공학박사학위논문

Development of Advanced RuO_2-based Electrocatalysts for Electrochemical Chlorine Production

전기화학적 염소 생성을 위한 RuO_2 기반의 고성능 코팅 전극의 개발

2015년 2월

서울대학교 대학원

화학생물공학부

트란 레 루

Development of Advanced RuO_2-based Electrocatalysts for Electrochemical Chlorine Production

by

Tran Le Luu

Under the supervision of

Professor Jeyong Yoon, Ph. D.

A dissertation submitted in partial fulfillment of the requirements for

the Degree of

Doctor of Philosophy

FEBRUARY 2015

SCHOOL OF CHEMICAL AND BIOLOGICAL ENGINEERING

SEOUL NATIONAL UNIVERSITY

Development of Advanced RuO_2-based Electrocatalysts for Electrochemical Chlorine Production

전기화학적 염소 생성을 위한 RuO_2 기반의
고성능 코팅 전극의 개발

지도교수 윤 제 용

이 논문을 공학박사 학위논문으로 제출함

2014년 12월

서울대학교 대학원

공과대학 화학생물공학부

TRAN LE LUU

TRAN LE LUU 의 공학박사 학위논문을 인준함

2015년 1월

위 원 장 이 종협 (인)

부 위 원 장 윤 제용 (인)

위 원 성 영은 (인)

위 원 탁 용석 (인)

위 원 강 경석 (인)

Abstract

Chlorine, which is produced industrially by the electrolysis of brine solution (chlor-alkali), is an important chemical in industry and is widely used in many applications. Currently, the most commonly used electro-catalysts for chlorine evolution are so-called Dimensionally Stable Anodes (DSA), based on RuO_2 or its mixtures with valve metal oxides, which brought a revolution in technical electro-chemistry during the past 50 years. When fabricating a RuO_2 electrode, the high electro-catalytic activity and the low energy consumption in chlorine evolution are considered as the most important factors. This requirement can be satisfied with the development of novel heterogeneous nanostructures RuO_2-based electrodes which can increase the accessible surface area and mass transfer. In addition, the using of green preparation methods for RuO_2-based electrodes that can reduces the cost, time, and environmental compatibility is necessary. In order to develop novel advance nanostructure morphologies as well as novel green synthesis routes for preparing RuO_2-based electrodes with improved chlorine electro-catalyst activities and understand on the mechanism of the chlorine evolution reaction at the interface between electrode surface - electrolyte, the following studies were conducted:

First, effect of various fabrication conditions in thermal decomposition including the types of solvents, precursors, and calcination times which can produce various surface areas to the electro-catalytic activity of RuO_2 electrode in chlorine

evolution was discovered. It was observed that the RuO_2 electrode fabricated with ethanol as the solvent showed highest chlorine evolution efficiency. Using $Ru(AcAc)_3$ as precursor and increase the calcination time to 3 h are also the good choices for increasing chlorine electrocatalytic activities. The chlorine evolution efficiency was not significantly related to the total voltammetric charge but to the outer voltammetric charge, which is affected by the morphology of the RuO_2 electrode surface. The size and number of cracks on the electrode surfaces or the outer voltammetric charges increased with easily evaporated solvents, decomposed precursors, and tensile stress under longer thermal treatments.

Second, the design in the advanced 1-D, 2-D, 3-D nanostructure morphologies as nanorod, nanosheet and macroporous of RuO_2-based electrodes have been successful achieved by using templates synthesis. The obtained nanorod, nanosheet and macroporous RuO_2 based electrodes show enhanced about the chlorine electrocatalytic activities compare to the conventional nontemplated electrode, respectively. The chlorine evolution efficiencies increase up to 20% in case of nanorod electrode, 35% in case of nanosheet electrode, and 50% with macroporous electrode compare to the conventional one. These results are strongly attributed to the more outer active sites favor chlorine evolution resulting from fast charge and easy mass transport in nanorod, nanosheet and interconnectivity macroporous structures. The RuO_2 nanorod with morphological features of 80 nm length, 20-30 nm width and the RuO_2 nanosheet with 40-60 nm length, 40 nm width are formed

on the surfaces of Ti substrates. In addition, the RuO_2-TiO_2 macropores structures of 50–600 nm in diameter with the worm hole-like and ordered cycle pore system were observed. These findings manifest that the templated nanorod, nanosheet and macroporous RuO_2-based electrodes are promising anode materials for chlor-alkali industry in future application.

Third, the performance enhancement both electrocatalytic and stability of RuO_2-based electrodes with chlorine evolution was attained by using novel green preparation routes as sonoelectrodeposition and microwave-assisted sol-gel. These novel green synthesis routes can also reduce the cost, time, energy consumption, and increase the outer active surface area, which is the main working part in chlorine evolution. The RuO_2 electrodes prepared by sonoelectrodeposition contain large hemispheres, mushroom-likes with the smaller and more uniform nanoparticles sizes (7-10 nm) compare to the conventional one made by mechanical stirring electrodeposition (20-25 nm). The formation of Ru metal by-product is inhibited using the sonoelectrodeposition method. Sonication accelerated the mass transport in the electrodeposition process, facile the deposition step and so on enhanced the quality of the RuO_2 electrodes. In the same manner, microwave-assisted sol-gel method can produce smaller size and more uniform distribution of RuO_2-TiO_2 nanoparticles with mean diameter of 8-10 nm on the big crack size surface compared with conventional heating method. Microwave-assisted sol-gel

route also has been identified as a novel and powerful method for quick synthesis of RuO_2–TiO_2 electrodes with excellent chlorine evolution performances.

Keywords: DSA, electrocatalyst, RuO_2, chlorine evolution, outer surface area, nanorod, nanosheet, macroporous, thermal decomposition, sol-gel, sonoelectrodeposition, microwave.

Student number: 2011-30796.

Contents

List of Figures

List of Tables

1. Introduction

1.1. Research background

Chlorine is produced by the electrolysis of brine solution (chlor-alkali industry) and now become one of the most important chemical in the chemical industry, pharmaceuticals, and wastewater treatment [1-3]. Chlor-alkali process represents one of the most energy- and resource-intensive technological applications of electrocatalysis. The growth rate of chlor-alkali industry in the world through has increased more than 350% since last 5 decades. The demand for Cl_2 supply reaches about 65 Mtons in 2010 worldwide, and the overall energy consumption is 1.5×10^{11} kWh/year, while the most efficient membrane process consumes around 2600-2800 kWh/Cl_2 ton [4]. The total energy consumption in the chlor-alkali process is proportional to the total cell voltage, including thermodynamic potential of anodic and cathodic reactions, electrode overpotential, ohmic drop from the electrolyte, membrane and bubble effect, etc. From a practical point of view, a possible efficiency improvement of the electrolytic chlorine production and reduce the energy consumption become a critical issue for the sustainable development with multilateral significance. This way provides highly environmentally benign electrical devices to address the problems of climate change, the impending exhaustion of fossils fuels [5].

Dimensionally Stable Anodes (DSA®) are now become the most popular electrode in chlor-alkali industry. These electrodes were discovered 50 years ago

and are still described as one of the most striking and greatest technological breakthrough of the history of electrochemistry in the last century [6-10]. RuO_2 is the main component in DSA® because of a very high catalytic activity and incredible stability for chlorine and oxygen evolutions [11, 12]. Most commonly, the active catalyst layer consists of RuO_2 or mix metal oxide RuO_2 + TiO_2, RuO_2 + IrO_2 + TiO_2 supported with metallic Ti as substrate material [13, 14]. It is critically needed to boost the energy efficiency in industrial processes by using selection electrocatalysts with improved performance [4, 5]. Thus it is a key for chemists to develop and evaluate new catalytic materials and accordingly new preparation routes to meet the continuous expansion of industrial requirements. Since their microstructures, phase compositions and surface morphologies are inhomogeneous, the electrocatalytic activities of these coatings are strongly dependent on the preparation conditions [13].

The thermal decomposition methods conducted with various preparation parameters such as types of solvents, precursors, and calcination times have led to the development of the RuO_2 electrode for the chlorine evolution [14]. The enhanced electro-catalytic activity of RuO_2 electrodes is attributed to the increased outer surface area, which is an easily accessible region for the electrolyte, and has become a significant factor in chlorine evolution [14-18]. Nevertheless, it has not fully been investigated on how these fabrication parameters affect to the chlorine evolution efficiency in the RuO_2 electrode prepared by thermal decomposition method.

In spite of remarkable electrocatalytic effects, there are remains a drawback in the conventional nanograins or nanospheres with zero dimensional effortlessly agglomerate under the fabrication or reaction conditions, which leads to low catalytic activity as well as the mass transport limitation [19]. The improvement electrocatalytic activity can be achieved by using the special nanostructure morphologies of RuO_2-based electrodes which can increase the surface area as well as mass transfer, and so on favor the chlorine evolution. Especially one, two and three dimensional nanostructured materials such as nanorods, nanosheets or macroporous morphologies have been shown to exhibit unique properties such as high active surface area, fast mass transfer, charge/discharge process and high stability [20-22]. Previous studies suggested that attainment nanostructures of RuO_2 nanorod or nanosheet electrodes have been obtained mostly through vacuum sputtering techniques [23-25] and chemical vapor deposition [26-28] in the form of thin films. In these methods, the high temperature (1500°C) vapor-phase processes are expensive and also limited by their low yield. In particular, the promising nanostructure materials as nanorod, nanosheet, macroporous RuO_2-based electrodes which intend to have a controlled pore size without collapse of the wall structure can be simply prepared by employing soft templates based on surfactant has not been investigated so far for chlorine evolution. This process is easy, reliable, versatile, low cost and applicable to a wide variety of electrodes.

In addition, many conventional methods were used for fabrication RuO_2-based electrode as thermal decomposition [14], sol-gel [29], polyol [30], Adams fusion

[31], electrodeposition [5], chemical vapour deposition [26-28], reactive sputtering [23-25]. These methods still having some drawback as low efficiency, by-product forming, high cost, require high temperature, high electrical energy and not environmental friendly. As a solution, using novel green fabrication methods as sonoelectrodeposition and microwave-assisted sol-gel which reduces the time, cost, energy consumption, and so on increase the chlorine electrocatalyst activity or stability should be examined. By these ways, the increasing in the utilization of active Ru species and reducing the use of Ru noble metal can be achieved.

1.2. Objective of the study

Towards this goal, the present work is aimed to synthesis the novel advanced RuO_2-based electrocatalysts exhibit an extraordinary surface morphology which provides a high active surface area, improves the catalyst utilization and mass transfer comparing to conventional electrocatalysts, then following the understanding the mechanism of the electrochemical chlorine evolution. Later, the developments of RuO_2-based electrocatalytic by using alternative green preparation routes with control the coating' structures, reduce the cost and time, increase the chlorine evolution efficiency and electrode stability has been investigated systematically in this study:

1. To investigate the effect on the chlorine evolution efficiencies of RuO_2 electrodes depending upon preparation parameters in thermal decomposition. For this purpose, RuO_2 electrodes were prepared at various fabrication conditions including the types of solvents, precursors, and calcination times. The coating layers of the metal oxides were prepared with precursor solutions containing 50 μL of 0.2 M $RuCl_3$, $Ru(NO)(NO_3)_3$, or $Ru(AcAc)_3$ (Ruthenium acetylacetonate) dissolved in HCl 1:1 (v:v), ethanol, or iso-propanol as the solvent and then sintered at 450℃ for predetermined times (1, 2, and 3 h). The total or outer voltammetric charges were analyzed by cyclic voltammetry (CV) and the microstructures of the RuO_2 electrode surfaces were examined by scanning electron microscopy (SEM). The electro-catalytic performance of the RuO_2 electrodes in chlorine evolution was evaluated with linear sweep voltammetry (LSV) and aqueous chlorine

measurements. The possible mechanisms of chlorine evolution at the interface between electrode surface and electrolyte were also discussed.

2. To synthesis advanced 1-D, 2-D, and 3-D nanostructure morphologies of RuO_2-based electrodes as nanorod, nanosheet, macroporous which increase the surface area as well as mass transport. For this purpose, three organic templates as sodium dodecyl sulfate (SDS), polyethylene glycol (PEG), polystyrene microspheres (PS) were used as surfactants assemblies to prepare nanorod, nanosheet, macroporous RuO_2-based electrodes. The properties of the obtained RuO_2-based nanorod, nanosheet and three dimensional ordered macroporous electrodes were compared with the conventional nontemplated electrode in chlorine evolution. The microstructures of as-prepared electrodes were characterized using scanning electron microscope (SEM), transmission electron microscopy (TEM), X-Ray diffraction (XRD). The electrochemical properties were examined with cyclic voltammetry (CV), linear sweep voltammetry (LSV), total chlorine concentration (DPD) methods. The electrode morphologies, active surface area and chlorine evolution efficiency improvement were discussed based on the observation.

3. To apply novel green fabrication methods for RuO_2-based electrodes which can reduces the time, cost, energy consumption, and so on increase the chlorine electrocatalyst activity and stability. For this purpose, the sonoelectrodeposition and microwave-assisted sol-gel methods were used to synthesis RuO_2-based electrodes. The properties of as-prepared electrodes as morphologies, active

surface area, and chlorine evolution efficiency were compared with the electrodes prepared by conventional method without sonication or microwave-assisted. The properties of as-prepared electrodes were examined using scanning electron microscope (SEM), transmission electron microscopy (TEM), X-Ray diffraction (XRD), cyclic voltammetry (CV), linear sweep voltammetry (LSV), total chlorine concentration (DPD) methods.

2. Literature review

2.1. Chlor-alkali industry

Chlorine is now become one of the most important chemical in the industry, which is produced by the electrolysis of brine solution (chlor-alkali process). The annually chlorine production now is about 70 million tons, which is used in a lot of application. Approximately 50% of the products marketed by the chemical industry and 85% of the pharmaceuticals, 98% water treatment plant are derivatives of chlorine chemistry [1-3]. Dimensional Stable Anodes (DSA) are such kind of catalytic electrodes for chlorine evolution, which consist of RuO_2, IrO_2 or a mixture of its metal oxides coated on metal substrate, mainly titanium. Large-scale use of DSA in chlor-alkali electrolysis industry came in the 1960s when Henri Beer invented this type of electrode, and further P.C.S. Hayfield, were then developed and industrialized by De Nora. From a broad point of view, electrocatalysis can be regarded as the search for new materials and new operating conditions in order to: (i) improve activity, efficiency and selectivity of electrodes, (ii) reduce investment and operational costs, (iii) increase the electrode or cell lifetime, and (iv) avoid pollution [4, 5]. Electricity is essential to produce chlorine in the chlor-alkali industry, which accounts for about half of the total production cost [4]. Energy savings arise primarily through using more efficient technologies, such as the replacement of the less energy-efficient mercury, diaphragm processes by the most energy-efficient and environment friendly membrane technology with 2600-2800

kWh per produced ton of Cl_2 [1, 2]. This power consumption can be further reduced to 1600-1700 kWh per ton Cl_2, if the cathode is replaced by an oxygen-depolarized cathode in which oxygen is reduced to water in somewhat internal fuel cell ($O_2 + 2H_2O + 4e^- \rightarrow 4OH^-$, $E_o = 0.4$ V/SHE), as shown in Figure 2-1 [32, 33]. Meanwhile, chlor-alkali industry is also one of the resource-intensive production processes, which depends highly on the use of the rare strategic metal ruthenium as catalysts [14].

In chlor-alkali process, chlorine is produced by the electrolytic of sodium chloride, to convert chloride ions (Cl^-) into molecular chlorine (Cl_2) at the anode as follows reactions [4]:

Cathode: $2H_2O + 2e^- \rightarrow H_2 + 2OH^-$ (1)

Anode : $2Cl^- \rightarrow Cl_2 + 2e^-$ (2)

Total : $2Na^+ + 2Cl^- + 2H_2O \rightarrow H_2 + Cl_2 + 2Na^+ + 2OH^-$ (3)

Simultaneously with chlorine evolution, sodium hydroxide (NaOH) solution and hydrogen (H_2) are produced at the cathode side, induce the increasing pH. High electrical efficiency is closely related with the electrocatalysis performance. High-quality electrodes can improve the electrocatalytic activity of the desired reactions, such as chlorine gas evolution, but depress the electrocatalytic activity of the side reactions, such as oxygen gas evolution.

The total consumption of electric power is proportional to the voltage applied to the cell for a given current density (the rate of electrode reaction). The cell voltage consists of several components [5]:

$$\Delta V = \Delta E + \Delta \eta + IR + \Delta v \qquad (4)$$

Where ΔV is the thermodynamic potential difference for a given anode/cathode reaction, $\Delta \eta$ is the sum of the overpotentials for the anodic and cathodic reactions (which are dependent on the electrocatalysts), *IR* is the ohmic drop of the electrolyte and Δv is the additional ohmic drop from the membrane, gas bubble effect, stability of the electrode etc.

In general, the intrinsic electrocatalytic properties of an electrode material can be simplified to the exchange current density and the Tafel slope. Chlorine evolution is characterized by a low Tafel slope about 40 mV at pure RuO_2 electrode and 30 mV with RuO_2-TiO_2 electrode at current densities of 200–250 mA/cm^2 in 5 M NaCl solution at 80–90◦C. High exchange current density, low Tafel slope, and a high density of active sites are beneficial for electrocatalysis [4, 5, 14].

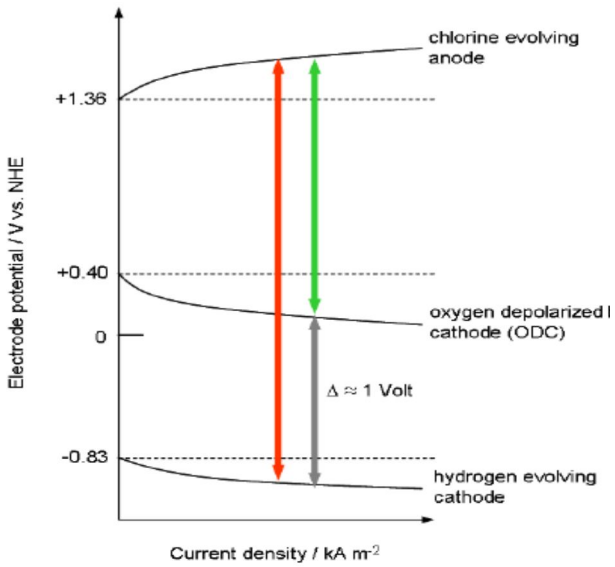

Fig. 2-1. Electrode potential in chlor-alkali electrolysis from NaCl aqueous solution as a function of current density [5].

2.2. RuO_2-based electrodes

2.2.1. Physicochemical properties of RuO_2

Ruthenium is a chemical element that can easily adopt various formal oxidation states from −II to +VIII in chemical bonds. RuO_2 is a noble and expensive metal oxides, the price of ruthenium is about 10 times lower than that of platinum. RuO_2 reveals a complex and unique redox surface chemistry, act as a versatile oxidation catalyst and electrocatalysis in many applications as chlor-alkali cells, organic electrosynthesis, as well as electrochemical supercapacitors and photocatalysis [34]. RuO_2 exhibits excellent corrosion resistance, electronically conducting and low overpotential for anodic chlorine evolution reaction [13, 14]. Roughly 10-15% of the annual production of ruthenium goes into the production of such DSA (in 2010 about 3 tons) while most of the ruthenium is deployed as buffer layers and thin film resistors in the electronic industry (about 20 tons) [2]. The performance of RuO_2/Ti was so outstanding that all graphite anodes were replaced by these anodes in a few years of their discovery [8-14].

The electronic configuration of elemental Ruthenium is $4d^7 5s^1$. In general, the electrons in d^n oxides can quite easily be removed from the partially filled d orbitals so that d^n oxides are considered to be much more chemically active than d^o oxides. Its first valence state is Ru^{3+}, occurring as Ru_2O_3 at 0.738V vs HE. Because this oxidized species is insoluble in the absence of complexing agents, the metal is passive in the higher potential range. The next redox step is Ru^{4+} as RuO_2 at 0.937

vs HE, volatile yellow ruthenium tetroxide (melting point 25.51^{o}C, decomposition at 1081^{o}C), RuO_4, or soluble H_2RuO_5 (Ru^{8+}, yellow hyperruthenate), depending on the solution pH [35]. In a DFT study, the corundum structure of Ru_2O_3 has shown to be thermodynamically less stable than rutile RuO_2, but it may exist as a metastable phase [4, 36]. RuO_2 crystallizes with rutile structure, reflecting a strong tendency of Ru^{4+} to acquire octahedral coordination, which is shown in Figure 2-2. Red balls are ruthenium atoms (this site is shared by other transition metal for the mixed oxide), and green balls are oxygen atoms. At high pressures (typical values of 100 GPa), the rutile structure of RuO_2 transforms into the cubic fluorite structure, with an increase in the metal coordination number from 6 to 8. Interestingly, the bulk modulus of cubic-RuO_2 is close to that of diamond [37, 38]. RuO_2 belongs to the class of metallic conducting transition metal oxides whose electrical resistivity is 35.2 ± 0.5 μΩ.cm at room temperature, higher than that of metallic ruthenium (about 16 μΩ.cm). The high electronic conductivity of RuO_2 is one prerequisite for its intensive use as electrocatalyst and electric contacts in microelectronic devices. The electrical resistance of RuO_2 is virtually isotropic and increases with increasing temperature (characteristic for metallic conductivity) [39]. Within the molecular orbital (MO) theory two of the five d-orbitals of Ru in RuO_2 are combined with s and three p functions of Ru to form the six hydrid orbitals e_g $2sp^3$ [40-42].

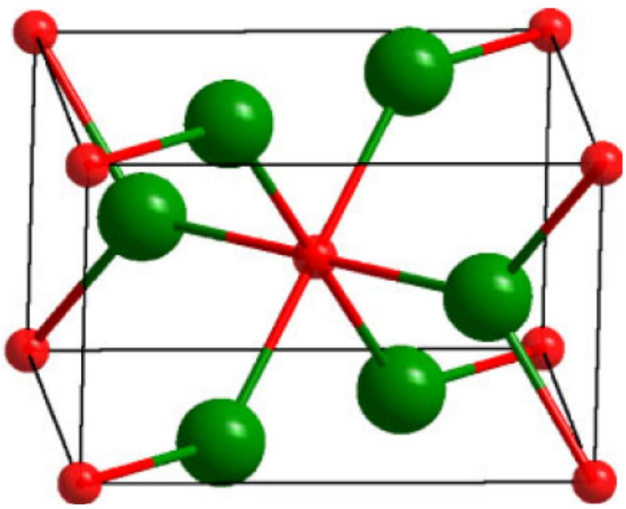

Fig. 2-2. Tetragonal rutile structure (*P*42/mnm, space group 136) of the active phase [5].

2.2.2. Electrochemical properties of RuO_2

The electrochemical and interfacial properties of RuO_2 are of utmost importance for a deeper understanding of how RuO_2 catalyzes electrochemical reactions. A number of investigations have pushed forward the idea that most of the features of oxide electrodes may be governed by the acid−base properties of the oxide/solution interface. For instance, the state of oxide surfaces depends critically on solution pH, which may point to the formation of surface hydroxyl complexes. Or the reaction order of the oxygen evolution and chlorine evolution in H^+ or in OH^- has often been found to be fractional [43-46]. Equally important for the state of the electrode surface in solution is the specific adsorption of anions. The acid/base properties of RuO_2(110) are related to the 1f-cus Ru and bridging O sites which serves as Lewis acid/base and Bronsted base, respectively. The potential of zero charge (PZC) is the potential value at which the surface is uncharged, that is, the surface dipole which also includes possible adlayer species is compensated. The PZC is governed by the strength of the interaction between the surface Ru atoms and the oxygen of the surface OH groups attached to it. Therefore electrocatalytic properties and the PZC of oxide surfaces may be intimately interconnected. Using the Gouy−Chapman−Stern model for the double layer, the experimental capacitance is composed of two capacitors in series [47-50]:

$$1/C = 1/C_d + 1/C_i \qquad (5)$$

With C_d is the diffuse layer capacitance and C_i is the inner layer capacitance. The inner capacitance is independent of the electrolyte concentration and can be

extracted from concentration-dependent measurements of 1/C. Assuming a planar geometry of the double layer, values of C_i = 60−80 μF/cm^2 are derived, while C_i is 300−500 μF/cm^2 for a spherical double layer. In an aqueous environment the oxide surface is normally covered by OH groups (due to water dissociation) which are stabilized by "co-adsorbed" and coordinated water and which mediate the interaction of the underlying metal ions with chemical species in the solution [48, 49]. RuO_2 in aqueous solution adsorbs water rapidly with a constant H/Ru ratio throughout the thickness of the oxide layer. Active sites on hydroxylated oxide surfaces act preferentially as Bronsted acids and bases. Hydrous RuO_2 is permeable to protons while dry RuO_2 is not. The surface response in CV (Figure 2-3) is related to redox reactions at the surface active sites which is assisted by proton exchange δH^+ with the solution and electron transfer δe^- according to equation [46]:

$$RuO_x(OH)_y + zH^+ + ze^- \rightarrow RuO_{x-z}(OH)_{y+z} \qquad (6)$$

This behavior plays an important role for hydrous-RuO_2 when applied as supercapacitors. The ionic adsorption strength on RuO_2 electrode is constant as the electrode potential is varied. There are two ways to charge an oxide surface: one is driven by the electrode potential, the other by the pH. While the electrode potential acts on the metal sites whose charge variation is compensated by proton exchange, the pH variation acts on the surface hydroxyl complexes whose dissociation with the formation of a surface charge is compensated by adsorption of ions from the solution [51, 52].

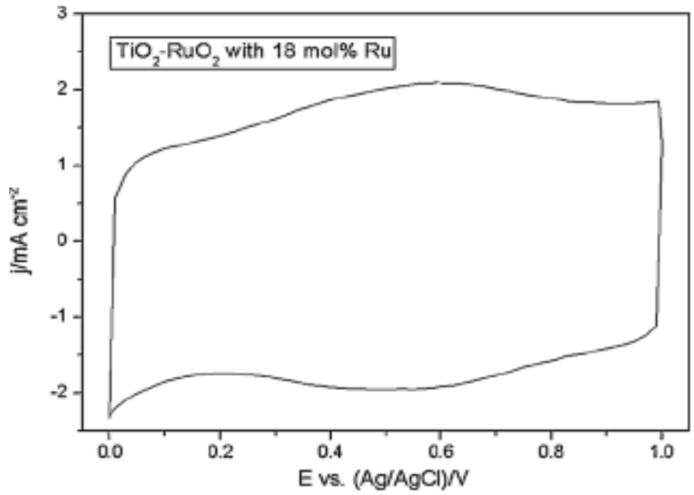

Fig. 2-3. CV of a TiO_2–RuO_2/Ti coating with 18 mol% Ru, recorded in 0.5 M H_2SO_4, room temperature, 100 mV s^{-1} [52].

2.2.3. Mechanism of chlorine evolution reaction

The model mechanism of chlorine evolution at the electrode surface is described following the Volmer–Kristalik–Tafel mechanism (2002). Three different reaction mechanisms are distinguished according to the kinetics and the rate of the separate reaction steps [53]:

$$-S^{Z} + H^{+} \rightarrow SH^{Z+1} \quad (7)$$

$$-S^{Z} \rightarrow S^{Z+1} + e^{-} \quad (8)$$

$$-S^{Z+1} + Cl^{-} \rightarrow -SCl^{Z+1} + e^{-} \quad \text{Volmer-step} \quad (9)$$

$$-SCl^{Z+1} + Cl^{-} \rightarrow -S^{Z+} + Cl_2\,(g) \quad \text{Krishtalik-step} \quad (10)$$

$$2{-}SCl^{Z+1} \rightarrow 2{-}S^{Z+1} + Cl_2\,(g) \quad \text{Tafel-step} \quad (11)$$

Where $-S^{Z}$ and $-S^{Z+1}$ are the non-oxidized and oxidized superficial sites in different oxidation states, respectively, and reaction (7) is an equilibrium step independent of the chlorine evolution reaction, being an intrinsic property of the oxide. This step explains the dependence of the electrode behavior on pH. Reaction (8) is the oxidation of the superficial sites (S^{Z}), which generate the active sites where the adsorbed chlorine intermediate is formed from the chloride ions. In this step, the active sites (S^{Z+1}) are generated as one electron is released. In reaction (9), the chloride ion is electro-adsorbed on the generated active sites since the active site is the metallic cation site to give the atomic chlorine intermediate (SCl^{Z+1}). There are δ and π interactions or construction from t_{2g} orbital of the surface

between metal cation and p orbital of the adsorbed Cl atom. The later discharge of chlorine can occurs either by the reaction of an intermediate with a chloride ion or the recombination of the adsorbed intermediates (reaction 10, 11). These reactions involve the formation of the Cl-Cl and the cleavage of the bond between the adsorbed Cl atom and the electrode surface accompanying with the electron transfer. Theoretical potential decay curves were deduced for both the Tafel reaction ($2Cl^- \leftrightarrow Cl_2$) and the Krishtalik reaction ($Cl^- + Cl_{ad} \leftrightarrow Cl_2 + e^-$) as a rate determining step in the formation of molecular chlorine. To maintain a current it is essential to supply reactants to the electrode surface and also remove the products (the mass-transfer processes, such as diffusion and convection of the reacting species between the electrode surface and bulk of the solution). The electrocatalytic properties of different oxides are correlated with the energy change involved in the lower → higher valency state transition [54-56]. Electrocatalysis can be expressed, to a first approximation, in terms of bond strength between the electrode surface and reaction intermediates. The concepts applied to the oxygen evolution electrocatalysis can thus be extended to chlorine evolution, including the calculation of the change in the crystal field stabilization energy for the transition from one surface complex to another [57-59].

Another mechanism of chlorine evolution can be proposed by Erenburg and Jansen in 1981 and 1984 [55, 56]. Since metal cations on oxide electrodes are not directly accessible to Cl^- discharge because they are covered with surface OH

groups. The oxidation of the anode surface precedes the Cl^- oxidation, and the Cl^- discharge happens over adsorbed oxygen. In case removal of chlorine from the electrode surface, reaction 13-14 below, are the slow step. The reactant Cl^- moves to the interface (mass transport), electron transfer occurs close to the interface (electron transfer reaction), the product Cl_2 moves away from the anode to allow the fresh reactants to the anode surface:

$$S\text{-}OH \rightarrow S\text{-}O + H^+ + e^- \qquad (12)$$

$$S\text{-}O + Cl^- \rightarrow S\text{-}OCl + e^- \qquad (13)$$

$$S\text{-}OCl + Cl^- + H^+ \rightarrow S\text{-}OH + Cl_2 \qquad (14)$$

Figure 2-4 shows the reaction pathway of the Cl_2 evolution reaction was investigated by combining electrochemical and Raman spectroscopy to monitor vibrations of the crystal lattice of RuO_2 and changes in the surface concentration of the adsorbed species as a function of the electrode potential. It is shown that oxidation and reconstruction of the catalyst surface during chlorine evolution is a consequence of the interaction between RuO_2 and water. Water (more precisely the OH adlayer) is understood not just as a medium that allows adsorption of intermediates, but also as an integral part of the intermediate formed during the electrochemical reaction. HClO was a crucial intermediate for the catalytic reaction. The vibrational modes of the crystal lattice of RuO_2 were very similar to the vibration of the ClO bond in HClO dissolved in water [60]:

$H_2O \leftrightarrow OH_{ad} + H+ + e^-$ (15)

$OH_{ad} + Cl^- \leftrightarrow HClO + e^-$ (16)

Rate determining step b = 40 mV dec^{-1}

$HClO + H^+ + Cl^- \leftrightarrow Cl_2 + H_2O$ (17)

Interpretation of the derived “volcano” curve suggests that electrocatalysis is governed by a resonance phenomenon using a dynamic catalytic descriptor. The characteristic vibration of the MO bond and the maximum of the volcano curve corresponded to the vibration of the ClO bond in HClO [60].

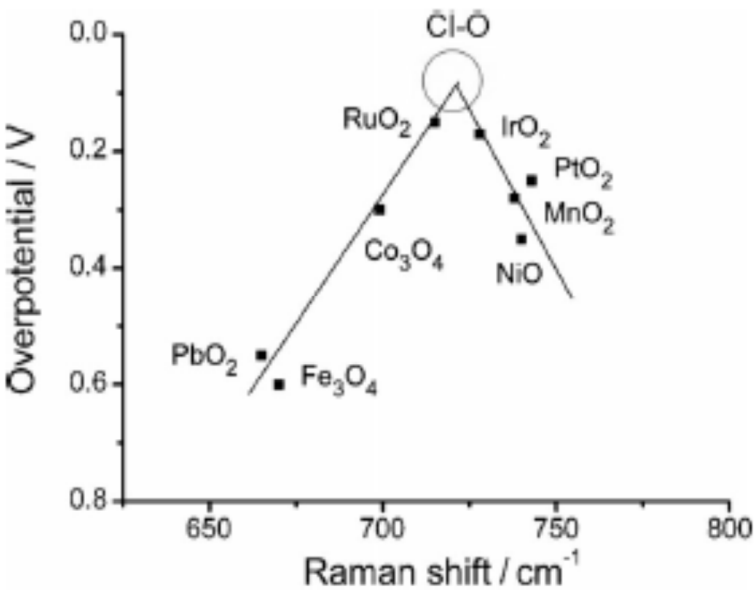

Fig. 2-4. Overpotentials of the chlorine evolution as a function of the characteristic Raman shifts of the ClO bond vibration of HClO in aqueous solution [60].

2.3. Factors affect to the chlorine evolution reaction

2.3.1. The surface area

In view of the reversibility of the chlorine/chloride electrode system, especially as compared oxygen, the main factor influencing the rate of chlorine evolution was assumed to be transfer of chlorine gas away from the electrode surface. These electrode systems also difference at least one other important respect, namely that while the chlorine system is highly reversible, the oxygen system is quite irreversible. It seems reasonable, therefore, to assume that in the case of chlorine evolution the surface process is fast and mass transfer of the gaseous product away from the interface plays a major role in this reaction. This is borne out by the fact that the low Tafel slope can apparently be maintained at high current densities if quite vigorous stirring is maintained [16, 18, 61]. The pores may be small, thereby inhibiting the transport both of chloride ions or chlorine gas. The chlorine gas bubble effectively blocking off the internal surface, difficult supply of Cl^- to the inside of the pores, additional ohmic drops. The activity of the RuO_2 nanocrystals towards oxygen evolution reaction decreases with increasing particle size, the activity towards chlorine evolution is insensitive to the particle size/shape [62]. The observed tendency indicates that the oxygen evolution is significantly affected by the crystal edges while chlorine evolution reaction proceeds mainly on crystal faces. In contrast to the oxygen evolution reaction, the rate of chlorine evolution apparently occurs at the external surface of these microporous electrodes [63]. The

internal surface area is not a critical factor in the chlorine evolution process at practical current density [64].

2.3.2. Chlorine gas bubbles behaviour

In the electrolytic production of chlorine-soda, high current density produces bubbles that can cover some parts of the electrode surfaces, causing an undesirable decrease in mass transfer. Since the Cl_2 is evolved from a highly concentrated electrolyte, diffusional limitation of the product is expected as a consequence of its accumulation in the proximity of the electrode surface. The equations of the steady-state polarization curve and the potential decay curve (pdc) upon current interruption were analysed for the electrochemical gas-evolving processes on the electrodes with high electrocatalytic activity under conditions when removal of reaction product is the rate-determining step of the overall process. The entire gas evolution process can be summarized into three crucial steps involving: (1) nucleation, (2) bubble growth, and (3) detachment. Chlorine gas bubbles generated at the electrode surface result in additional ohmic drop due to the shielding and blocking effects, which is shown in Figure 2-5. Diffusional overpotential coupled with the "gas-bubble effect", that is causing the loss of active surface area due to the produced Cl_2 gas masking active spots, introduces a decline in activity that can be more than 40% with respect to the initial value of the current density. Supersaturation of the electrolyte near the electrode surface with the produced Cl_2 and gas formation is possible even at relatively low current densities [50, 63]. The sample with the highest active surface area should hence produce more gas per unit of geometric surface area which results in higher density gradients, better natural

convection of the electrolyte and better penetration of the electrolyte towards the active spots. Thus, the increase in the volume of bubbles adsorbed per unit area causes a decrease in mass transfer at the electrode surface. For these reasons, there has been increased interest in finding electrode geometries that promote the detachment of gas bubbles in order to increase mass transfer and ultimately efficiency. It was proposed that in a regime of very high current densities, the inner parts of the coating start to participate in the reaction due to increased convective flow of the electrolyte in the pores [50, 65, 66].

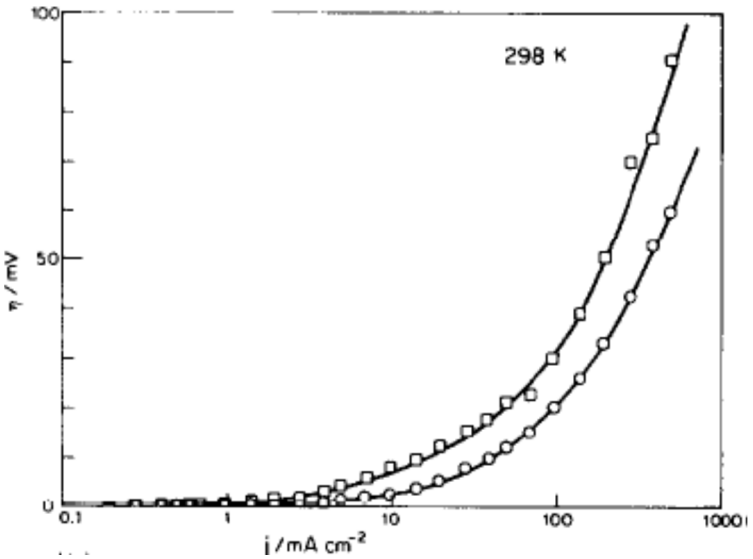

Fig. 2-5. Log j vs. n curves for Cl_2 evolution from 1M Cl^- ion solution of a RuO_2 + TiO_2 anode in an active state, with (o) and without (□) stirring (298°K) [65].

2.3.3. Stability and mixed metal oxide electrodes

In the electrochemical production of chlorine, high stability and high electrocatalysis performance are the two most important research topics for studying or developing electrodes and marked tendency to corrosion under high potential. High stability means long working life time with stable working performance and little contamination to the environment from the dissolving of the metal oxides. Proceeding from laboratory tests to the general behavior observed in industrial situations, the deactivation mechanism can be classified into five large classes, which clearly are not to be considered as rigidly separated: metal base passivation, coating consumption, coating detachment, mechanical damages and mixed mechanism. Passivation is the most frequent deactivation mechanism associated with operations at high current densities. Only a slight increase of the potential, and a different mode of gas evolution (beginning with uniform evolution of fine bubbles, which gradually changes to uneven distribution of large ones), from the surface is observed. Deactivation occurs with a sudden increase of electrode potential, rapidly reaches very high values, signifying a complete electrochemical failure. Since the typical support of activated anodes is titanium (in any case, a "valve" metal), the growth of an insulating TiO_x film can distorts the Tafel line, related to the presence of ohmic drop. Insulating films can form during the preparation if the calcination temperature exceeds or under electrodeposition process (Figure 2-6). Another possibility is that the support becomes passive during the anodic reaction because of oxygen evolution inside the pores whose deepness

can reach the underlying interface. The latter effect is however expected to become a problem in long-term experiments. Because the usual support of activated oxide coated anodes is titanium, the growth of an insulating film can increase the potential of the system [63, 67].

RuO_2 is barely stable at high potentials. It is believed that the oxidation of RuO_2 to soluble perruthenates, ruthenates, and RuO_4 is the main source of instability of RuO_2. The dissolution rates of RuO_2 raises with increasing current density and increasing percentage of O_2 generation [4, 56, 68]. The oxygen evolution reaction cannot be totally suppressed and becomes a significant process (a) at high anolyte pH, (b) at temperatures approaching ambient and (c) at low concentration of chloride ions. There are several successful strategies available to minimize the loss of Ru. For instance, if the chlorine evolution is run in the low pH region the percentage of O_2 evolving at the anode will be lower for thermodynamic and kinetic reasons and hence Ru losses via oxygen evolution can be reduced [63]. Corrosion can be reduced or minimized by lifting the limit of the redox reaction. This can be done by mixing RuO_2 with other oxides. The development of the mixed metal oxide electrodes significantly increased the stability, current efficiency and operating voltages of dimensionally stable electrodes and enabled the introduction of new electrochemical processes [43, 69]. The multi-component $RuTiMO_x$ system improved effectively the stability performance with M = Ir, Sn, V, Ta, Ni, Ce, or can be binary, many metal oxides as TiO_2-RuO_2, TiO_2-Co_3O_4, RuO_2-TiO_2-CeO_2-Nb_2O_5, etc [70-89]. The nonconducting oxides are especially

attractive due to their considerably lower cost compares to the noble metal oxide, become economic benefit for the making of electrode. Actually, inert oxides such as valve metal oxides exhibit much lower voltammetric charges because the redox mechanism is not operating (Ti^{4+} in TiO_2 cannot be further oxidized; the same is the case with SnO_2, etc.). The stability of IrO_2 is somewhat better than that of RuO_2. Therefore, anodes in the chlor-alkali industry usually comprise RuO_2 and IrO_2 combined intimately with TiO_2 to form an anode which is mechanically robust, readily releases chlorine, and does not undergo passivation or severe dissolution with extensive use. The electrocatalytic stability of TiO_2-RuO_2 with variable concentration profiles of RuO_2 has found to be higher than that of pure RuO_2-IrO_2 coatings [5]. The excellent stability and performance of mixed RuO_2-TiO_2 coatings is attributed to the existence of a metastable solid solution through a charge transfer from the RuO_2 to the TiO_2. With extended usage in electrolytic chlorine cells the chlorine overpotential increases from 40–50 mV (fresh electrode) to 300–400 mV so that the RuO_2-TiO_2-based anode is considered to be deactivated. Because of their excellent chemical and electrochemical resistance under anodic polarization for chlorine evolution, the Ti/RuO_2−TiO_2 electrode can reach very long operating times of up to 35000 Ah cm^{-2} for the brine electrolysis [70, 71, 74, 89].

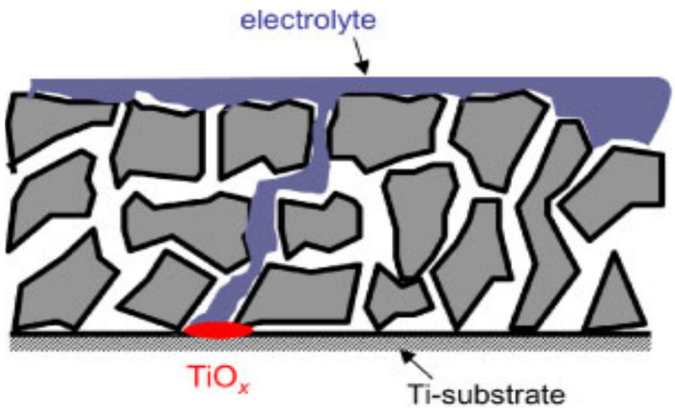

Fig. 2-6. Sketch of the cross-section at the RuO_2 coating – Ti substrate interface [5].

2.4. Synthesis of RuO_2 electrode

2.4.1. Thermal decomposition

DSA-type metal oxides can be prepared in various ways, but the most applied procedure in technology is the thermal decomposition of appropriate precursors, mainly $RuCl_3$ salts, dissolved in suitable solvents and painted on the metal substrates, mainly titanium and firing the deposit in air or oxygen at 450^{o}C [43]. The thermal decomposition method is preferred, due to its specialties of simple conduction and low cost. The painting and firing procedure is usually repeated some 10-12 times to produce a relatively thick conducting film. RuO_2 nanocrystalline films were produced by dip-coating, brush painting, spin coating techniques. Oxide electrodes prepared by thermal decomposition of suitable precursors consist of porous layers of sintered crystallites [43, 58]. Figure 2-7 shows the schematic diagram for the metal-oxide electrodes fabrication process with thermal decomposition methods. Pretreatment on the metal substrate should be conducted before thermal deposition, in order to enhance the adhesion of produced metal oxide on the substrate. Normally, pretreatment process includes: first, thoroughly cleaning of the substrate by organic solvent and degreasing agent and second, etching of the substrate in concentrated HCl at high temperature for 30 min to 1 h, to remove the original surface oxides and increase the surface roughness. The chemical composition, crystallinity and crystal grain size, surface morphology, electrical conductance, electrocatalysis performance, and electrode

stability are determined by the precursor composition, solvents and loadings, substrate pretreatment, and thermal decomposition parameters especially the temperature and duration of the preparation and calcinations processes [90, 91]. It is reported that RuO_x exists the most when annealed at around 450^oC, and disappears at 600^oC [92].

Porosity and crystallite size are depended on the calcinations temperature. SnO_2 is frequently used as an additive in industrial RuO_2-based electrodes to enhance their selectivity for chlorine evolution with respect to oxygen evolution [56]. In a recent paper the chlorine evolution and oxygen evolution were studied on well-defined RuO_2 nanocrystals with a typical size of 10-50 nm [93].

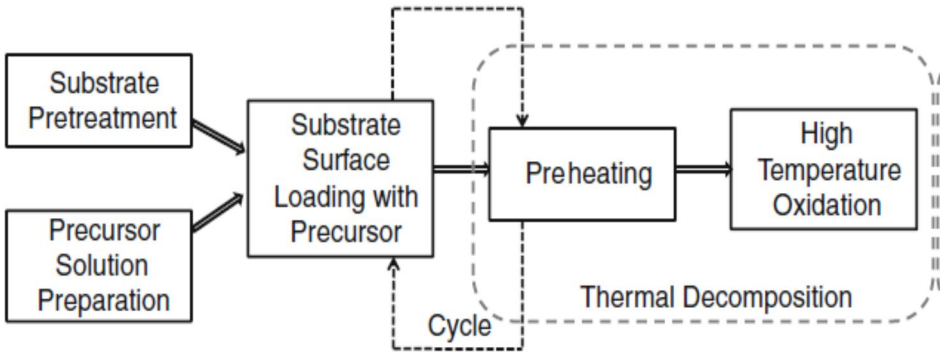

Fig. 2-7. Schematic diagram of thermal decomposition method for making DSA type electrodes [90].

2.4.2. Sol-gel

Both thin and thick RuO_2 coatings on Ti substrate can be produced by the sol−gel process. An approach based on the attractive sol–gel route for the preparation of noble metal oxides seems to be promising both electrocatalytic and stability with oxygen, chlorine evolutions. It has been suggested that electrocatalytic properties and stability of DSA can be significantly improved if the active coating is prepared by a sol−gel procedure, as an alternative to the commonly used preparation procedure that involves thermal decomposition of metal chlorides [94]. The improvement is due to an enlargement of the coating active surface area, increased contribution of the so-called geometric catalytic factor, caused by the formation of finely dispersed oxide particles during the sol–gel procedure. The electrochemical behavior for the chlorine evolution depends sensitively on the aging time of RuO_2 and TiO_2 sols [95]. A typical cracked-mud catalytic layer during synthesis is typically achieved by inducing a large enough tensile stress in the layer. During sol–gel synthesis a wet layer of salt precursors of the catalyst is deposited on a solid substrate. After drying, the catalyst is exposed to thermal annealing to transform it into the active state. The volume change of the gel-body during the drying and thermal treatment steps is morphology of a RuO_2-based DSA is depicted in Figure 2-8 [5]. The formation of “cracks” in a restricted by the substrate, which results in an internal stress that depends on the density change of the coating during drying and the mismatch in the coefficients of thermal expansion. If the internal stress is large enough, surface cracks or channel cracks

may nucleate and release energy. Owing to the controlled hydrolysis and polycondensation reactions, sol–gel synthesis of mixed oxides has shown to be superior to other synthesis techniques [96-98].

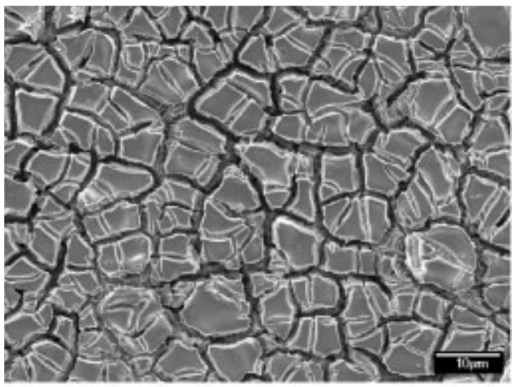

Fig. 2-8. A typical cracked-mud morphology of a sol-gel RuO_2-based DSA [5].

2.4.3. Electrodeposition

Electrodeposition has proved to be simple and versatile, one-step, film thickness control and cost effective method for electrode preparation [99-105]. The two key mechanisms that have been identified as the rate determining steps for crystal formation are charge transfer and diffusion of supersaturated ions or mass transport at the electrode surface. With cathodic electrodeposition, metal ions can be precipitated in the form of amorphous oxide and hydroxides which are transformed into the crystalline oxides by subsequent thermal treatment. Zhitomirsky succeeded first in the simultaneous electro-deposition of TiO_2 and RuO_2 onto a Ti plate in the form of a mixed oxide layer [106]. Since the electrodeposited films are thicker than those produced by painting, fewer calcinations steps are required to produce a similarly thick DSA coating. The electrodeposition of a metal oxide proceeds via a wet chemical precipitation induced by a cathodically electro-generated base seems very promise [46]. This method produces typical morphology with a decrease of the chlorine overpotential and simultaneously a reduction of the noble metal content can be achieved, which is favorable in terms of energy and resource efficiency of the chlor-alkali industry [20]. A titanium wire (Goodfellow Metals, 99.9% purity, 0.25 cm^2 geometrical area) sealed in glass served as a substrate for electrodeposition. It was polished with emery paper and alumina powder, washed with quadruply distilled water. The electrodeposition route for a metal oxide preparation uses a cathodic reaction to increase the pH locally near the electrode

surface. The main cathodic reaction to produce OH^- is the decomposition of water under hydrogen evolution as followed reactions [48, 107, 108]:

$$O_2 + 2H_2O + 4e^- \leftrightarrow 4OH^- \quad (18)$$

$$2H_2O + 2e^- \rightarrow H_2 + 2OH^- \quad (19)$$

These reactions consume H_2O, generate OH^- and increase pH at the cathode. In cathodic deposition, metal ions or complexes are hydrolyzed by electrogenerated base to form oxide, hydroxide or peroxide colloidal particles deposit on cathodic substrates. Hydroxide and peroxide deposit can be converted into corresponding oxides by thermal treatment. The assumed reactions can be represented as:

$$Ru^{3+} + OH^- \rightarrow RuO_x(OH)_y \rightarrow RuO_2 \quad (20)$$

The cathodic decomposition of water can be competed with the cathodic electro-deposition of Ru metal:

$$Ru^{4+} + 4e^- \rightarrow Ru^o \quad (21)$$

The anodic electrodeposition of ruthenium was carried out galvanostatically from a stirred solution of 1 g dm^{-3} $RuCl_3$, 0.1 M HCl (Fluka, puriss.) at a current density of 40 mA cm^{-2} for 15 min at room temperature or treated by a potentiodynamic sweeps from -0.2 V to +1.2 V at 2 Hz for 2 min in 0.5 M H_2SO_4.

2.4.4. Templates synthesis

2.4.4.1. Hard template

Four general steps are needed to synthesize a porous material from a hard template, starting with the synthesis of a precursor solution. Although gas-phase molecules or solid particles can be used as precursors, solution-based precursors are principally used for multiple templating [21]. For the formation of a template inorganic material, the simplest solution-based precursor is a salt dissolved in a polar solvent. Metal alkoxides dissolved in aliphatic alcohols are also commonly used as precursors. With metal alkoxides, formation of the final inorganic material generally needs to be catalyzed by acid or base.

Step two consists of filling or coating a hard template with a precursor. This is done by either letting a precursor solution infiltrate the void spaces of a hard template via capillary action (Figure 2-9, left), or by soaking a hard template in the precursor solution (Figure 2-9, right) [21]. Ensuring that the precursor uniformly fills or coats the template is a crucial part of this step. Several important things need to be considered in order to achieve this goal. First, the precursor solution should easily wet the template surface (i.e., have similar polarity). Second, the precursor needs to have sufficiently low viscosity so it can easily fill or coat the template. Additional solvent in the precursor often helps in this respect, provided the precursor does not become too dilute to fill adequately a template. Different methods that rely on the assistance of vacuum suction can also improve the infiltration of low viscosity precursors (and remove excess solvent). After the

template has been coated or filled, the precursor needs to be transformed a solid-phase material. Chemical or thermal treatments are required for this step. Sol–gel chemistry is generally used to form templated inorganic oxides. In the initial step, hydrolysis of the salt (1) or alkoxide (2) takes place. Acid or base-catalyzed condensation occurs next, which produces oxo- (3) or hydroxo- (4) linkages between metal/metalloid atoms. Colloidal oxide clusters form during this process, producing a sol (a solid colloid dispersed in a liquid). Continued condensation, often at elevated temperatures, leads to the formation of a three dimensional gel.

$$M–X + H_2O \rightarrow M–OH + ROH,\ X = \text{Anion} \quad (22)$$

$$M–OR + H_2O \rightarrow M–OH + ROH \quad (23)$$

$$M–OH + XO–M \rightarrow M–O–M + X–OH,\ X = H \text{ or } R \quad (24)$$

$$M–OH + M–OX \rightarrow M–(OH)–M–OX,\ X = H \text{ or } R \quad (25)$$

Removal of the template is the final and sometimes optional step. Chemical etching is an option for many different templates, including oxide templates. Templates containing SiO_2 are etched away in hot, concentrated alkali hydroxide or hydrofluoric acid (HF). Other metal oxide templates, such as AAO membranes, can be dissolved in strong acids. Suitable organic solvents are often used to dissolve polymeric templates. Unfortunately, it is difficult to remove all residual template material via etching, and several cycles of etching may need to be performed. One must also make sure that the etching chemical does not dissolve the porous hard templated material. Plasma can also be employed to etch out polymeric templates. A further advantage of this is that residual organic groups can be removed, and

infiltrated nanoparticles can be sintered together into a cohesive network. With polymeric templates, a common option for this final step is thermal treatment in an O_2-containing environment (calcination). This approach is quite effective at removing the template; however, appropriate temperature ramps should be used to avoid localized heating that can disrupts the structure during combustion. The treatment increases the degree of condensation for the templated material and also helps to remove residual solvent from the structure. Proper control of the temperature, heating rate and hold times are critical. Excessive temperatures or prolonged thermal treatment can cause undesired solid-state reactions, sintering, and crystalline growth, leading to densification of the structure and closure of pores (if the template is already removed) [22].

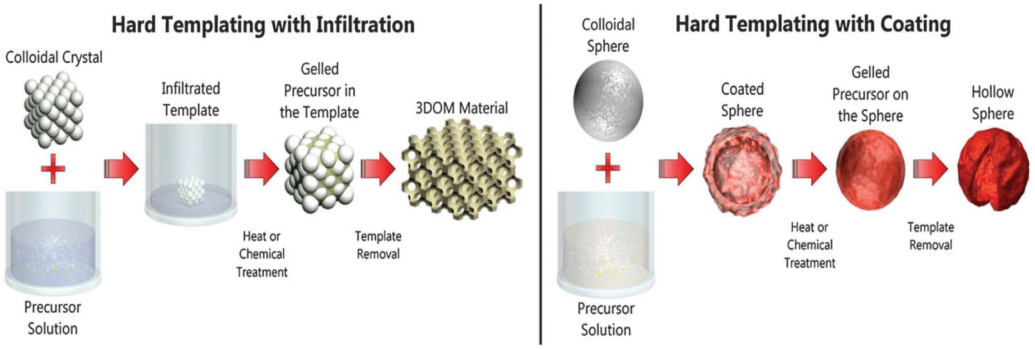

Fig. 2-9. Schemes detailing the hard templating process: hard templating conducted using an infiltration process (left), hard templating conducted via a coating process (right) [21].

2.4.4.2. Soft template

The self-assembly that occurs during soft templating is a remarkable phenomena that involves the structuring of surfactant, precursor, and solvent molecules [21]. Figure 2-10 shows the schemes detailing the soft templating process, the sequence of steps in evaporation-induced self-assembly. Understanding the processes that govern self-assembly may seem daunting, but by understanding three interrelated topics, a solid foundation in soft templating can be gained. The most important part of soft templating is ensuring that micelle and a liquid crystalline phase develop. Two conditions have to be met before micelles can form in any solution. The surfactant concentration can then be increased to a narrow concentration range at which micelles spontaneously form. This is the critical micelle concentration (cmc); the second condition mentioned above. After reaching the cmc, any added surfactant is incorporated into micelles. Once micelles form in solution, their shape dictates what liquid crystalline phases can form. The shape of a micelle depends on the structure of the surfactant molecule.

Adding a precursor to a surfactant-containing solution can cause fairly substantial changes to the self-assembly process that leads to micelle/liquid crystal formation. These changes are a result of the new interactions between the precursor, surfactant, and solvent. Flexibility in synthesis conditions, mesopore size, and precursor compounds are possible in soft templating by changing the surfactant. Fortunately, there are many surfactants that have been synthesized for their utility in consumer and industrial products. Amphiphilic molecules have many roles to

play in commercial products, such as detergents for cleaning, emulsifiers (including those used in latex paints), and wetting agents. While one may not be able to choose a soft template by reading the ingredients of a shampoo bottle, the rich chemistry of surfactant molecules is ready to be used in conjunction with inorganic and organic precursors.

Three major classes of surfactant molecules can be harnessed for soft templating: cationic, anionic, and non-ionic surfactants. These surfactants are named because of the charge the head group does or does not carry in neutral pH solution. Cationic surfactants are comprised of at least one amine functional group that serves as a hydrophilic head group and at least one hydrophobic tail. A greater diversity of head groups is available for anionic surfactants, including sulfates, sulfonates, carboxylates and phosphates (which are attached to a hydrophobic tail). In soft templating, ionic surfactants typically interact with precursors via electrostatic interactions, including interactions with intervening ions. The structure of non-ionic surfactants varies widely from Brij surfactants, which contain a linear alkyl chain connected to a hydrophilic polyethylene oxide (–CH_2–CH_2–O–, PEO) chain to block copolymeric surfactants. Tri-block polyethylene oxide -block-polypropylene oxide–block-polyethylene oxide (PEO_x–PPO_y–PEO_x) surfactants, known as Pluronics are commonly used. In water, the PPO block is sufficiently hydrophobic relative to the PEO block, allowing for micelle formation. Self-assembly processes with non-ionic surfactants are primarily mediated by Van der Waals interactions and hydrogen bonding [22].

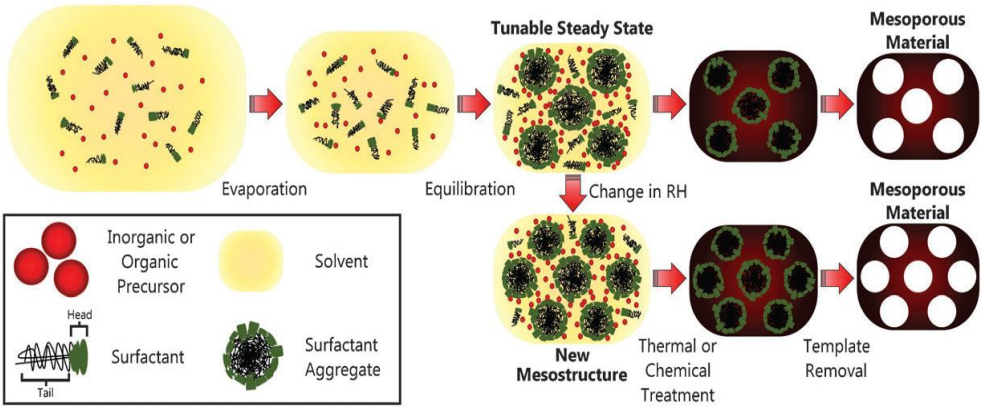

Fig. 2-10. Schemes detailing the soft templating process, the sequence of steps in evaporation-induced self-assembly [21].

2.4.5. Sonochemistry

Ultrasound occurs at a frequency above 16 kHz, higher than the audible frequency of the human ear, and is typically associated with the frequency range of 20 kHz to 500 MHz [109]. The frequency level is inversely proportional to the power output. Sonochemistry is the use of ultrasound to enhance or alter chemical reactions. Sonochemistry in the true sense of the term occurs when ultrasound induces “true” chemical effects on the reaction system, such as forming free radicals which accelerate the reaction [110]. However, ultrasound may have other mechanical effects on the reaction, such as increasing the surface area between the reactants, accelerating dissolution, and/or renewing the surface of a solid reactant or catalyst. Much of the pioneering work in the field has been done by chemists and physicists who have found that the chemical, and some mechanical, effects of ultrasound are a result of the implosive collapse of cavitation bubbles, as shown in Figure 2-11. Cavitation is a process in which mechanical activation destroys the attractive forces of molecules in the liquid phase. Applying ultrasound, compression of the liquid is followed by rarefaction (expansion), in which a sudden pressure drop forms small, oscillating bubbles of gaseous substances. These bubbles expand with each cycle of the applied ultrasonic energy until they reach an unstable size; they can then collide and/or violently collapse. The applied energies in this case can be several hundred times higher. Laboratory equipment uses frequencies between 20 kHz and 40 kHz, but cavitation can be generated well above these frequencies and recent research uses a much broader range [111].

There are two types of effects mediated by ultrasound: chemical and physical. When the quantity of bubbles is low - using standard laboratory equipment - it is mainly physical rate acceleration that plays a role. For example, a specific effect is the asymmetric collapses near a solid surface, which forms microjets. This effect is the reason why ultrasound is very effective in cleaning, and is also responsible for rate acceleration in multiphasic reactions, since surface cleaning and erosion lead to improved mass transport. Ultrasound has proven to be a very useful tool in enhancing the reaction rates in a variety of reacting systems. It has successfully increased the conversion, improved the yield, changed the reaction pathway, initiated the reaction in biological, chemical, and electrochemical systems. This non-classical method of rate enhancement, a field termed sonochemistry, is becoming a widely used laboratory technique. In addition, research is continually underway to make it a feasible option in the ongoing effort to intensify large-scale processes [110].

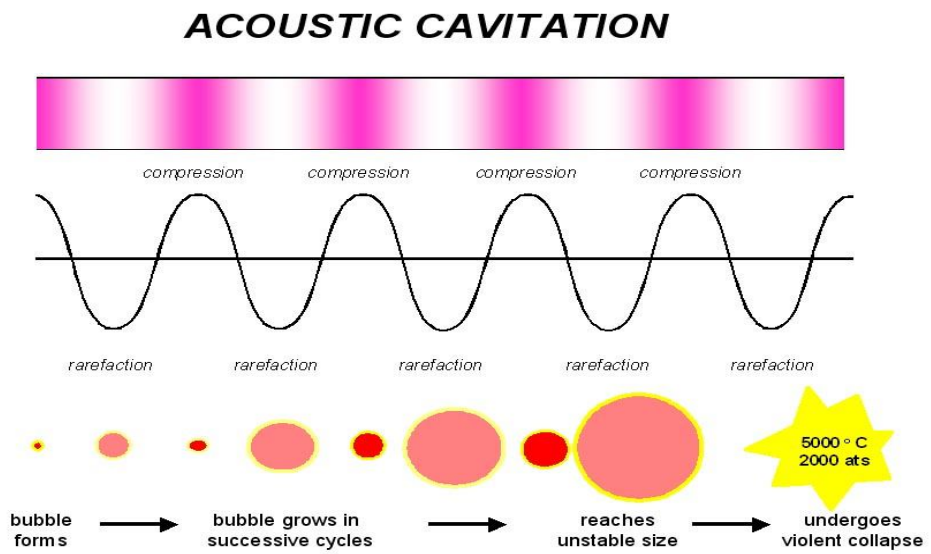

Fig. 2-11. Ultrasound mechanism in bubble cavitation [109].

2.4.6. Microwave-assisted synthesis

Microwave is electromagnetic radiation, whose wavelengths lie in the range of 1 mm to 1 m (frequency range of 0.3 to 300 GHz). A large part of the microwave spectrum is used for communication purposes and only narrow frequency windows centered at 900 MHz and 2.45 GHz are allowed for microwave heating purposes. As is well-known, microwaves are produced by magnetrons, which are principally thermionic diodes with heated cathodes acting as sources of electrons. From the magnetrons the microwaves are generally directed toward a target (placed in so-called microwave cavities) with the use of micro-waveguides [112]. These guides are usually made of sheet metal, and the intensity distribution within the waveguides is homogenized by the use of mode stirrers.

Since the first reports in 1986, the use of microwave ovens became an indispensable tool in modern synthetic chemistry, including inorganic synthesis. In particular, the synthesis of nanoparticles and nanostructures, whose growth is highly sensitive to the reaction conditions, could benefit from the efficient and controlled heating as provided by microwave irradiation. A variety of materials such as carbides, nitrides, complex oxides, silicides, zeolites, apatite, etc. have been synthesized using microwaves. Microwave-assisted synthesis is generally much faster, cleaner, energy efficient and more economical than the conventional methods. The microwave heating does not only reduce the chemical reaction times by several orders of magnitude, but also suppresses side reactions, and thus improves the yield and reproducibility of a specific synthesis protocol. All these

features represent important parameters that have to be considered during the development of ‘‘greener’’ synthesis methodologies, and therefore it can be expected that the microwave technique will also play a fundamental role in a future environmentally friendlier ‘‘synthetic nanotechnology”. Accordingly, the main question addressed is how liquid-phase synthesis of inorganic nanomaterials can efficiently take advantage of the unique features of microwave chemistry.

The energy transfer from microwaves to the material is believed to occur either through resonance or relaxation, which results in rapid heating. It is well-known that the interaction of dielectric materials with microwaves leads to what is generally described as dielectric heating. An understanding of the microwave interaction with materials has been based on concepts of the resonance absorption due to rotational excitation in the alignment of the dipoles (Fig. 2-12a) and of ions in dielectric heating (Fig. 2-12b). Due to the fact that the electromagnetic radiation produces an oscillating field, the dipoles or ions continuously attempt to realign themselves in the electric field. Depending on the time scales of the orientation and disorientation phenomena relative to the frequency of the irradiation, different amounts of heat are produced through molecular friction and dielectric loss.

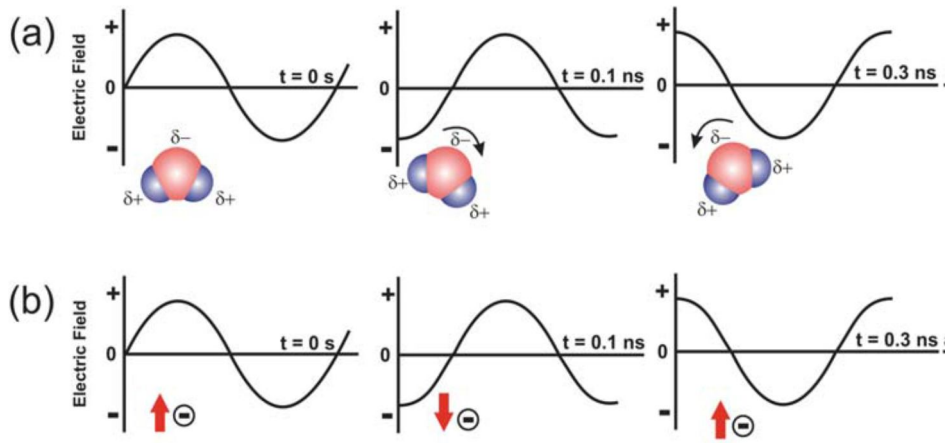

Fig. 2-12. Two main heating mechanisms under microwave irradiation: (a) dipolar polarization; (b) ionic conduction mechanism [112].

3. Experimental

3.1. Fabrication of RuO_2-based electrodes

3.1.1. Substrate pretreatment

The insoluble anodes consisting of a RuO_2-based catalytic layer formed on titanium substrates were prepared in this study. Ultrapure water was obtained by a Millipore purification system (Barnstead NANO Pure, USA). Titanium foils (dimensional 30 x 20 x 0.25 mm, purity 99.7%, Aldrich-Sigma) were used as the substrate materials, of which the contaminants were removed by emery paper, degreased in acetone and then etched in boiling concentrate hydrochloric acid at 86℃ in 1 h to produce gray surface with uniform roughness. Afterwards, the titanium substrates were dried and freshly coated with precursor solutions. All the other chemicals were purchased from Sigma-Aldrich with reagent grade and used without further purification.

3.1.2. Thermal decomposition of RuO_2 electrodes

The coating layers of the metal oxides were prepared with precursor solutions containing 50 μL of 0.2 M $RuCl_3$, $Ru(NO)(NO_3)_3$, or $Ru(AcAc)_3$ (Ruthenium acetylacetonate) dissolved in HCl 1:1 (v:v), ethanol, or iso-propanol as the solvent. The precursor solutions were withdrawn and coated on the pretreated Ti substrate with the spreading method (controlled by pipetting) in order to obtain similar molecules of RuO_2 metal oxides for a fair comparison. Then, the electrodes were annealed at 100°C within 10 min to dry the solvents, and then sintered at 450°C for the predetermined times (1, 2, and 3 h) to allow for the complete decomposition of the precursors and the formation of the metal oxides. The sintering temperature was chosen based on the previous studies which showed the highest electro-catalytic activities [113, 114]. The amount of RuO_2 catalyst loadings on these anodes was intended to be similar at 0.22 ± 0.01 mg/cm^2. Unless specified, the standard condition chosen to fabricate the RuO_2 electrodes was as follow: HCl as solvent, $RuCl_3$ as the precursor, and 1 h calcination time. The back side of the electrode was covered with epoxy to prevent its exposure to the electrolytes. Table 3-1 shows all the experimental details for fabricating the various RuO_2 electrodes used in this study.

Table 3-1. The experimental details for fabricating various RuO_2 electrodes.

Sample ID	**Solvent**	**Precursor**	**Calcination time (h)**
No. 1 (Standard: HCl, $RuCl_3$, 1 h)	HCl	$RuCl_3$	1
No. 2 (Iso-propanol)	Iso-propanol	$RuCl_3$	1
No. 3 (Ethanol)	Ethanol	$RuCl_3$	1
No. 4 ($Ru(NO)(NO_3)_3$)	HCl	$Ru(NO)(NO_3)_3$	1
No. 5 ($Ru(AcAc)_3$)	HCl	$Ru(AcAc)_3$	1
No. 6 (2 h)	HCl	$RuCl_3$	2
No. 7 (3 h)	HCl	$RuCl_3$	3

3.1.3. Nanorod and nanosheet RuO_2 electrodes

Three difference methods were carried out for preparing the nanorod, nanosheet and conventional nanograin RuO_2 electrodes [115, 116]. The nanorod structure was synthesized by using sodium dodecyl sulfate as a template. Ruthenium chloride, sodium dodecyl sulfate, urea, and water were mixed at a molar ratio of 1:2:10:200 and stirred at 40°C for 2 h to obtain a homogeneously mixed solution. Urea was used to raise gradually the pH value of the reaction mixture because on heating at above 60°C urea is hydrolyzed to release ammonia and then in the quiescent state the precipitation occurred. After a reaction time of 10 h, the resulting mixture was immediately cooled to room temperature to prevent further hydrolysis of urea. With nanograin type, 0.1 M $RuCl_3$ dissolved in 20 mL de-ionized water was taken in a two neck flat bottom flask stirred with magnetic stirrer and 20 mL of 0.1 M NaOH was added drop wise in a course of 3 h. For achieving nanosheet structures, about 0.4 g polyethylene glycol (dissolved in 20 mL H_2O) was added extra with the same concentrations of the reactants used in the nanograin experiment (0.1 M $RuCl_3$ + 0.1 M NaOH + 0.4 g polyethylene glycol). The temperature of the solution was maintained at 75°C for the entire reactions. At the end of each reaction, a black precipitate was formed. After discarding the supernatant, the precipitates were centrifuged, washed many times with de-ionized water in order to remove the unreacted chemicals and then dried at 80°C within 5 h, respectively. Weight 3 mg of sol $Ru(OH)_x$, dissolved in isopropanol and then coated on the pretreated Ti

substrates. Next, the electrodes were sintered at 450℃ for 1 h to allow hydrous removal and formation of the metal oxides [113]. One side of the electrode was covered with epoxy to prevent the exposure of the electrolytes.

3.1.4. Three dimensional macroporous RuO_2-TiO_2 electrodes

The titanium coated macroporous RuO_2-TiO_2 electrodes were prepared using the thermal decomposition method with several sizes of polystyrene (PS) microspheres (0.1 µm, 0.46 µm and 1.1 µm in diameter) to examine their effect on the macroporous structure including pore sizes. $RuCl_3$ 42 mg, $TiCl_3$ 72.5 mg (proportion of Ru:Ti was 30:70, % mol/mol), 0.1 mL of hydrogen peroxide solution (30 wt %), and 0.1 g of PS microspheres were dissolved in a solution of 3 mL of ethanol. As a reference, coating without templated macroporosity (nontemplated) was prepared by dissolving Ru:Ti (30:70) as above but without PS microspheres present. The precursor solution was sonicated for 30 min before spreading onto the titanium substrates. Next, the electrodes were sintered at 450^{o}C for 1 h to allow for hydrous removal and formation of the metal oxides [113]. One side of the electrode was covered with epoxy to prevent the exposure of the electrolytes.

3.1.5. Sonoelectrodeposition of RuO_2 electrodes

RuO_2 nanoparticles were deposited onto commercial titanium substrates using an electrochemical deposition step followed by calcination [106-108]. Ti substrate was served as the working electrode (cathode). A Pt electrode (Samsung Chemicals, South Korea) was used as the counter electrode (anode). The electrochemical bath was prepared by dissolving 5 mM $RuCl_3$ and 20 mM $NaNO_3$ as supporting electrolyte (99.9 %, Aldrich) in deionized water at room temperature (25^oC). Cathodic deposition was performed at constant current density 50 mA cm^{-2} controlled by a power supply (Unicorn 1501, South Korea), under sonication at 20 kHz (Branson 1510, USA) or mechanical stirring at 200 rpm with difference deposition time. Next, the electrodes were calcined at 450◦C for 1 h to allow hydrous removal and formation of the metal oxides. Back side of the electrode was covered with epoxy to prevent its exposure to the electrolytes.

3.1.6. Microwave-assisted sol-gel synthesis of RuO_2-TiO_2 electrodes

A solution containing 40 mM $RuCl_3$, 60 mM $TiCl_3$, 0.2 M $(NH_4)_2CO_3$, 0.1 M H_2O_2 (Sigma–Aldrich, 99%) were employed as the precursor. The metal ratio Ru:Ti (4:6 mol/mol) was chosen depend on the optimization of some previous reports to obtain highest electrocatalytic and stability performances of RuO_2-TiO_2 electrodes. The pH of the mixture was maintained between 9 and 10. The mixture was treated under microwave irradiation (oven MARS 5, CEM Corporation, US) with the energy intensities of 400 W/g and 800 W/g for 20 minutes at the temperature 80°C [112]. For comparison, conventional RuO_2-TiO_2 electrode was prepared using classical route by heating the mixture to 80°C for 6 h, with a temperature controlled hot plate. The synthesized metal oxide nanoparticles were separated from solution by centrifugation under 10,000 rpm. The products were then washed with deionized water until free of chloride and then dried at 80°C within 5 h. Weight 3 mg of sol mixtures RuO_2-TiO_2, dissolved in isopropanol and then coated on the pretreated Ti substrates. Next, the electrodes were sintered at 450℃ for 1 h to allow hydrous removal and formation of the metal oxides [113]. Back side of the electrode was covered with epoxy to prevent its exposure to the electrolytes.

3.2. Surface analysis

3.2.1. Thermal gravimetric analysis (TGA)

A TGA instrument (Perkin-Elmer 7 - USA) was used to monitor the sample weight loss of the precursor solutions and record the temperature at which the metal oxides formed. A derivative weight loss curve can identify the point where weight loss is most prominent. The procedure for the thermo-analytical experiments was as follow: sample is placed in a small electrically heated oven with a thermocouple for accurate measurement of the temperature. The atmosphere was supplied with an inert gas to prevent oxidation or other undesired reactions. The precursor was evaporated at 100^{o}C and then transferred to the TGA cell. The temperature was raised to 700^{o}C using air as carrier gas. The sample was heated at the rate of 10^{o}C min^{-1}. The resultant data was finally analyzed with Pyris Version 4.01 software.

3.2.2. Field emission scanning electron microscopy (FE-SEM)

Field emission scanning electron microscopy (FE-SEM, JSM-6701F, JEOL Co., Japan) images a sample with a high energy beam of electrons in a raster scan pattern was used. The electron interacts with the sample that produces signal that contains information about the sample's surface topography, composition and other properties such as electrical conductivity. Secondary electrons (generated by inelastic scattering during the energy exchange between the electron beam and the sample) are the common type to produce the SEM signals by the interactions between the electron beam and the atoms at or near the sample surface. The size of the interaction volume depends on the electron energy, the atomic number of the specimen and the density of the specimen. The SEM images in this study were taken at a working distance of 7 mm and an accelerating voltage of 10 kV. The samples were positioned horizontally [116].

3.2.3. Energy dispersive X-ray spectroscopy (EDX or EDS)

EDX coupled with SEM analysis is used to obtain the qualitative element analysis from the emission of characteristic X-rays from a specimen when a material is bombarded with electrons in an electron beam instrument. When the sample is bombarded by the electron beam of the SEM, electrons are ejected from the atoms comprising the sample surface. A resulting electron vacancy is then filled by an electron from the higher shell, and an X-ray is emitted to balance the energy difference between the two electrons. The EDX detector counts the emitted X-rays, measures their energy and quantitative determinations of the elements.

3.2.4. Transmission electron microscopy (TEM)

TEM is an imaging technique with a significantly higher resolution than light microscopes owning to the small de Broglie wavelength of electrons. A beam of electrons is transmitted through an ultra-thin solid sample, interacting with the specimen. The transmitted beam containing information about the electron density, phase, and periodicity is used to form an image. In this study, crystal's imaging were examined using a transmission electron microscope (TEM, JEOL 2000EXII, JEOL Co., Japan). The TEM samples were prepared by scraping off the coating using a sharp knife and collecting the powder of RuO_2-based nanoparticles, then dispersing the powders in isopropyl alcohol. A few drops of these solutions were deposited on carbon film-coated Cu grids and analyzed with transmission electron microscope. A beam of electrons with accelerating voltage was 110 kV is transmitted through an ultra-thin solid sample, interacting with the specimen. The vacuum system was 10 Pa, tilting angles were $\pm 25^o$ [117].

3.2.5. High resolution X-ray diffraction (HR-XRD)

The three-dimensional atomic arrangement in a crystal is deduced from the directions and intensities of the diffracted X-ray beams. Crystalline material can be considered as an infinite recurrence of parallel atomic planes with an inter-planar distance d. When a beam of monochromatic X-rays is incident on the atoms in a crystal, the wavelets scattered by the atoms in each plane combine to form a reflected wave. The interference patterns of the scattered radiation are recorded by a detector. In order to study the crystallinity of RuO_2-based electrodes, high resolution X-ray diffraction pattern was obtained with the grazing incidence technique on a D8 Discover (Bruker-AXS, Germany) diffractometer (CuKα, λ = 1.5406 Å). A scintillation counter detector scanned between 25° and 100° in 2θ with an angle of incidence was 0.5°, the working distance was 12 mm and the accelerating voltage was 25 kV [118]. The volume-weighted crystallite size (D, the mean size of the ordered domains or the mean dimension of the coherently diffracting domains) can be estimated from the main diffraction peak by using Scherrer's equation [117]:

$$D = \frac{0.9\lambda}{\beta \cdot \cos\theta}$$

where λ is the X-ray wavelength, β is the full width at the half-maximum intensity in radians, and θ is the Bragg angle.

3.3. Electrochemical measurement

The electrochemical characterizations of the metal oxide electrodes were carried out using cyclic voltammetry (CV), linear sweep voltammetry (LSV) measurements [10]. The experiments were performed at room temperature in a conventional single compartment cell with three electrodes using a computer-controlled potentiostat (PARSTAT 2273A, Princeton Applied Research, USA). The volume of electrolyte solution in the cell was 150 ml. RuO_2-based was used as the working electrode (anode), Pt (Samsung Chemicals, Korea) as the counter electrode (cathode), and Ag/AgCl (in saturated KCl) as the reference electrode.

3.3.1. Cyclic voltammetry (CV) and active surface area

CV is used for obtaining qualitative information about the electrochemical reactions of an electrode surface, such as the redox processes, heterogeneous electron - transfer reactions, phase formations or adsorption processes. In this study, CV was measured using 0.5 M H_2SO_4 as electrolyte. The range of scan rate was 5-320 mV/s. The CV curves were recorded in a range of potential between 0-1 V vs Ag/AgCl. The pseusdo-capacitive reaction which consists of coupled redox transitions involving proton exchange with the solution at a broad reversible peak around 0.6 V vs. Ag/AgCl can be described as follows [15]:

$$RuO_x(OH)_y + zH+ + ze- \rightarrow RuO_{x-z}(OH)_{y+z} \quad (26)$$

The voltammetric charge q obtained by integration of the voltammetric curves in the potential range with the Faradaic reaction is a measurement for the number of electrochemically active Ru sites, which are accessible by the electrolyte:

$$q_a = \frac{S}{\nu}$$

where S (mA V cm^{-2}) is the integrated area of the anodic branch, and υ, (mV s^{-1}) is the potential scan rate.

Total or outer active surface area can be obtained by varying the scan rate of the applied potential in CV. For example, total active surface including both the inner and outer active surfaces can be obtained at a low scan rate. On the other hand, the outer active surface can be obtained at a high scan rate [15]. This is explained as follows: at a low scan rate, the total active surface including both the inner and

outer active surfaces can exchange protons with the solution, while at a high scan rate, the inner active surface fails to participate in this reaction. Thus, the total or outer active surface area can be estimated by plotting and extrapolating the voltammetric charge according to an infinitely low (0) and high (∞) scan rate with the following equations (Eqs. (1) - (3)) [15]:

$$q_{total} = q_{inner} + q_{outer} \qquad \text{Eq. (1)}$$

$$q(v) = q_{outer} + A(1/\sqrt{v}) \qquad \text{Eq. (2)}$$

$$1/q(v) = 1/q_{total} + B\sqrt{v} \qquad \text{Eq. (3)}$$

, where: v is the scan rate; $q(v)$ is the voltammetric charge at the scan rate v; q_{total} is the voltammetric charge obtained at an infinitely low (0) scan rate; q_{outer} is the voltammetric charge obtained at a high (∞) scan rate; q_{inner} is related to the voltammetric charge of the inner surfaces, and A, B are constants.

3.3.2. Linear sweep voltammetry (LSV)

LSV is a voltammetric method where the current at a working electrode is measured while the potential between the working electrode and a reference electrode is swept linearly in time. Oxidation or reduction of species is registered as a peak in the current signal at the potential at which the species begins to be oxidized or reduced. Prior to the polarization measurement, the electrode should be activated firstly. LSV measurements were conducted in the electrolyte containing 5 M NaCl + 0.01 M HCl (pH = 2), which is a favored condition for chlorine evolution over oxygen evolution [14]. The LSV curves were recorded in a range of potential between 0-2 V vs. Ag/AgCl and the scan rate was 10 mV/s.

3.3.3. Total active chlorine concentration (DPD)

In this study, chlorine is evolved from electrolyte contains NaCl by electrolysis in two electrode system. As electrochemical reaction terminated, the chlorine was detected immediately from the reactor. The concentration of total active chlorine dissolved in the solution of 0.1 M NaCl, pH = 2 as electrolyte was determined by the DPD (N, N-diethyl-p-phenylenediamine) colorimetric method. In this method, DPD is oxidized to form a purple product and chlorine concentration was analyzed immediately using a spectrophotometer (DR/2010, HACH Co., Loveland, US) at 530 nm [10]. The chlorine concentrations were replicated three times and the average values were obtained.

3.3.4. Accelerated stability test (AST)

For any electrode, life is equally important to its degradation efficiency. Only long service life of electrode makes the electrochemical process economic, but the problem is testing service life of any electrode in real conditions. Testing of an electrode under normal condition may takes years and years. To reduce the testing time from years to months or hours, AST were used to assess electrode stability. The stability of prepared anodes in this study was examined by AST using two electrode cell systems with DC power [94, 96], with a current density considerably higher and an electrolyte solution more dilute than those usually applied in industrial electrochemical conditions. It provided information about the electrode stability and lifetime (via the electrode potential - time dependence at constant current density). The experiments were performed galvanostatically at the current density of 1 A cm^{-2} in a solution of 0.5 M NaCl, pH = 2 at room temperature ($25^{o}C$). The anode potential was recorded during the electrolysis. A suddenly increase of the potential implies that the anode can no longer be used in practice (the end of service life).

4. Results and discussion

4.1. The effect on the chlorine evolution efficiencies of RuO_2 electrodes depending upon preparation parameters in thermal decomposition

4.1.1. Background

Dimensionally Stable Anodes (DSA) for not only oxygen but also chlorine evolutions has been widely used for over 40 years in the electrolysis industry due to their versatile electro-catalytic properties and stability [1, 2]. DSA electrodes usually consist of a Ti support coated with active noble metal oxides or their mixtures with other non-noble metal oxides on the surfaces [3-5]. Ruthenium dioxide (RuO_2) is a technologically good and important electrode in chlor-alkali electrolysis because of its unique characteristics such as high thermal and chemical stability, low resistivity, and low over-potential with oxygen and chlorine evolutions [6-12]. Recently, the RuO_2 electrode has been reported to be superior to the IrO_2 electrode in terms of electro-catalytic properties for chlorine evolution because the RuO_2 electrode has a lower oxygen/metal atomic fraction, a more positive surface charge, lower binding energy, lower resistance, and more hydrophilic properties than that of the IrO_2 electrode [119]. Various methods have been used to fabricate high electro-catalytic RuO_2 electrodes for chlorine evolution such as sputtering [23-25], thermal decomposition [14], Adams fusion [31], sol-gel

[29], and electro-deposition [100-103]. Among them, Ti/RuO_2 electrodes have been mainly developed by the thermal decomposition method due to their convenient fabricating, cost effectiveness, high stability from the strong adhesion between the noble metal oxides and the substrate surfaces.

The thermal decomposition methods conducted with various preparation parameters such as types of solvents, precursors, and calcination times have led to the development of the RuO_2 electrode for the chlorine evolution. The enhanced electro-catalytic activity of RuO_2 electrodes is attributed to the increased outer surface area, which is an easily accessible region for the electrolyte, and has become a significant factor in chlorine evolution [14-18]. The activity of the RuO_2 nanocrystals towards the chlorine evolution is insensitive to the particle size/shape, and chlorine evolution reaction proceeds mainly on crystal faces [62]. Nevertheless, it has not fully been investigated on how these fabrication parameters affect to the chlorine evolution efficiency in the RuO_2 electrode. Thus, this study investigated the effect on the chlorine evolution efficiency in RuO_2 electrodes depending upon the three major preparation parameters. The total or outer voltammetric charge was analyzed by cyclic voltammetry (CV) and the microstructures of the RuO_2 electrode surface were examined by scanning electron microscopy (SEM). The electro-catalytic performance of the RuO_2 electrodes was evaluated with linear sweep voltammetry (LSV) and aqueous chlorine measurements.

4.1.2. Chlorine evolution under varying fabrication conditions

Figure 4-1 shows the chlorine evolution expressed as chlorine concentration (a) with the various RuO_2 electrodes fabricated with the three major parameters (Table 3-1) and the linear sweep voltammetry (LSV) (b) for the change in solvents: No. 1 (Standard: HCl, $RuCl_3$, 1 h), No. 2 (Iso-propanol), and No. 3 (Ethanol), for the change in precursors: No. 4 ($Ru(NO)(NO_3)_3$), and No. 5 ($Ru(AcAc)_3$), and for the change in calcination times: No. 6 (2 h), and No. 7 (3 h). As shown in Fig. 4-1 (a), the chlorine evolutions after 10 minutes for the RuO_2 electrodes varied from 85 mg/L (No. 1, Standard) to 115 mg/L (No. 3, Ethanol), depending upon the fabrication conditions. The highest chlorine concentrations for the three major parameters was obtained when the electrode was fabricated with ethanol as the solvent, $Ru(AcAc)_3$ as the precursor, and 3 h as the calcination time. The chorine concentration increased to 35% when the solvent was changed from HCl to ethanol, to 13% when the precursor was changed from $RuCl_3$ to $Ru(AcAc)_3$ and to 22% when the calcination time was increased from 1 h to 3 h, respectively. The chlorine concentration was the highest for ethanol followed by isopropanol and then HCl for the solvents, $Ru(AcAc)_3$ followed by $Ru(NO)(NO_3)_3$ and then $RuCl_3$ for the respect to precursors, and 3 h followed by 2 h and then 1 h for the calcination times. At this chlorine measurement condition, the oxygen evolution is suppressed by the increasing of oxygen overpotential and selectivity for chlorine evolution [120, 121]. Differences in current densities from the different fabrication conditions were

also observed in the LSV measurements. Figure 4-1 (b) shows the current density, which indicates the electro-catalytic activity of the RuO_2 electrode, from the made by different solvents in the order of ethanol > isopropanol > HCl, the different precursors in the order of $Ru(AcAc)_3$ > $Ru(NO)(NO_3)_3$ > $RuCl_3$, and the different calcinations times in the order of 3 h > 2 h > 1 h. The results were in good agreement with results for the chlorine concentrations shown in Figure 4-1 (a). There is a good linear relationship between the chlorine evolution and current density (R^2 = 0.92) (Figure S1 in Appendix). Reportedly, the amount of charge that flows is primarily related to the chlorine concentration, showing that a larger current density means a larger chlorine evolution [119]. These results suggest the different fabrication parameters induce different chlorine evolution efficiencies and their corresponding LSV in the RuO_2 electrodes.

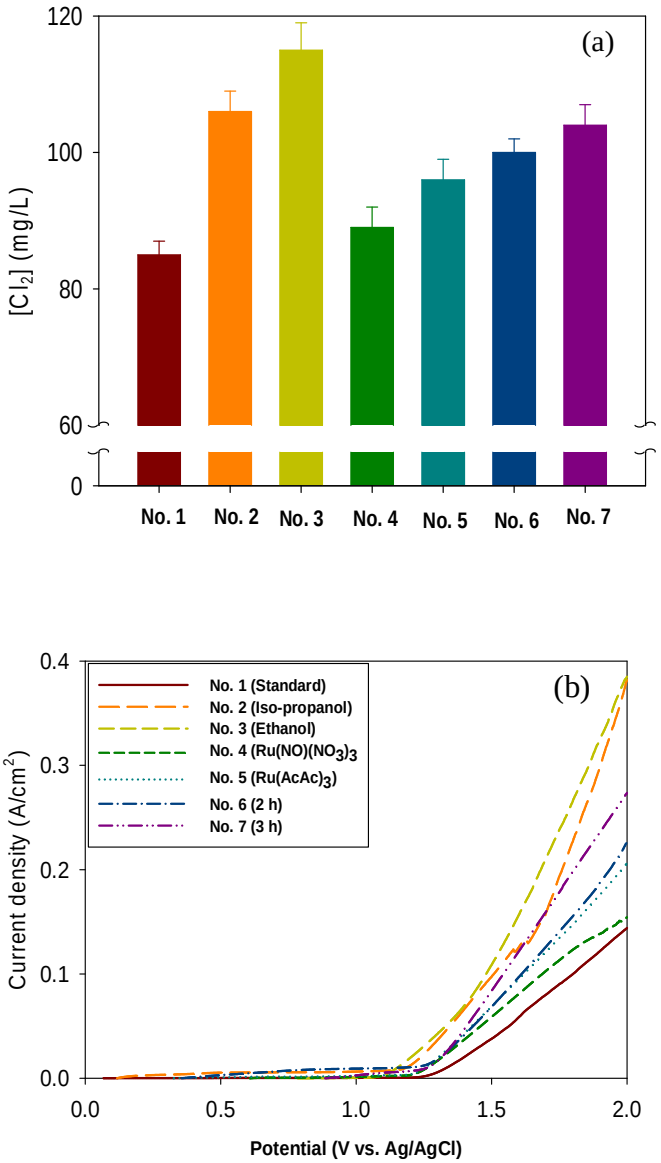

Fig. 4-1. The total chlorine evolution expressed as chlorine concentration (a) and the linear sweep voltammetry (LSV) (b) of the various RuO_2 electrodes fabricated under three different conditions for the solvents: No. 1 (Standard : HCl, $RuCl_3$, 1 h),

No. 2 (Iso-propanol), and No. 3 (Ethanol); for the precursors: No. 4 ($Ru(NO)(NO_3)_3$), and No. 5 ($Ru(AcAc)_3$); and for calcination times: No. 6 (2 h), and No. 7 (3 h) (details in Table 1). Electrolysis conditions were as follows : (a) [NaCl] = 0.1 M, pH = 2, I = 16.7 mA/cm^2, t = 10 min; (b) [NaCl] = 5 M, pH = 2.

4.1.3. Relationship between chlorine evolution - outer voltammetric charge

Figure 4-2 shows the relationship between chlorine evolution and the outer voltammetric charges of the RuO_2 electrodes. Chlorine concentrations and voltammetric charges shown in Figure 4-2 are from Figure 4-1 (a) and Figure S2-3 in Appendix, respectively. As shown in Figure 4-2, clearly, the chlorine concentrations increase linearly with the outer voltammetric charges. Active sites for chlorine evolution facilitate the electro-catalytic performance only conditionally in the accessibility of the active sites for effective transport of the electrolyte [16, 17]. Chlorine evolution is a well-known reversible and fast reaction. Thus, the outer surface of the electrode contributes the active sites for chlorine evolution [14-18]. In contrast, the inner surface of the electrode is blocked by the adhered chlorine gas bubbles and becomes partially inactive in chlorine evolution [14, 16-18, 98]. As shown in Figure S4 in Appendix, chlorine evolution does not follow the total voltammetric charge. The highest outer voltammetric charge and chlorine evolution for the three conditions was obtained with an electrode fabricated with ethanol as the solvents, $Ru(AcAc)_3$ as the precursor, and 3 h as the calcination time, and correlating with the chlorine evolution efficiency. These results suggest the outer voltammetric charge significantly affects the chlorine evolution efficiency compared to the total voltammetric charge.

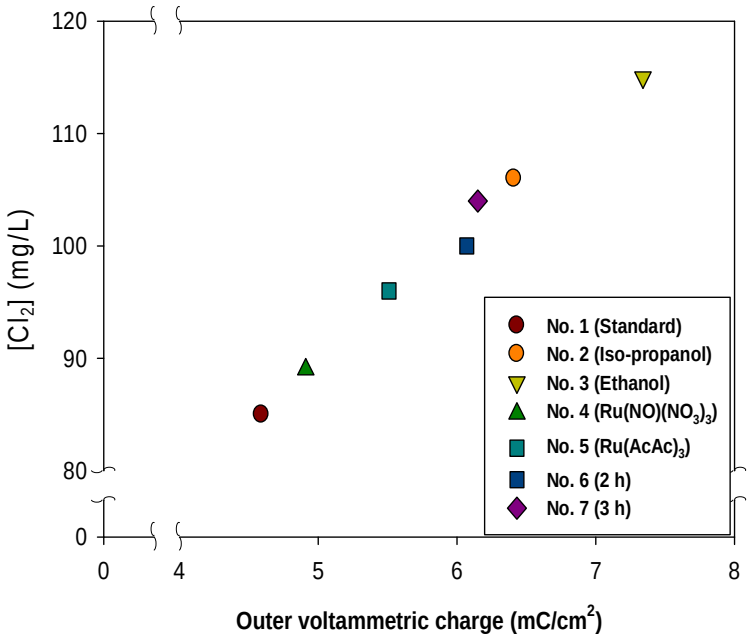

Fig. 4-2. Relationship between outer voltammetric charge and chlorine evolution of the RuO_2 electrodes fabricated under different conditions: No. 1 (Standard: HCl, $RuCl_3$, 1 h), No. 2 (Iso-propanol), No. 3 (Ethanol), No. 4 ($Ru(NO)(NO_3)_3$), No. 5 ($Ru(AcAc)_3$), No. 6 (2 h), and No. 7 (3 h). Refer to Table 3-1 for details on the fabrication conditions.

4.1.4. Morphology

Figure 4-3 shows the SEM images of the RuO_2 electrodes fabricated under the various conditions: (a) No. 1 (Standard: HCl, $RuCl_3$, 1 h), (b) No. 2 (Iso-propanol), (c) No. 3 (Ethanol), (d) No. 4 ($Ru(NO)(NO_3)_3$), (e) No. 5 ($Ru(AcAc)_3$), (f) No. 6 (2 h), and (g) No. 7 (3 h). As shown in Figure 4-3, the morphologies of the RuO_2 electrodes appear to be diverse with the different fabrication conditions. The RuO_2 electrodes exhibited a characteristic surface morphology with a mud-cracked structure which is a typical morphology for electrodes prepared with the thermal decomposition method [4, 5, 14].

It is speculated that these cracks formed during solvent evaporation and precursor decomposition during the thermal treatment. It is clear that No. 2 (Iso-propanol) and No. 3 (Ethanol) have larger cracks and defects (crack size 1.5-2.0 μm) and these samples have a higher chlorine evolution as well as larger outer voltammetric charge (Figure 4-2). This difference in cracks with respect to the solvents can be explained by the different boiling points and surface tensions of the solvents: HCl (103-108^{o}C) > iso-propanol (82.5^{o}C) > ethanol (78^{o}C). In general, organic solvents have a lower boiling points and surface tensions as well, thus, they can evaporate very quickly off the electrode surface, leading to deeper and larger cracks on the electrode surface. In contrast, No. 1 (Standard: HCl, $RuCl_3$, 1 h) and No. 4 ($Ru(NO)(NO_3)_3$) with smaller cracks (crack size 0.5-1.0 μm), had lower chlorine evolution accompanied with a lower outer voltammetric charge (Figure 4-2). One

explanation for these observations is that the increasing number and size of the cracks reduce the bubble coverage on the electrode surfaces, allowing more electrolytes to come into contact with the active surface area of the electrode [17]. The cracks are responsible for the increase in outer surface area [16].

The longer calcination times (No. 1 (1 h), No 6 (2 h), and No. 7 (3 h)) also contributed to increasing the number and size of the cracks. Under thermal conditions, the surface of the electrode is not stable and splits because of tensile stresses. This observation is consistent with previous studies reporting on the effect of different temperatures on electrode surfaces [16, 122]. Figure 4-4 shows the TGA spectra of the RuO_2 electrodes fabricated with different precursors. As shown in Figure 4-4, the TGA spectra of the RuO_2 electrode shows different decomposition temperatures, possibly related to the morphology of the surfaces of the electrodes. For example, No. 4 ($Ru(AcAc)_3$), and No. 5 ($Ru(NO)(NO_3)_3$), which have more cracks on the electrode surfaces (Figure 4-3) have a decomposition temperature of 330^{o}C and 350^{o}C, respectively, while No. 1 (Standard: HCl, $RuCl_3$, 1 h) has the least cracks with a higher decomposition temperature of 450^{o}C.

In addition, the XRD spectra (Figure S5 in Appendix) of RuO_2 electrodes fabricated under different preparation conditions. As a result, precursors reveal the similar diffraction peaks of RuO_2 nanoparticles without the forming of Ru metal by-product. This is implied that the crystal and phase structures of RuO_2 electrodes are analogoues with different precursors.

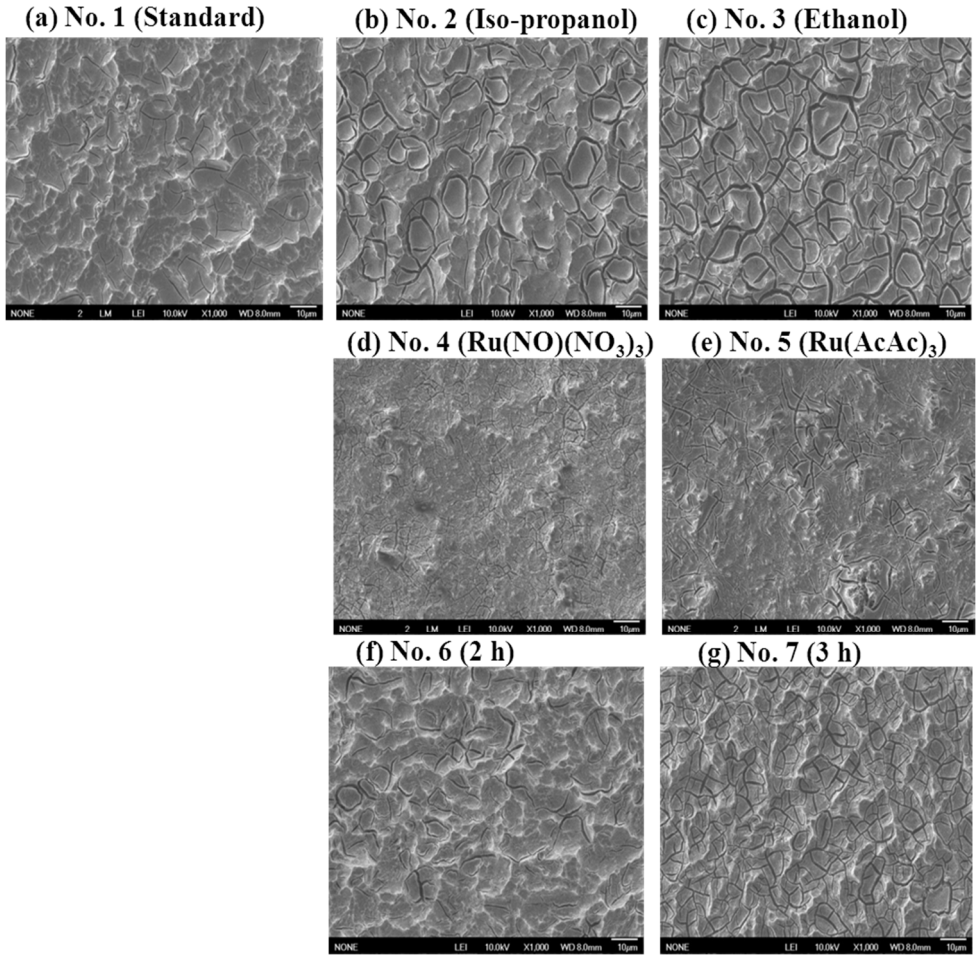

Fig. 4-3. The SEM images of the RuO_2 electrodes fabricated under various conditions: No. 1 (Standard: HCl, $RuCl_3$, 1 h), No. 2 (Iso-propanol), No. 3 (Ethanol), No. 4 ($Ru(NO)(NO_3)_3$), No. 5 ($Ru(AcAc)_3$), No. 6 (2 h), and No. 7 (3 h). Refer to Table 1 for the details on the fabrication conditions.

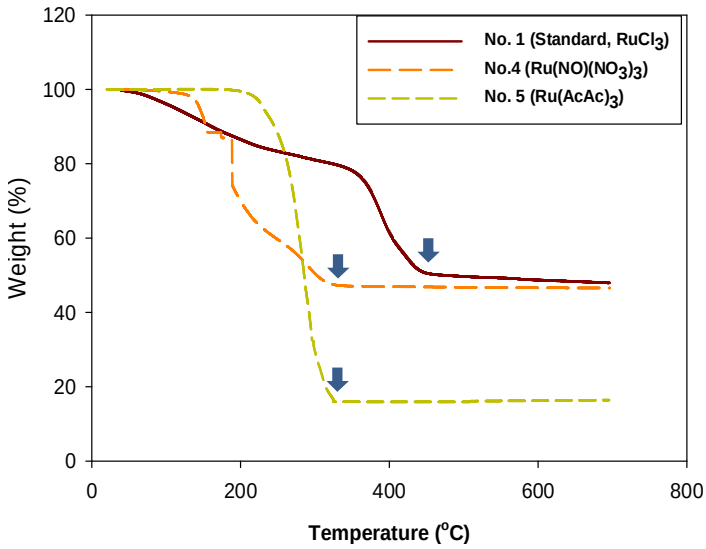

Fig. 4-4. TGA spectra of the RuO_2 electrodes with different precursors: No. 1 (Standard: HCl, $RuCl_3$, 1 h), No. 4 ($Ru(NO)(NO_3)_3$), and No. 5 ($Ru(AcAc)_3$). Refer to Table 1 for details on the fabrication conditions.

4.1.5. Conclusions

In this study, the effect on chlorine evolution was investigated by focusing on the preparation parameters of the RuO_2 electrodes which included solvents, precursors and calcination times using the thermal decomposition method. It was investigated that using ethanol as solvent played the most critical factor for increasing the chlorine evolution efficiency of the RuO_2 electrode. Using $Ru(AcAc)_3$ as precursor and increase the calcination to 3 h are also the good choices for increasing chlorine electrocatalytic activities. It can be explained that the increasing number and size of the cracks on the electrode surfaces or the outer voltammetric charges were caused by the easily evaporated solvents, decomposed precursors and tensile stress under longer thermal treatments. The chlorine evolution efficiency was not significantly related to the total voltammetric charge but the outer voltammetric charge.

4.2. Development templated RuO_2 nanorod and nanosheet electrodes for chlorine evolution reaction

4.2.1. Background

Chlorine is an essential product and widely used in the fields of chemical industry, pharmaceutical, and wastewater treatment [1]. Currently, the most commonly used electrocatalysts for chlorine evolution are so-called Dimensionally Stable Anodes (DSA), which brought a revolution in technical electrochemistry [2]. This type of anodes usually consists of a Ti support coated by noble metal oxide catalysts as RuO_2, IrO_2 or their mixtures with valve metal oxides [3]. RuO_2 possesses excellent electrocatalytic features for chlorine evolution as low overpotential, low cost, enhanced selectivity, mechanical and chemical stability [4]. Roughly 10-15% of the annual production of Ru goes into the fabrication of such DSA-type [5]. Although the electrolytic production of chlorine is a well-established industrial process, it is still necessary to further improve the chlorine electrocatalytic activity of RuO_2 electrodes in order to reduce amount of consumed electrical energy [4-5]. This way provides highly environmentally benign electrical devices to address the problems of climate change, the impending exhaustion of fossils fuels [5]. In spite of remarkable electrocatalytic effects, there are remains a drawback in these catalysts as the nanograins or nanoparticles effortlessly agglomerate under the fabrication or reaction conditions, which leads to low catalytic activity as well as the mass transport limitation [19]. In the recently year,

promising heterogenous nanostructure materials are known as advance materials strongly improved the electrochemical properties and garnered great interest due to their wide range of applications such as solar cell, fuel cell, supercapacitor, catalyst [20, 21]. Especially one and two dimensional nanostructured materials such as nanorods, nanowires, nanobelts or nanosheets morphologies have been shown to exhibit unique properties such as high active surface area, fast mass transfer, charge/discharge process and high stability [22]. Previous studies suggested that attainment nanostructures of RuO_2 nanorod or nanosheet electrodes have been obtained mostly through vacuum sputtering techniques [23-25] and chemical vapor deposition [26-28] in the form of thin films. In these methods, the high temperature (1500°C) vapor-phase processes are expensive and also limited by their low yield. In contrast, the solution phase method which is called as sol-gel can be carried out in soft-environments on a large scale and seems to be promising in fabrication of RuO_2 electrode both high electrocatalytic and stability in chlorine evolution [29, 94, 96]. Contribution of stabilizers such as sodium dodecyl sulfate (SDS) or polyethylene glycol (PEG) in sol-gel process for achieving desired shape is received a lot of attention now, proposed on the basis of surfactant induced growth mechanism of nanomaterial [115, 117, 123-126].

Herein, we report the facile synthesis of RuO_2 nanorod and nanosheet electrodes with structures templated by using PEG and SDS as surfactants assemblies. The properties of the obtained RuO_2 nanorod and nanosheet electrodes are compared with the conventional nanograin electrode for chlorine evolution. The

microstructures of as-prepared electrodes were evaluated using scanning electron microscope (SEM), transmission electron microscopy (TEM), X-Ray diffraction (XRD). The electrochemical properties were examined with cyclic voltammetry (CV), linear sweep voltammetry (LSV), total chlorine concentration (DPD) methods.

4.2.2. Microstructure characteristic

Figure 4-5 shows the SEM (a) and TEM (b) images of the obtained RuO_2 electrodes with difference morphologies: nanorod, nanosheet and conventional nanograin deposited on the Ti substrates. As shown in Figure 4-5 (a), the one dimensional nanorod structure directly grows almost in random direction rather than through epitaxial deposition. The rods seem stable with a single layer and separated with each other. On the other hand, RuO_2 nanosheet electrode consists of hierarchical sheet nanostructures in an assembly two dimensional subunits porous network with high interconnectivity. The nanosheet structure is perpendicular to the substrate and leading to a flower-like projected view with the sheet thickness approximately 10 nm. The formation of pores could be attributed to the release of volatile gas such as H_2O and CO_2 during the heat treatment because of precursor decomposition, in which organic additives were burnt up and left behind porous structures. In contrast, the nanograin electrode is composed of crystal RuO_2 nanoparticles with zero dimensional. The grains are fine, agglomerated and seem in uniform size, which is the characteristic of sol-gel process. Overall, the RuO_2 nanorod and nanosheet electrodes are more open structures and roughness factor in comparison with the nanograin electrode. Clearly, the electrode morphologies are strongly influenced by using difference organic templates. The morphologies of templated RuO_2 nanorod and nanosheet electrodes prepared by the sol-gel method were somewhat difference to that prepared by the reactive sputtering or chemical

vapor deposition methods, which are total perpendicular and align to the substrate surfaces [23-28].

It can be seen from Figure 4-5 (b) displayed the TEM images with difference shape pattern of the obtained RuO_2 nanorod, nanosheet, and nanograin, respectively. The nanorods present a core shape with a length of 80 nm and width of 20-30 nm were observed. The rods are polygonal prisms and continuous with a smooth surface, which may because the effect of thermal treatment at 450^{o}C. Moreover, individual sheets about 40-60 nm length and 40 nm width are formed. The size of the nanosheets is uneven which might because of the growth controlled process due to PEG addition. The total length and width of the RuO_2 nanorod and nanosheets are reveals a good crystallinity. On the other hand, the nanograin composed the aggregated nanoparticles with diameter size of about 20-30 nm are exhibited. Undoubtedly, the organic template precursors play a crucial role in the shape evolution of the RuO_2 nanomaterials. These difference morphologies are expected the different about the electrocatalytic efficiency with chlorine evolution of RuO_2 electrodes.

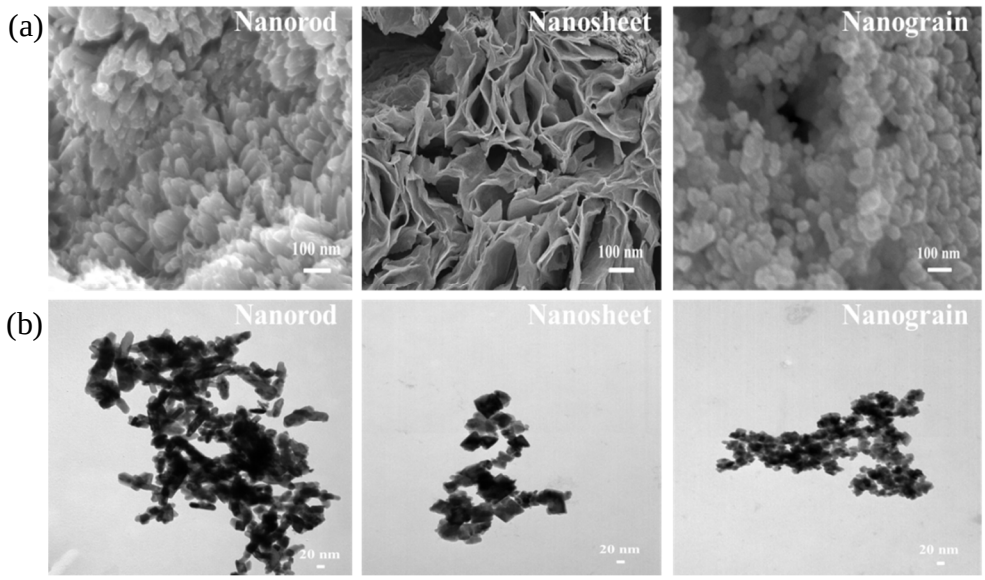

Fig. 4-5. SEM (a) and TEM (b) images of RuO_2 nanorod, nanosheet, and nanograin electrodes.

4.2.3. XRD spectra

Figure 4-6 shows the diffraction patterns of the obtained RuO_2 electrodes with difference morphologies: nanorod and nanosheet and nanograin. There is a little difference about crystal structures of these electrodes. The most pronounce peaks of RuO_2 are easily detected as: 110, 101 planes at 28^o and 35^o in all the electrodes. While the peak of 211 plane is very weak in nanorod electrode and the peak of 310 plane seem not exist in the nanorod and nanosheet electrodes. Nevertheless, all these peaks of RuO_2 were observed in nanograin electrode, which mean that the nanograin electrode is more polycrystallinity. The presence of sharp peaks of RuO_2 indicates the high purity and crystallinity of the as-synthesized RuO_2 nanostructures. The RuO_2 peaks reveal the formation of rutile and solid phase, which is desired in terms of electrode stability. The forming step of RuO_2 metal oxide can be expressed as followed: addition of NaOH or urea with $RuCl_3.xH_2O$ forms the precipitate of $Ru(OH)_3$ at the end of the reaction. $Ru(OH)_3$ is unstable and oxidizes in the presence of air during initial heat treatment (100^oC drying process) which form $RuO_2.nH_2O$ [26]. Further heat treating the samples up to 450^oC causes the completely removal of water molecules and produce crystalline RuO_2. Because the catalyst layers are thin, so that X-ray can penetrate through the coating layers and the absorption peaks of Ti metal can be realized. No evidence of Ruthenium metallic phase by-product was observed, which is the easy corrosion component in the chlorine electrolysis [52].

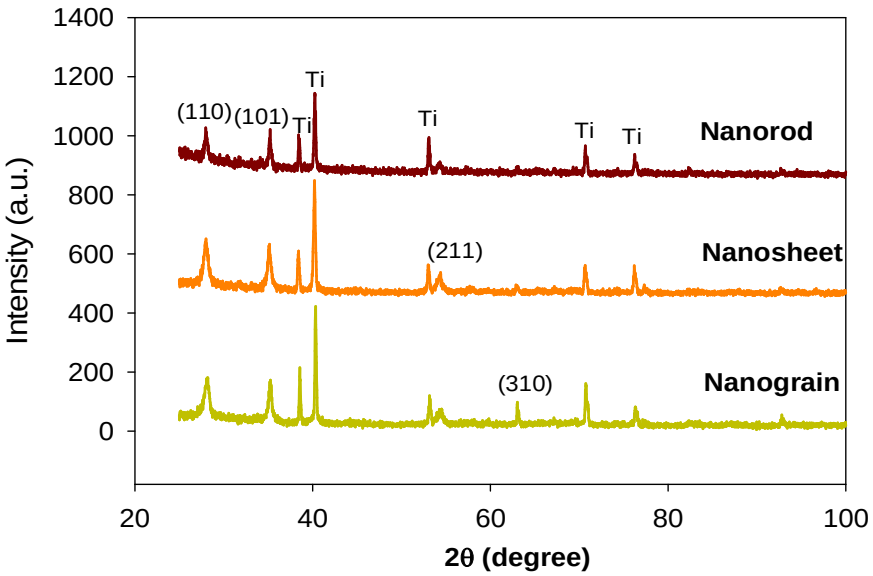

Fig. 4-6. XRD spectra of RuO_2 electrodes with difference morphologies: nanorod, nanosheet, and nanograin.

4.2.4. CV and active surface area

Figure 4-7 shows the voltammetric charges at difference scan rate (a) cyclic voltammograms at scan rate 4 mV/s (b) of the RuO_2 electrodes with difference morphologies: nanorod, nanosheet and nanograin. As shown in Figure 4-7 (a), the voltammetric charge decrease with the increase of scan rate, which is attributed to the difficulty of the electrolyte to penetrate to the inner surface of the electrode likes micropores, microcracks, grains boundary. Since the electrode's morphologies are difference, which means that the kinetics of electrochemical reactions may vary on different parts of the electrode's surface. At fast scan rate the protons have no time to diffuse to the less accessible areas before the scan direction is reversed. At low scan rate the diffusion processes reach deeper into the oxide structure, the voltammetric charge is larger and decreases towards a constant value when the scan rate is increased. The values of voltammetric surface charges at both high and low scan rates are higher with the templated nanorod and nanosheet electrodes than the conventional nanograin electrode, respectively. The total voltammetric charges of the nanosheet and nanorod electrodes are 121.3 mC/cm^2, 49.2 mC/cm^2 compare to nanograin electrode 28.8 mC/cm^2. While the value of outer voltammetric charges of these electrodes are 43.0 mC/cm^2, 27.5 mC/cm^2 and 15.1 mC/cm^2, respectively. Due to the characteristics of RuO_2 nanorod and nanosheet electrodes in the highly open structures, roughness factor and the hierarchical pores with considerable interstices among them, the electrolyte is easy

to access inside the rod or sheet structures and thus beneficial for charge transport and ion diffusion compare to the conventional nanograin electrode. The nanosheet electrode shows biggest gap between total surface area and outer surface area, which could be attributed to the porous structure in the nanosheet which may provide more inner surface area.

Figure 4-7 (b) displayed all CV curves of the as-prepared electrodes, which are almost symmetrical to zero potential line. The rectangular shape of the CV curves of RuO_2 electrodes remains unchanged with scan rate, indicating the good reversibility of the system resulting from the insignificant iR (ohmic drop) loss. The redox proton exchange between the electrode and the acidic solution presents a broad reversible peak at 0.6 V vs. Ag/AgCl. The current densities of these electrodes in cyclic voltammograms are very consistent with the voltammetric charge which is shown in Figure 4-7 (a). The response current densities and sharp patterns in cyclic voltammograms of the nanorod and nanosheet electrodes are higher than the conventional nanograin electrode. Among these electrodes, the nanosheet electrode shows highest response current density and electrochemical property.

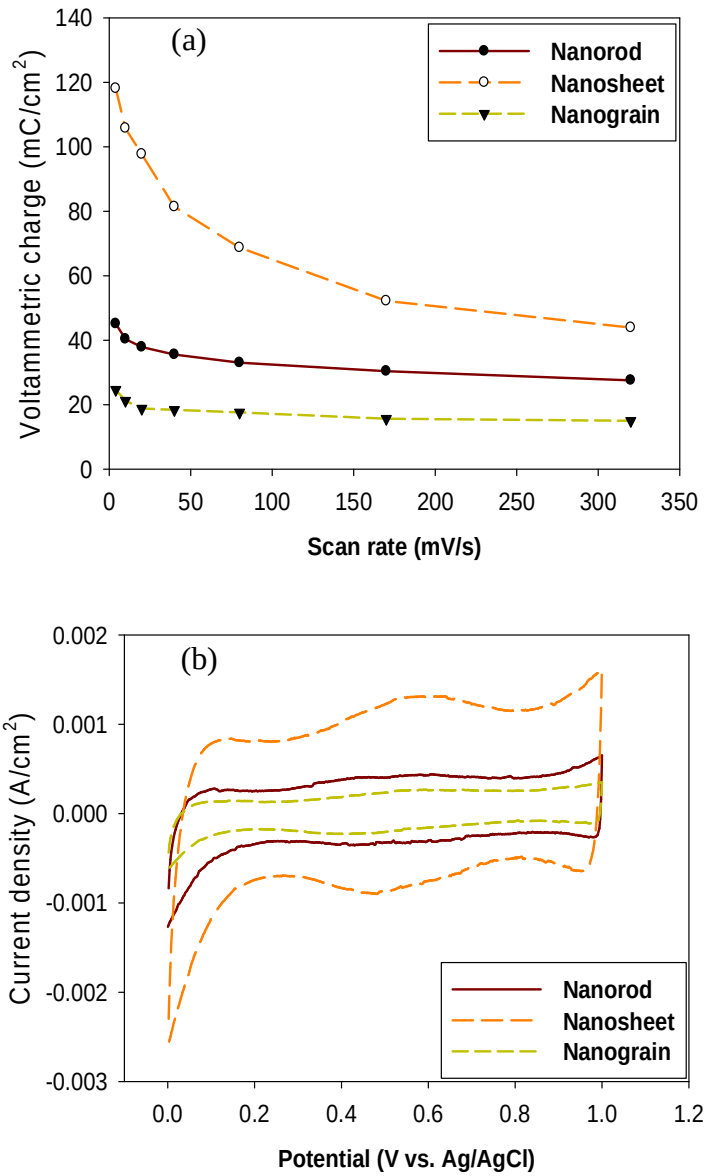

Fig. 4-7. Voltammetric charge at difference scan rate (a) and cyclic voltammetry at scan rate 4 mV/s (b) of RuO_2 nanorod, nanosheet, and nanograin electrodes in H_2SO_4 0.5 M.

4.2.5. Chlorine evolution efficiency

Figure 4-8 shows the chlorine concentrations (a) and LSV (b) of RuO_2 electrodes with difference morphologies: nanorod, nanosheet, and nanograin. As shown in Fig. 4-8 (a), there are different about chlorine evolution efficiency of as-prepared electrodes. The RuO_2 nanorod and nanosheet electrodes present higher chlorine concentrations than conventional RuO_2 nanograin electrode. The chlorine evolution efficiency increase up to 35% in case of nanosheet (200 mg/L) and 20% with nanorod electrodes (180 mg/L) compare to the conventional nanograin electrode (150 mg/L). At this chlorine measurement condition, the oxygen evolution is suppressed by the increasing of oxygen overpotential and selectivity for chlorine evolution [120, 121]. Chlorine concentrations are also supported by LSV results in brine solution (5 M NaCl, 0.01 M HCl), which is shown in Figure 4-8 (b). At potentials below 1.2 V vs. Ag/AgCl, no reaction takes place, but potentials exceeding 1.2 V vs. Ag/AgCl cause a steady increase in measured current density, which indicates chlorine formation. The steady state current of nanorod and nanosheet electrodes seem more linear compare to the interrupt line of nanograin electrode at 1.8 V, which can be affected by the chlorine gas bubbles. Overall, RuO_2 nanorod and nanosheet electrodes have higher current density in the region of chlorine evolution compares to the nanograin electrode. It is implied the nanorod and nanosheet RuO_2 electrodes possess higher chlorine electrocatalytic activities compare with nanograin electrode. This result can be attributed to the higher outer

surface areas of the nanorod and nanosheet electrodes. The outer surface area is the main working part for chlorine evolution because of highly reversible and fast reaction, while the inner surface is blocked by adherent chlorine gas bubbles, and becomes partially inactive [14-18]. Undoubtedly, these nanorod and nanosheet structures could not only provide more outer electroactive sites, effective electrolyte-accessible channels for ion transportations, but also substantially improved the chlorine electrocatalytic performances.

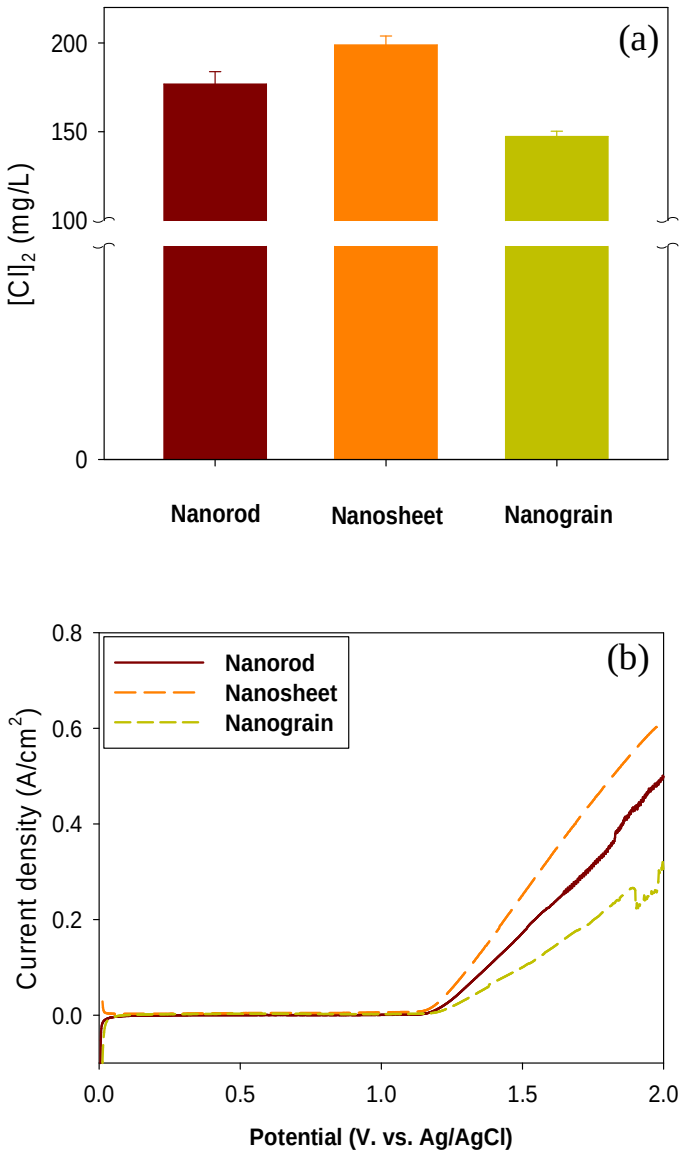

Fig. 4-8. Chlorine concentrations (a) and LSV (b) of RuO_2 nanograin, nanorod and nanosheet electrodes. Experiment condition: 0.1 M NaCl, pH = 2, j = 16.7 mA/cm^2.

4.2.6. Conclusions

In this study, the RuO_2 nanorod and nanosheet electrodes are synthesized with tailored architecture using organic templates and make the comparison with the conventional nanograin electrode. The organic template precursors as PEG or SDS surfactant played a major role in controlling the morphology of RuO_2 electrodes. We have demonstrated that the templated RuO_2 nanorod and nanosheet electrodes can be used as efficient electrocatalyst for chlorine evolution reactions, which show better activity than the nanograin electrode. The chlorine evolution efficiencies increase up to 20% in case of nanorod electrode and 35% in case of nanosheet electrode in comparison with nanograin electrode. These results could be attributed to the better mass transport of RuO_2 nanorod and nanosheet electrodes in comparison with the conventional nanograin electrode, allow more effective surface area to participate in the chlorine evolution reaction. The templated RuO_2 nanorod and nanosheet electrodes are promising materials for high-electrocatalytic performance and reducing the energy consumption in the future chlor-alkali industry.

4.3. Fabricating macroporous RuO_2-TiO_2 electrodes for high chlorine evolution efficiencies

4.3.1. Background

Chlorine, which is generally produced by the chlor-alkali process, is one of the most important chemical species in the chemical, and pharmaceutical industry, and wastewater treatment [1]. In the chlor-alkali process, Dimensionally Stable Anodes (DSA®) have led to great success as the electro-catalysts in chlorine evolution in technical electro-chemistry [2, 3]. These types of anodes usually consist of a Ti support coated by noble metal oxides including RuO_2, IrO_2 or their mixture with valve metal oxide [4-10]. Among them, the RuO_2–TiO_2 binary anode has notably gained interest in the practical application of DSA® due to its high stability and catalytic performance toward chlorine evolution [5]. Nevertheless, one significant limitation of the RuO_2–TiO_2 anode is still the high energy consumption in the industrial chlorine production process. Thus, it is still necessary to further improve the chlorine evolution efficiency of RuO_2–TiO_2 electrode as well as reduce the electrical energy consumed during the reaction [4].

The chlorine evolution efficiency of RuO_2–TiO_2 electrodes depends on several important parameters such as their surface area, composition, annealing temperature, etc [4, 5, 14, 94, 96]. Especially, the surface or pore structure leading to an increased surface area or contributing to fast mass transfer is thought to be a key parameter affecting to the chlorine evolution efficiency [21, 22]. For example,

various pathways have been investigated to enhance the surface area of RuO_2 with hollow aerogels [127], vertical nanorods [23-26], nanosheets [115] and nanotubes [128-130]. In particular, a porous framework by virtue of tiny crystallite dimensions has dramatically emerged as the fundamental method to enhance the surface area of RuO_2 electrodes [131-133]. The porous framework is well-known to contribute to the high chlorine evolution efficiency of the anode because the pore surface provides improved diffusional access for the electrolyte to reach the electrode surface, and faster transport of the evolving gas from the reactive pore surface due to the enhanced pore connectivity or the formation of gas channels inside [133-134].

In particular, the porous framework can be simply prepared by employing hard or soft templates with a narrow size distribution as the pore-directing agent, which has been extensively investigated in the synthesis of various nanostructures and seems to be significantly promising [135-138]. This process is easy, reliable, versatile, low cost and applicable to a wide variety of electrodes. A previous study showed successful improvement in oxygen evolution on an IrO_2 macroporous electrode fabricated with a SiO_2 template [139]. The macroporous structure decreases the mass transport resistance compared with mesoporous or microporous materials by enabling easy access to the active surface sites for the electrolyte [137-139]. However, a RuO_2-TiO_2 electrode with the macroporous framework which intends to have a controlled pore size without collapse of the wall structure has not been fully investigated for chlorine evolution.

Herein, this study fabricated a highly electrocatalytically active RuO_2–TiO_2 electrode for chlorine evolution using polystyrene microsphere templates (0.1, 0.46, and 1.1 μm) resulting in novel three dimensional ordered macroporous structures. The microstructures of the as-prepared electrodes were characterized with scanning electron microscope (SEM), transmission electron microscopy (TEM), and X-Ray diffraction (XRD). The electrochemical properties were examined with cyclic voltammetry (CV), linear sweep voltammetry (LSV), and total chlorine concentration (DPD) methods.

4.3.2. Surface analysis

Fig. 4-9 shows the SEM (a) and TEM (b) images of the RuO_2-TiO_2 electrodes fabricated with several different sizes of PS (diameters of 0.1, 0.46 and 1.1 μm) compared with the nontemplated electrode. As shown in Fig. 4-9 (a), the RuO_2-TiO_2 electrodes (PS 0.1 μm, PS 0.46 μm, and PS 1.1 μm) clearly exhibited three dimensional uniform macroporous structures, while the nontemplated electrode did not. In addition, the size of the macropores on the RuO_2-TiO_2 electrodes appeared to be smaller than the size of the PS microspheres. In other words, the 0.1, 0.46 and 1.1 μm diameters of the PS microspheres led to pore sizes of ca. 0.05, 0.2, and 0.6 μm, respectively. This observation can be explained by the contraction during the sintering process [132-134]. Furthermore, the distinct surface morphology of the macroporous electrodes (PS 0.1 μm, PS 0.46 μm and PS 1.1 μm) and the nontemplated electrode with it's irregularly shaped aggregates (11-20 nm) and no macroporous structure was also evidently observed in the TEM images (Fig. 4-9 (b)). This observation is in good agreement with the results of the SEM images in Fig. 4-9 (a). The results in Fig. 4-9 suggest that PS microspheres as templates have a fundamental role in the synthesis of macroporous RuO_2-TiO_2 electrodes.

Fig. 4-10 shows the XRD spectra of the macroporous and nontemplated RuO_2-TiO_2 electrodes. As can be seen in Fig. 4-10, the well-defined peaks of (110) and (111) corresponding to the polycrystalline RuO_2 are clearly observed on the macroporous RuO_2-TiO_2 electrodes (PS 0.1 μm, PS 0.46 μm and PS 1.1 μm) and

the nontemplated RuO_2-TiO_2 electrode. No evidence of a Ru metallic peak was observed, which means that the electrodes are high purity phase structures. Their average crystallite sizes calculated by the Scherrer equation [117] with peaks of (110) were approximately 15 nm. This indicates that both the macroporous and nontemplated RuO_2-TiO_2 electrodes possessed similar crystallite structure and sizes despite significantly different surface morphologies.

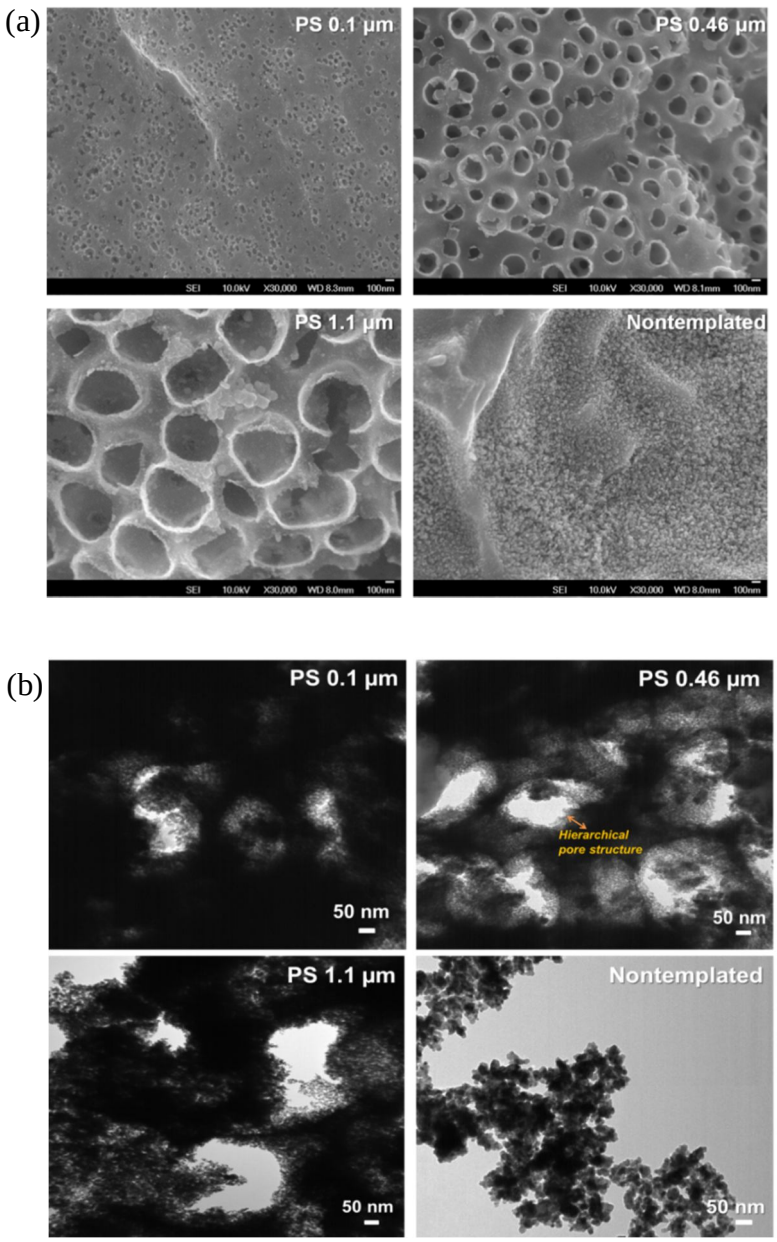

Fig. 4-9. SEM (a) and TEM (b) images of the macroporous RuO_2-TiO_2 electrodes fabricated with several ranges of the PS sizes (diameter of 0.1, 0.46 and 1.1 μm) and without PS template (nontemplated).

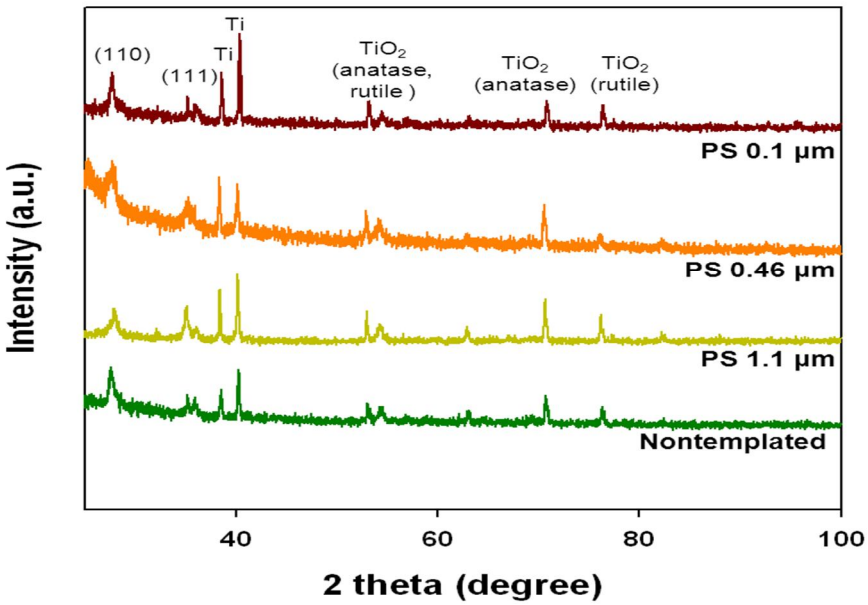

Fig. 4-10. XRD patterns of the macroporous RuO_2-TiO_2 electrodes fabricated with several ranges of of the PS sizes (diameter of 0.1, 0.46 and 1.1 µm) and without the PS template (nontemplated).

4.3.3. Chlorine evolution on the ordered macroporous RuO_2-TiO_2 electrodes

Fig. 4-11 shows the chlorine concentration (a) and voltammetric charge (b) for the macroporous and nontemplated RuO_2-TiO_2 electrodes. Two important observations can be made in Fig. 4-11 (a). First, as shown in Fig. 4-11 (a), the chlorine evolution on the macroporous electrodes (180~220 mg/L) was much higher than that of the nontemplated electrode (145 mg/L). Second, among the macroporous electrodes, PS 0.46 μm, not PS 0.1 and 1.1 μm, exhibited the highest chlorine evolution efficiency, indicating the existence of an optimal macropore size for RuO_2-TiO_2 electrodes. For example, the chlorine concentration (220 mg/L) for the macroporous electrode that used PS 0.46 μm in its fabrication was higher than that of the macroporous electrodes that used PS 0.1 μm and 1.1 μm (180 and 200 mg/L, respectively). Under this condition for the chlorine measurement, oxygen evolution is suppressed increasing the oxygen overpotential and selectivity for chlorine evolution [120, 121]. These different chlorine evolution efficiencies are further supported by the electrocatalytic activity examined by linear sweep voltammetry (Fig. 4-11 (b)). All the macroporous RuO_2-TiO_2 electrodes showed a higher current density as a result of the charge transfer reaction in chlorine evolution compared to the nontemplated electrode, and the highest current density was observed on macroporous electrodes that used PS 0.46 μm in its fabrication. It

is noted that the magnitude of the current densities was in same order of the chlorine concentrations on the RuO_2-TiO_2 electrodes (Fig. 4-11(a)).

Fig. 4-12 shows the voltammetric charge obtained from the cyclic voltammograms with the scan rate (5–320 mV/s) within a potential range of 0.0–1.0 V in 0.5 M H_2SO_4 (Fig S6 in Appendix) to estimate the total and outer surface areas of the RuO_2-TiO_2 electrodes [15, 52]. The total voltammetric charge including both the inner and outer active surfaces can be measured at a low scan rate. On the other hand, the outer voltammetric charge can be obtained at a high scan rate [15]. As shown in Fig. 4-12, it is interesting to note that the order of the total surface area for the electrodes was different with that of the outer surface area. That is, the total surface area was in decreasing order of PS 0.1 μm, PS 0.46 μm, PS 1.1 μm and the nontemplated electrode, while the outer surface areas was in decreasing order of PS 0.46 μm, PS 0.1 μm, PS 1.1 μm and the nontemplated electrode. Thus, the outer surface area was in good agreement with the results of the chlorine evolution efficiency for the macroporous RuO_2-TiO_2 electrodes, indicating that the outer surface area has a more critical role in enhancing the chlorine evolution efficiency than that of the total surface area, and pore size can affect the optimal development of the outer surface area. As mentioned earlier, the reason for this could be because of the increased mass transfer or the easy removal of chlorine gas bubbles based on the well-developed outer structure of the macroporous electrodes because the chlorine evolution reaction rate is very fast

and thermodynamically reversible [14-16]. Futhermore, it has been attributed that under intensive gas evolution, the inner surface is blocked by adherent gas bubbles and becomes partially inactive for chlorine evolution [14-18].

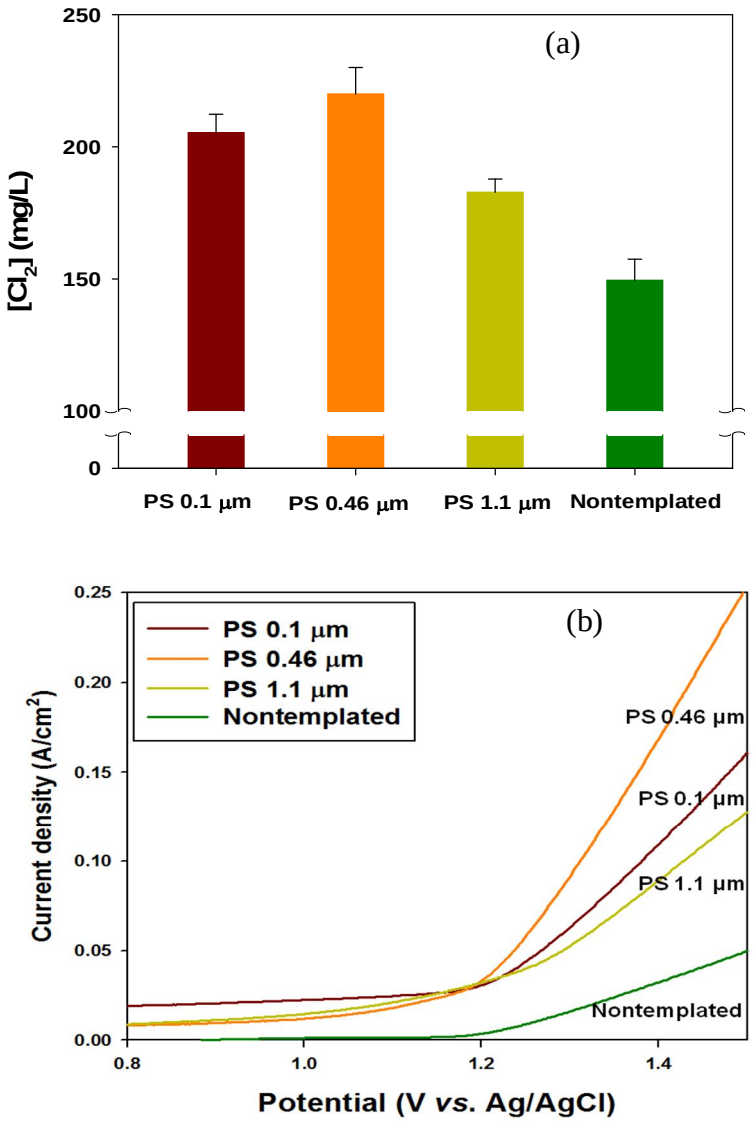

Fig. 4-11. Chlorine evolutions (i = 16.67 mA/cm^2, $[NaCl]_o$ = 0.1 M) (a) and linear sweep voltammetry (5 M of NaCl (pH = 2)) (b) of the macroporous RuO_2-TiO_2 electrodes fabricated with several ranges of the PS size (diameter of 0.1, 0.46 and 1.1 μm) and the nontemplated electrode.

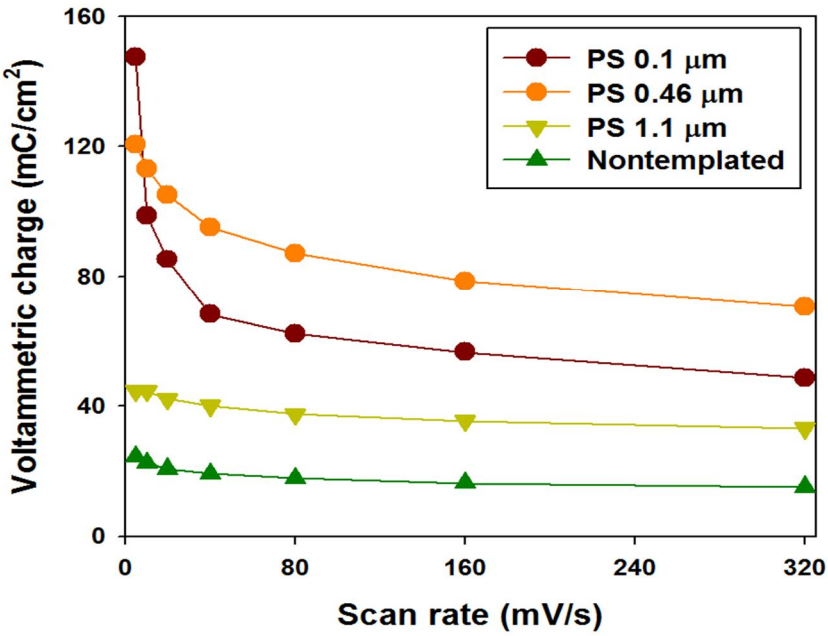

Fig. 4-12. Voltammetric charges of the macroporous RuO_2-TiO_2 electrodes with scan rate fabricated with several ranges of the PS sizes (diameter of 0.1, 0.46 and 1.1 μm) compared with that of the nontemplated electrode.

4.3.4. Conclusions

In this study, we fabricated highly electrocatalytically active RuO_2-TiO_2 electrodes for chlorine evolution with a structural ordered macroporous framework using PS microsphere templates (0.1 ~ 1.1 μm). The chlorine evolution efficiency of the macroporous RuO_2-TiO_2 electrodes was up to approximately 1.5 times higher than that of the nontemplated electrode at the same Ru loadings. Interestingly, in the macroporous RuO_2-TiO_2 electrode with the specific templated pore size of PS 0.46 μm, and not that of PS 1.1 μm or PS 0.1 μm, the outer surface area was the most well-developed, and it led to the highest chlorine evolution efficiency in this study, indicating the existence of an optimal macropore size for an effective chlorine evolution reaction. This result could be attributed to the structural properties of the macroporous electrodes providing easy mass transfer and removal of chlorine gas bubbles with good control over the pore size and pore walls connectivity. The macroporous RuO_2-TiO_2 electrodes can be considered as promising anode materials with high chlorine evolution efficiency and reduced the energy consumption in the future chlor-alkali industry.

4.4. High performance of RuO_2 electrodes using sonoelectrodeposition method for chlorine evolutions

4.4.1. Background

The chlor-alkali industry produces annually about 70 million tons of chlorine worldwide and therefore now become one of the largest electrochemical technologies in the world. The chlor-alkali process is energy intensive and is the second largest consumer of electricity among the electrolytic industries with about 2400 billion kWh per year [1]. RuO_2 is a well-known electrode material with excellent electrocatalytic features for chlor-alkali industry, as the active component of Dimensionally Stable Anodes (DSA) [2-4]. Roughly 10-15% of the annual production of Ru goes into the preparation of such DSA-type electrodes [1]. Using alternative green method for preparation RuO_2 electrode is necessary to reduce the cost, time, energy consumption, increase the chlorine evolution efficiency as well as stability [5]. Various methods for the synthesis of RuO_2 electrodes were developed, such as sol–gel [19], thermal decomposition [14], polyol [30], Adams fusion [31], reactive sputtering [23-25] and chemical vapor deposition [26-28]. Both these methods proceed via several coating applications and calcination steps until the desired catalyst loading is achieved. Beside this, the high temperature (1500°C) vapor-phase processes in reactive sputtering or chemical vapor deposition are expensive and also limited by their low yield. Electrodeposition method has proved to be simple, versatile, one-step, film thickness control and cost

effective for electrode preparation [99-105]. The two key mechanisms that have been identified as the rate determining steps for crystal formation in electrodeposition are charge transfer and diffusion of supersaturated ions at the electrode surface [106]. The electrodeposition of RuO_2-based electrode proceeds via a wet chemical precipitation induced by a cathodically electro-generated base seems very promise [107, 108, 52]. By this method, an increase of outer surface area, decrease of the chlorine overpotential and simultaneously a reduction of the noble RuO_2 can be achieved [52].

The electrodeposition route for preparation RuO_2 electrode uses a cathodic reaction to increase the pH locally near the electrode surface. The main cathodic reaction to produce OH^- is the decomposition of water under hydrogen evolution as followed reactions [106, 52]:

$$O_2 + 2H_2O + 4e^- \leftrightarrow 4OH^- \qquad (27)$$

$$2H_2O + 2e^- \leftrightarrow H_2 + 2OH^- \qquad (28)$$

These reactions consume H_2O, generate OH^- and then react with Ru ions to form Ru oxide, hydroxide or peroxide colloidal particles deposit on cathodic substrates. Ru hydroxide and peroxide deposits can be converted in to corresponding RuO_2 by thermal treatment. The assumed reactions can be represented as:

$$Ru^{3+} + OH^- \rightarrow RuO_x(OH)_y \rightarrow RuO_2 \qquad (29)$$

In addition, the cathodic decomposition of water can be competed with the cathodic electrodeposition of Ru metal:

$$Ru^{4+} + 4e^{-} \rightarrow Ru^{o} \qquad (30)$$

In recent decades, the use of sonoelectrodeposition has developed rapidly, efficient in the preparation of various nanomaterials [109-111, 139-147]. It has been shown that the effects of high intensity sonication on electrochemical processes lead advantage to both chemical and physical effects, for example, mass-transport enhancement, surface cleaning and radical formation. It is well accepted in the field that sonication decreases the diffusion layer thickness, therefore giving a substantial increase in limiting current. This can be attributed to the effects of collapse cavitation bubbles, micro, macrostreaming, increase electrolyte concentration at the electrode surface, and enhanced reaction rates [109-111].

In this study, the cathodic sonoelectrodeposition of RuO_2 electrodes from aqueous $RuCl_3$ bath on Ti substrates for chlorine evolutions was reported for the first time. The properties of the obtained electrodes prepared using the sonoelectrodeposition method are compared with the conventional one made by mechanical stirring electrodeposition. The microstructures of as-prepared electrodes were evaluated using scanning electron microscope (SEM), transmission electron microscopy (TEM), and X-ray diffraction (XRD). The electrochemical properties were examined using cyclic voltammetry (CV), linear sweep

voltammetry (LSV), total chlorine concentration (DPD), and accelerated stability test (AST) methods.

4.4.2. Chlorine evolution

Figure 4-13 shows the chlorine concentrations (a) and the LSV (b) of RuO_2 electrodes made by sonoelectrodeposition and conventional stirring electrodeposition. As shown in Figure 4-13 (a), there are different between the chlorine concentrations of the obtained RuO_2 electrodes. The chlorine evolution efficiency increase up to 17.1% in case of sonoelectrodeposition RuO_2 electrode (171 mg/L) compare to the one made by conventional stirring electrodeposition (146 mg/L) fabricated at the same deposition time of 15 minutes. Moreover, the chlorine concentration of the RuO_2 electrode made by sonoelectrodeposition after 10 minutes is also higher compare to the conventional one prepared after 15 minutes. Increasing the sonoelectrodeposition time from 10 to 15 minutes, the chlorine concentration increases. The chlorine concentration results in Figure 4-13 (a) are supported by the measured LSV in Figure 4-13 (b). At potentials below 1.2 V vs. Ag/AgCl, no reaction takes place. However, potentials exceeding 1.2 V vs. Ag/AgCl cause a steady state increase in measured current density, which indicates chlorine formation. The current densities extracted from linear sweep voltammograms in the region of chlorine evolution show higher with the electrodes made by sonoelectrodeposition than the one made by conventional stirring electrodeposition. Increasing the sonoelectrodeposition time from 10 to 15 minutes the current density also increases. The increasing of chlorine evolution efficiency of the RuO_2 electrodes made by sonoelectrodeposition may be related to the

increase of active surface area, which contributes to the electrochemical reaction. Clearly, sonoelectrodeposition has a positive role on improving the electrocatalytic performances of RuO_2 electrodes for chlorine evolution compares to conventional method.

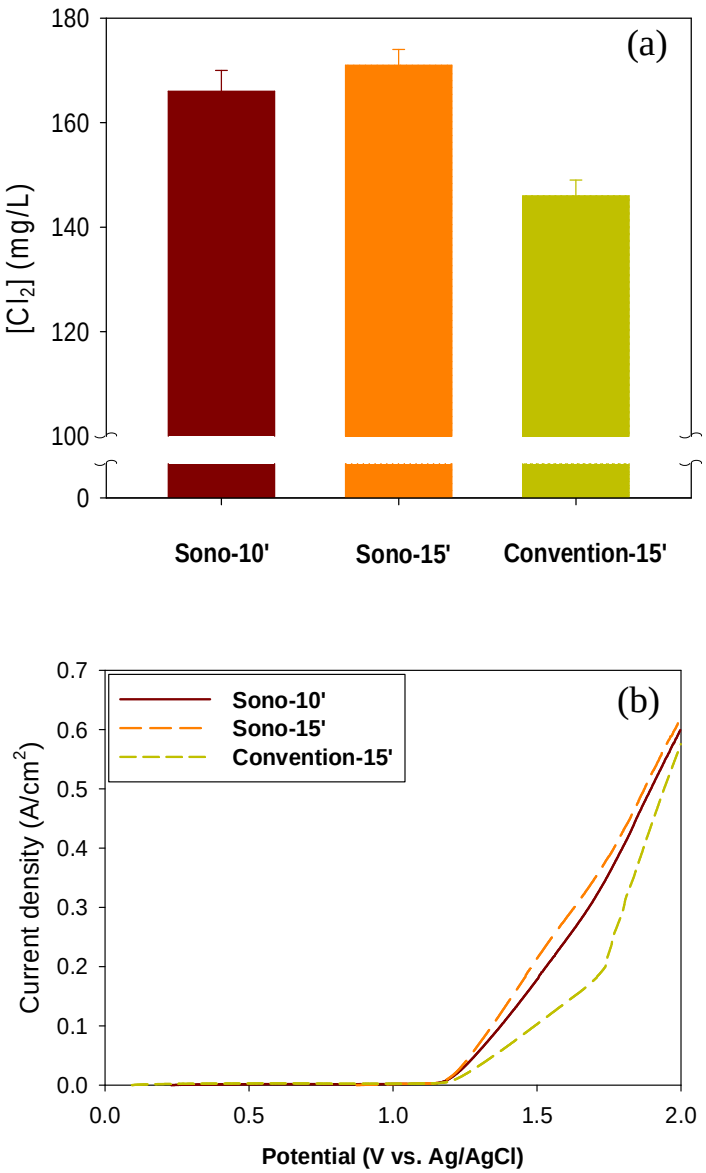

Fig. 4-13. Chlorine concentrations (a) and LSV (b) of RuO_2 electrodes prepared by sonoelectrodeposition and conventional stirring electrodeposition. Experimental conditions: (a) 0.1 M NaCl, pH = 2, t = 10 minutes; (b) 5 M NaCl, pH = 2.

4.4.3. Surface analysis

Figure 4-14 shows the SEM (a) and TEM images (b) of the RuO_2 as-prepared electrodes surfaces made by sonoelectrodeposition and conventional stirring electrodeposition. As the displayed SEM images in Figure 4-14 (a), there are different about the morphologies of these RuO_2 as-prepared electrodes. The electrodes made by sonoelectrodeposition composed of big hemispheres, fine grain and mushroom-like structures. A high roughness factor, island with layer by layer deposition in combination with an accumulation of compact surface has been formed with sonoelectrodeposition method while just a few of small spheres deposited in the conventional one. In conventional method, mass transport is dominated because of the limitation of the electrolyte concentration which reaches to the substrate. The roughness and surface coverage increase with the increasing of sonoelectrodeposition time, consistent with the RuO_2 mass increasing in the next session. It was found that sonication strongly affects the surface morphology of RuO_2 electrode. The capability of sonication to degas at the substrate/electrolyte interphase by in-situ cleaning due to the onset of cavitation phenomena removed all the hydrogen gas evolved from the surfaces, enhance the deposition process with the well covered deposits (Figure S7 in Appendix). Sonication waves could indeed thin down the diffusion layer and reduces the depletion of electroactive surface near the substrate, resulting in the formation of hemisphere on the existing nuclei [112].

Figure 4-14 (b) displayed the difference about the crystal size of RuO_2 nanoparticles made by sonoelectrodeposition and conventional stirring electrodeposition. Due to the annealing temperature, the water molecules in hydrous form are removed and well defined crystals of RuO_2 are obtained. The nanoparticles size of RuO_2 made by sonoelectrodeposition method is 7-10 nm in diameter with high dispersion, while with the conventional method is about 20-25 nm with high agglomerates. The nanoparticles made by sonoelectrodeposition procedure are smaller sizes, more uniform and finer distribution than the nanoparticles made by conventional stirring procedure. These observations can be attributed to the implosion of cavitation bubbles substrate's surface and acoustic streams enabling the deagglomeration and activating nucleation sites of RuO_2, leads to fine dispersion of RuO_2 nanoparticles in the coating [147]. As expected, there are not different between the crystal size of the electrode made by sonoelectrodeposition after 10 minutes and 15 minutes. This is inferred that the sonoelectrodeposition time is not affect to the crystal sizes of the RuO_2 electrodes. The special surface morphologies with broad hemispheres, mushroom-likes and the reducing of crystal size of the sonoelectrodeposition RuO_2 electrode are expected to fulfill the increasing of the outer surface area [52].

Figure 4-15 shows the diffraction patterns of RuO_2 electrodes made by sonoelectrodeposition and conventional stirring electrodeposition after 15 minutes. The typical peaks of rutile RuO_2 metal oxide are easily detected as: 110, 101, 211,

112 faces in all the electrodes, while the most intensity peaks are 110 and 101. The RuO_2 diffraction peaks of the electrode made by sonoelectrodeposition shows stronger intensity than the electrode made by conventional stirring electrodeposition, mean that the amount of RuO_2 nanoparticles is higher. The XRD spectra suggest that the oxide nanoparticles in all case are fine and polycrystalline structure, which is desired in terms of electrode stability. The peak of Ru metal presents with the electrode made by conventional stirring electrodeposition, but not with the electrode prepared by sonoelectrodeposition route. Ru metal is an undesired phase for the chlorine evolution, since Ru metal is sensitive to corrode under electrolysis. The electrodeposition processes, uniform forward and backward diffusion of adsorbing ions and desorbing by-products respectively, occur in this very thin region of substrate - solution interphase. With the present of sonication, the cathodic water decomposition is favoured and the rate of Ru metal deposition decreases. The undesired cathodic Ru metal deposition also can be suppressed by applying high current densities [52]. Because the catalyst layers are thin, so that X-ray can penetrate through the coating layers and the absorption peaks of Ti substrate can be realized. Overall, the applied sonication has a significant positive influence on the resulting phase formation of RuO_2 electrodes.

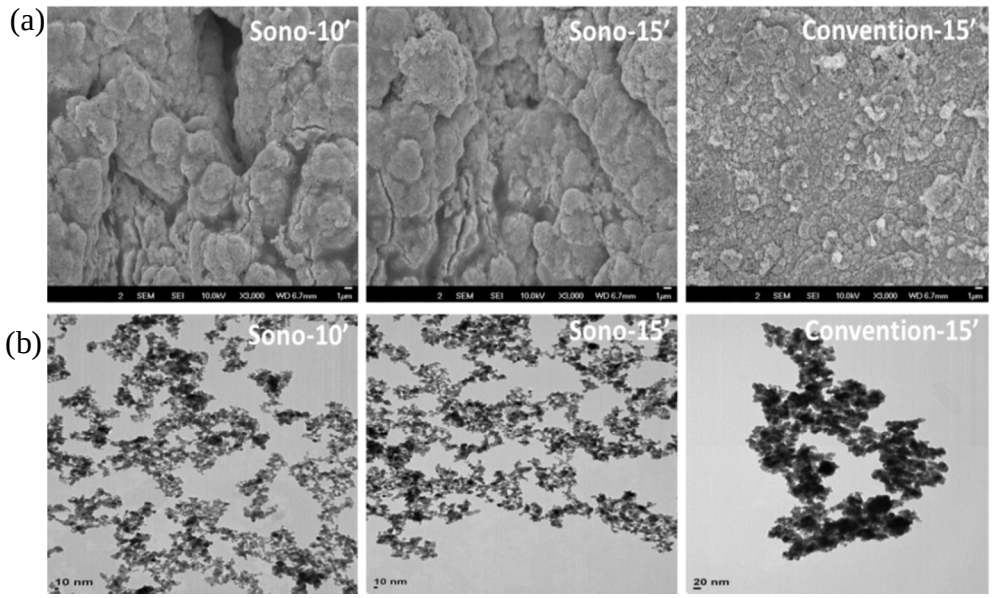

Fig. 4-14. SEM (a) and TEM (b) images of RuO_2 electrodes made by sonoelectrodeposition and conventional stirring electrodeposition.

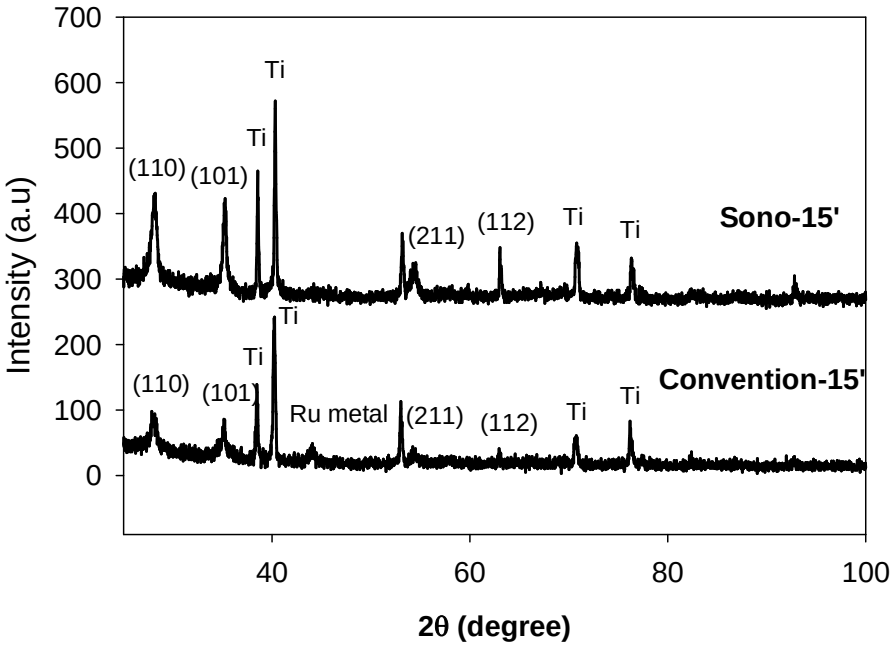

Fig. 4-15. XRD spectra of RuO_2 electrodes made by sonoelectrodeposition and conventional stirring electrodeposition.

4.4.4. CV and active surface area

Figure 4-16 shows the extrapolated voltammetric charges (a) and cyclic voltammograms (b) from a set of RuO_2 electrodes made by sonoelectrodeposition and conventional stirring electrodeposition. As show in Figure 4-16 (a), the voltammetric charges (active surface areas) decrease with the increase of scan rate, which mean that the difficulty of the electrolyte to penetrate to the inner surface of the electrode likes micropore, microcrack, and grain boundary. Since the formations of electrode morphologies are difference, which means that kinetics of electrochemical reactions may vary on different parts of the electrode surface. The results show that the total and outer voltammetric charges are higher in case of the electrode made by sonoelectrodeposition than the conventional one, respectively. The total and outer voltammetric charges at 15 minutes of sonoelectrodeposition electrode are 32.5 mC/cm^2, 23.9 mC/cm^2, while the values of conventional electrode are 22.2 mC/cm^2, 14.2 mC/cm^2. The higher voltammetric charges of the electrodes made by sonoelectrodeposition route can be attributed to the higher roughness factor, hemispheres, mushroom-like morphology, and decreasing of crystal sizes. Increasing of sonoelectrodeposition time from 10 to 15 minutes, the total and outer voltammetric charges increase, may because of the increasing of roughness factor and amount of RuO_2 deposited. The voltammetric charges of the electrodes made by sonoelectrodeposition after 10 minutes also higher than the conventional one after 15 minutes. Note that the outer active surface area of RuO_2

electrode is more importance than total active surface area for the chlorine electrocatalytic activity [14-18]. The outer surface area is the main working part for chlorine evolution because of highly reversible and fast reaction, while the inner surface is blocked by adherent chlorine gas bubbles, and becomes partially inactive [16-18].

As displayed in Figure 4-16 (b), all cyclic voltammetry curves of these obtained RuO_2 electrodes are almost symmetrical to zero potential line. Note that the rectangular shape of the cyclic voltammetry of RuO_2 electrodes remains unchanged with scan rate, indicating the good reversibility (redox reaction) of the system resulting from the insignificant iR (ohmic drop) loss. The response current density and sharp pattern in cyclic voltammetry enhances in case of the electrode made by sonoelectrodeposition than the conventional one, which mean that higher about the electrochemical property. The current densities extracted from cyclic voltammograms in Figure 4-16 (b) are very consistent with the voltammetric charges which are shown in Figure 4-16 (a) of these RuO_2 electrodes.

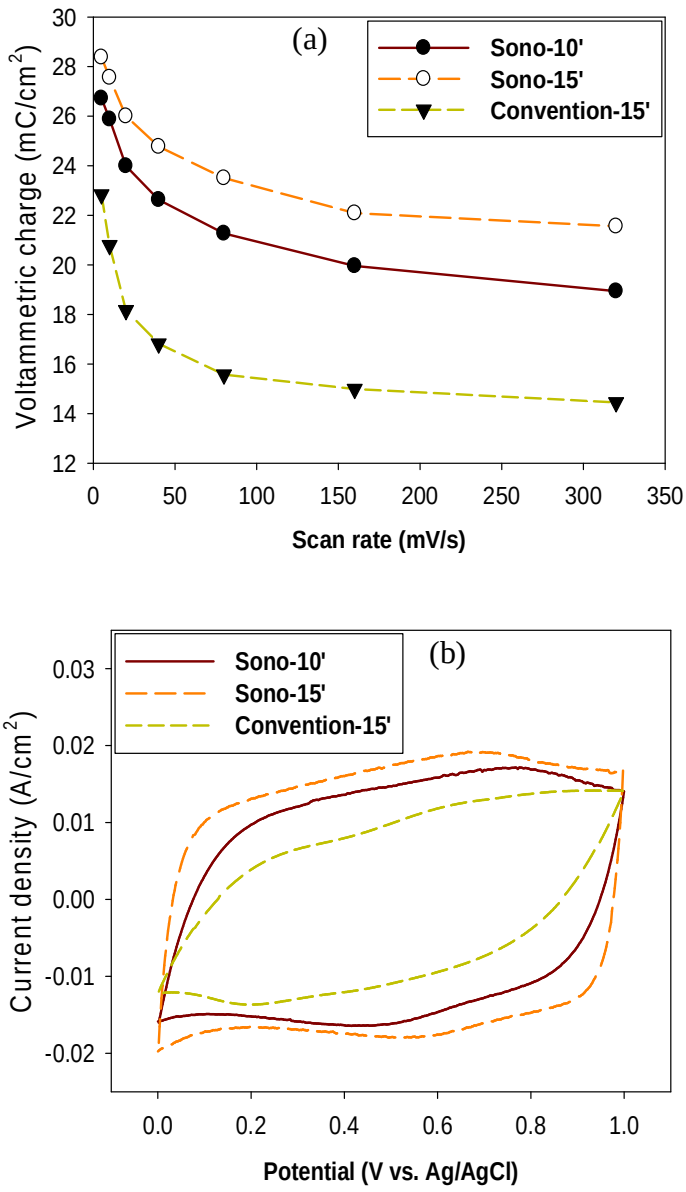

Fig. 4-16. Voltammetric charges (a) and cyclic voltammograms at scan rate 320 mV/s (b) in 0.5 M H_2SO_4 of RuO_2 electrodes made by sonoelectrodeposition and conventional stirring electrodeposition.

4.4.5. Amount of RuO_2 deposited

Electrodeposition experiments revealed the formation of black deposits on all the Ti substrates. The amount of RuO_2 nanoparticles deposited on the electrode surface can be measured by the film thickness or the increasing of electrode's weight after and before deposition. The accurate measurement of RuO_2 film thickness was not possible due to the rough morphology of the film. Therefore, the deposited weight (mg cm^{-2}) of RuO_2 film is measured instead of the thickness [106]. Figure 4-17 shows a various weight of RuO_2 films made by sonoelectrodeposition and conventional stirring electrodeposition at difference deposition times. It is seen that the deposit weight increases with time at a constant current density using the sonoelectrodeposition method, and maximum weight was obtained for the sonoelectrodeposition period of 15 minutes. For further sonoelectrodeposition time to 30 minutes, the deposited weight is not significant increase, which could be due to the empty of reactive species in the electrolytes. The weight of RuO_2 nanoparticles deposited with the present of sonication after 10 minutes (0.20 mg cm^{-2}) is nearly same, while after 15 minutes (0.30 mg cm^{-2}) shows higher than the conventional stirring (0.21 mg cm^{-2}) obtained for the deposition period of 15 minutes, respectively. Sonoelectrodeposition can produce a larger amount of RuO_2 nanoparticles deposited on the electrode's surface compare to the conventional method. The increasing of deposited weight in case of sonication-assisted can be attributed to the higher concentration of electrolyte at the electrode surface due to

the removal of H_2 bubble, enhance the mass transfer and deposition rate process [139, 140, 147].

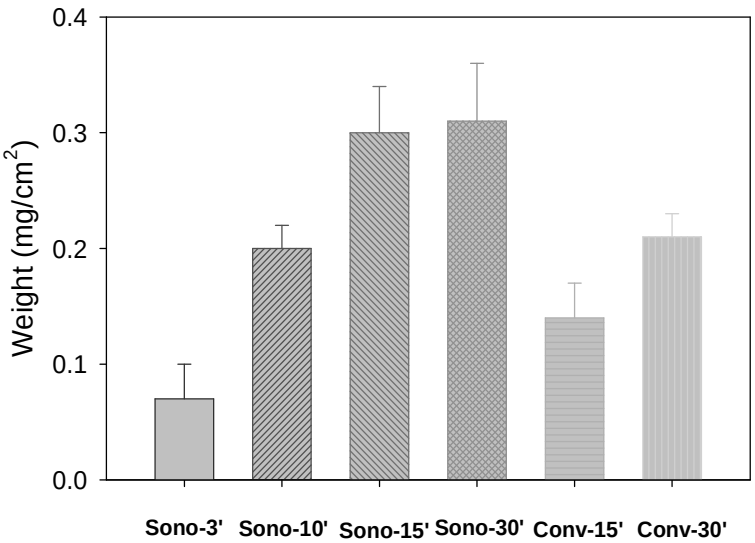

Fig. 4-17. Weights of RuO_2 deposits made by the sonoelectrodeposition and conventional stirring electrodeposition at difference deposition times, current density 50 mA cm^{-2}.

4.4.6. Accelerated stability test (AST)

In the electrochemical production of chlorine, it is undoubtedly the stability that plays the most important role. The sustainability of the electrocatalytic capability strongly relies on high electrode stability. The real service life of the electrode will be much longer than the lifetime obtained in the accelerated stability test due to the much lower current density used under normal operating conditions. The electrode lifetime in the stability test is defined by the time at which the potential of an electrode suddenly escalates under galvanostatic conditions in simultaneous oxygen and chlorine evolution reactions. Figure 4-18 shows the time dependencies of the electrode potential and the appropriate differential curves for the RuO_2 electrodes prepared by the sonoelectrodeposition and conventional stirring electrodeposition. The potential seem lightly decrease in the initial period of time, correlates with the activation process. The life time of the RuO_2 electrodes made by sonoelectrodeposition method (90 and 100 minutes) are longer than the electrode made by conventional stirring electrodeposition (60 minutes) under the same electrolysis condition. The electrode stability increase with the increasing of sonoelectrodeposition time from 10 to 15 minutes can be explained by the mass coverage enhancement. The failure mechanisms of a RuO_2 electrode are complex. In general, there are three mechanisms including the growth of an insulating TiO_2 layer at the coating – substrate interface that becomes less doped with the catalytic oxide, the removal of the catalytic material by the intense gas production, and the

dissolution of Ru due to formation of soluble Ru^{8+} species during the long-term electrolysis [94-96]. The morphology of the coating may favor any or all of them together. The RuO_2 particles size is smaller and the distributions are more uniform in the case of the sonoelectrodeposition procedure, which produces a larger surface area than in the conventional method. Consequently, the rate of dissolution of the Ru species on the electrode obtained by the sonoelectrodeposition procedure is lower. In the same manner, the structures of the catalytic coating of the sonoelectrodeposition prepared electrodes are more compact, layer by layer deposition, hemisphere structure and the penetration of electrolyte toward the Ti substrate is limited. Then it allows less non-conductive intermediate TiO_2 layer formation as compared to the conventional electrode. Totally, the stability of the electrodes made by sonoelectrodeposition is higher than conventional stirring electrodeposition.

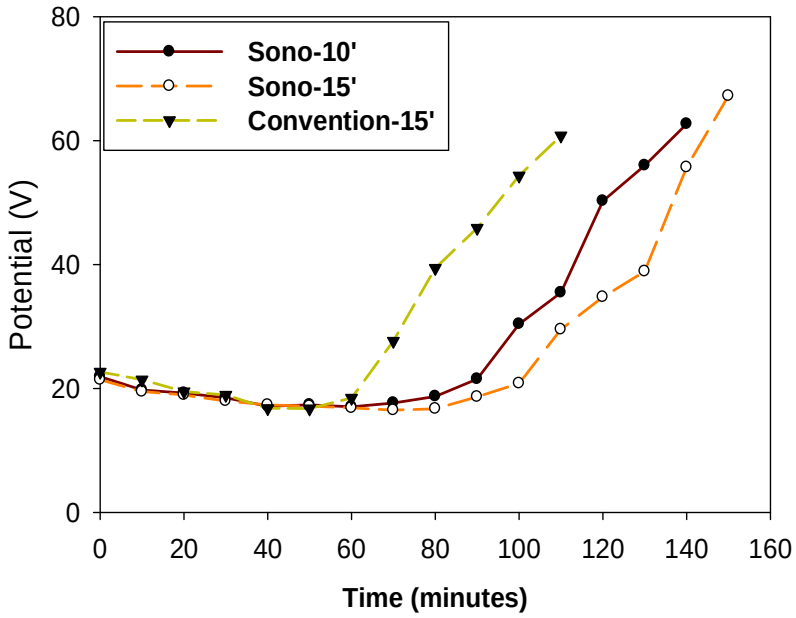

Fig. 4-18. The AST of RuO_2 electrodes prepared by sonoelectrodeposition and conventional stirring electrodeposition (0.5 M NaCl, pH = 2, t^o = 25^{o}C, current density 1 A cm^{-2}).

4.4.7. Conclusions

This study reported the first time for the sonoelectrodeposition of RuO_2 electrodes for chlorine evolution. The electrodes obtained by the sonoelectrodeposition procedure present a strong improvement about the electrocatalyst efficiency and stability with chlorine evolution in comparison with the one made by conventional stirring electrodeposition. Sonoelectrodeposition can increase the outer surface area of RuO_2 electrodes than the conventional procedure, significance for chlorine evolution enhancement. Increasing of sonoelectrodeposition time of RuO_2 electrode, the chlorine evolution efficiency and electrode's stability also increase. By using sonoelectrodeposition technique, we can successfully synthesize RuO_2 electrodes with broad hemispheres, mushroom-like, and compact structures. Sonoelectrodeposition method also can produce large amount of RuO_2 nanoparticles with more uniform and smaller crystal sizes than the mechanical stirring procedure. Ru metal, which is undesired composition in DSA, is not present by using sonoelectrodedosition route. The critical effect is the increasing of mass transport, which is high enough to decrease the diffusion layer into a charge controlled system by the capable of degassing produced H_2 free adherent surfaces.

4.5. A novel microwave-assisted synthesis of RuO_2-TiO_2 electrodes with improved chlorine evolutions

4.5.1. Background

Titanium based anodes nowadays become very importance anodes in the chlor-alkali industry, due to their excellent electrocatalytic activity for the chlorine and oxygen evolutions: low overpotential, low cost, enhanced selectivity, mechanical and chemical stability [1]. This type of electrodes usually consist of a Ti support coated by noble metal oxides as catalyst or their mixtures with valve metal oxide to prevent corrosion [2]. Mostly, the RuO_2–TiO_2 binary electrode is used in the practical application [3]. The using novel green fabrication method for synthesis RuO_2–TiO_2 electrodes now is received a lot of attention in order to enhance the efficiency and the environmental compatibility of this process [4]. Beside this, the electrode stability for a long time performance also should be considered [5]. Various methods for the synthesis of RuO_2-TiO_2 electrodes were developed, such as sol–gel [29], thermal decomposition [14], polyol [30], Adams fusion [31], electrodeposition [99-106], etc. Despite of its extensive use in industry and potential applications, the synthesis of RuO_2-TiO_2 electrode by a method giving high yield at the expense of less amounts of precursors or in less duration time needs to be considered. In this regard, an approach based on the attractive sol–gel route for the preparation of noble metal oxides seem to be promising in both

electrocatalytic and stability with chlorine evolution [94, 96]. The improvement is due to an enlargement of the coating active surface area, increased contribution of the so-called geometric catalytic factor, caused by the formation of finely dispersed oxide particles during the sol–gel procedure. The microwave heating, which is rapid, easy and energy efficient, has been used for synthesis a lot of nanomaterials over the two last decades, especially to improve the capacitance of RuO_2 for supercapacitors [112, , 148-151].

In the present study, a novel microwave-assisted synthesis of RuO_2-TiO_2 electrodes using the sol-gel method is investigated for chlorine evolution performances. The physicochemical and electrochemical properties of the obtained electrodes prepared by microwave-assisted are compared with the electrode formed by the conventional heating procedure. The microstructures of as-prepared electrodes are evaluated by scanning electron microscope (SEM), transmission electron microscopy (TEM), X-Ray diffraction (XRD). The electrochemical properties are examined with cyclic voltammetry (CV), linear sweep voltammetry (LSV), total chlorine concentration (DPD) and accelerated stability test (AST) methods.

4.5.2. Chlorine evolution

Figure 4-19 shows the difference about chlorine concentrations (a) and LSV (b) of RuO_2-TiO_2 electrodes made by microwave-assisted and conventional heating method. The chlorine concentrations are higher with the RuO_2-TiO_2 electrodes prepared by microwave-assisted synthesis method compare to conventional one by the order: convention < 800 W/g < 400 W/g. Increase the microwave intensity from 400 W/g to 800 W/g lead to decrease the chlorine evolution efficiency. The chlorine evolution efficiency increase up to 15.6% in case of microwave-assisted RuO_2-TiO_2 electrodes compares to the one made by conventional method. The increase of chlorine evolution efficiencies of the RuO_2-TiO_2 electrodes made by microwave irradiation may be related to the increase of accessible active surface area, which contributes to the electrochemical reaction. The decrease in electrocatalytic activity at high energy intensity may related to the loss of water molecule in RuO_2, which favor aggregation process of nanoparticles, leading to decrease in the accessibility for the active surface sites of the catalyst. Chlorine concentrations in Figure 4-19 (a) are consistent with current density in the region of chlorine evolution measured by LSV, which is shown in Figure 4-19 (b). At potentials below 1.2 V vs. Ag/AgCl, no reaction takes place. However, potentials exceeding 1.2 V vs. Ag/AgCl cause a steady increase in measured current density, which indicates chlorine formation. The current densities in the chlorine evolution region of RuO_2-TiO_2 electrodes are higher with the microwave-assisted synthesis

method compares to conventional one. Clearly, microwave irradiation has a positive role on improving the electrocatalytic performances of RuO_2-TiO_2 electrodes for chlorine evolution.

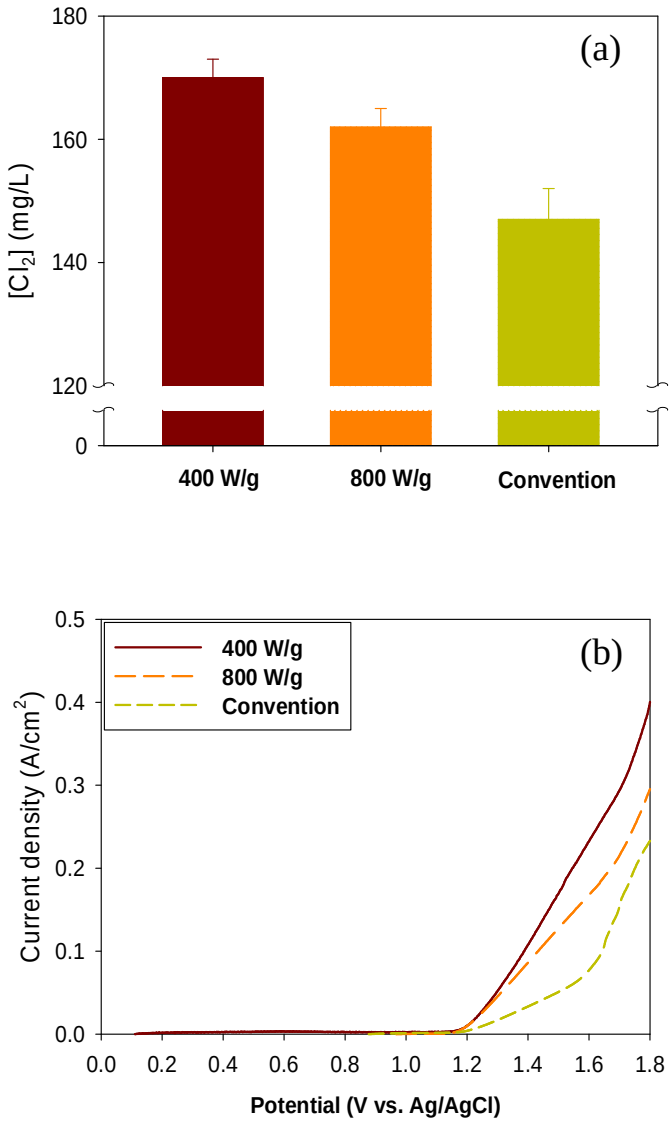

Fig. 4-19. Chlorine concentrations (a) and LSV (b) of RuO_2-TiO_2 electrodes made by microwave-assisted and conventional heating methods. Experimental condition: (a) 0.1 M NaCl, pH = 2, I = 16.7 mA/cm^2, t = 10 minutes; (b) 5 M NaCl, pH = 2, scan rate 10 mV/s.

4.5.3. Microstructure analysis

Figure 4-20 shows the SEM (a), TEM (b) imagines and XRD spectra (C) of RuO_2-TiO_2 electrodes made by microwave-assisted and conventional heating methods. Clearly, the electrode surfaces made by microwave-assisted at energy intensity 400 W/g, 800 W/g compare with the conventional heating route are difference, which are shown in Figure 4-20 (a). The morphology of the electrode made by conventional method seems mud-cracks (average crack width 1.5 µm) and porous, while the electrodes under microwave synthesis show the bigger crack sizes (average crack width is 2 µm), shaped island-gap and more compact structure, respectively. Each island on the microwave-assisted electrode consists of close-packed catalyst nanoparticles. In this case, the size of the cracks can be regarded as a sort of porosity whose sizes influence mass transfer into the inner part of the catalyst layer and proton exchange during the charge uniform assembly of nanoparticles architecture. The formation of the crack structure is generally attributed to the thermally induced tensile stress during the stage of solvent evaporation. The shrinkage of the xerogel body during the thermal processing is restricted by the underlying Ti substrate. Once the developed stresses exceed the tensile strength of the gel body, cracks develop to release the stress [5].

The homogeneous distribution of nanoparticles is observed from TEM images, which is clearly seen in the Figure 4-20 (b). Due to the annealing temperature, the water molecules in hydrous form are removed and well defined crystals of mixing

RuO_2-TiO_2 is obtained. The crystal size of RuO_2-TiO_2 nanoparticles made by microwave synthesis show more uniform and smaller sizes than the electrode made by conventional heating method. The average diameter of RuO_2 particles with microwave-assisted synthesis at 400 W/g are in the order of 8-10 nm, while the conventional heating method shows a big range from 15-20 nm of particles size. Moreover, the distribution of particle diameter size is bigger when the microwave energy increases (around 12-14 nm with microwave energy intensity 800 W/g). This can be attributed to the high energy absorption can lead to the agglomeration of nanoparticle by the reducing of hydrous. It was reported that the absence of structural water may result in the coalescence and growth of RuO_2-TiO_2 nanoparticles to form larger crystal [151]. Note the presence of a clearly lattice spacing on certain particulates, corresponding to TiO_2 crystallites. Ti species are relatively concentrated in the central portion, whereas the density of Ru species is slightly higher in the outer portion of this composite although the distributions of both Ti and Ru are uniform. The above results suggest that RuO_2 and TiO_2 should be formed independently under the sol-gel hydrothermal environment. Because crystalline TiO_2 can be formed in aqueous media at room temperature but crystalline RuO_2 could only be formed at 80°C under the microwave irradiation or thermal heating. This effect is believed to enhance the exposure of RuO_2 in the electrolyte, leading to high RuO_2 catalyst utilization [150]. The reduce of crystal size and the increase of crack sizes in the SEM imagines may increase the outer and total active surface area of the electrodes made by microwave-assisted

synthesis than the conventional method. In general, the microwave route produces RuO_2-TiO_2 nanoparticle can reduce the synthesis time and a better control of the temperature resulting in uniform RuO_2-TiO_2 nanoparticles which could induce the higher current density observed in chlorine evolution than the conventional procedure. The understanding of the microwave interaction with materials has been based on concepts of dielectric heating and of the resonance absorption due to rotational excitation [148]. The temperature is raised more uniformly throughout whole liquid volume (in-core volumetric heating) under microwave irradiation compare to conventional route is the explanation for this observation.

The diffraction patterns obtained by XRD analysis for RuO_2-TiO_2 electrodes made by difference microwave energy intensities and conventional heating methods are shown in Figure 4-21. The XRD spectra suggest that the oxide nanoparticles in all case are fine and crystalline structure in a set of broad and nearly symmetrical peaks. This indicates the formation of a solid solution, which is desired in terms of electrode stability. The typical peaks of rutile RuO_2 metal oxide are easily detected as: 110, 101 planes at about 28^o and 35^o in all of the electrodes. The most intense peak is 110. Because the catalyst layers are thin, so that X-ray can penetrates through the coating layers and the absorption peaks of Ti metal can be realized. TiO_2 metal oxide crystals are presented in both anatase and rutile structures. No evidence of Ruthenium metallic phase was observed, which can be found at the higher microwave energy because of Ruthenium reduction [148]. The

width of the RuO_2 peaks from the diffraction profiles show very consistent with the crystal size of the RuO_2 nanoparticles measured by TEM imagines, agrees to Scherrer equation [117].

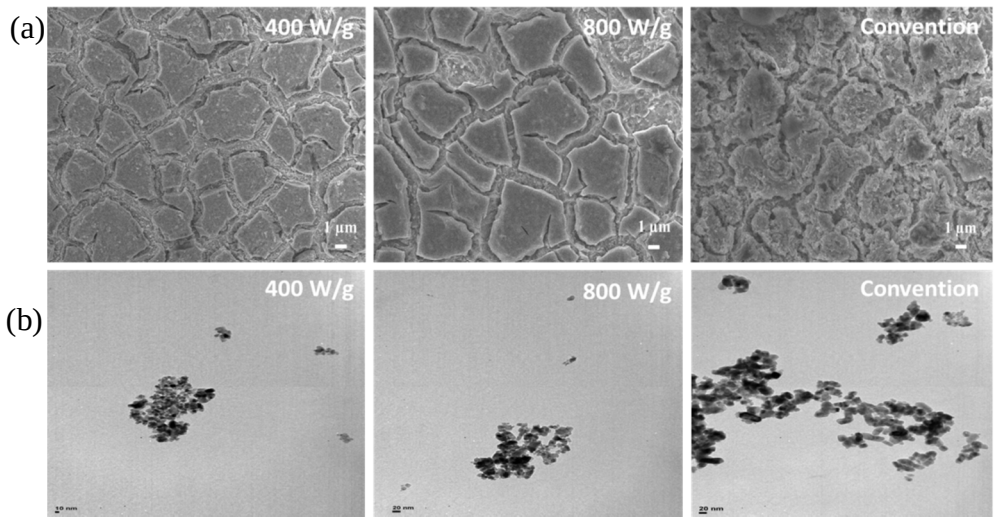

Fig. 4-20. SEM (a), TEM (b) imagines and of RuO_2-TiO_2 electrodes made by microwave-assisted and conventional heating methods.

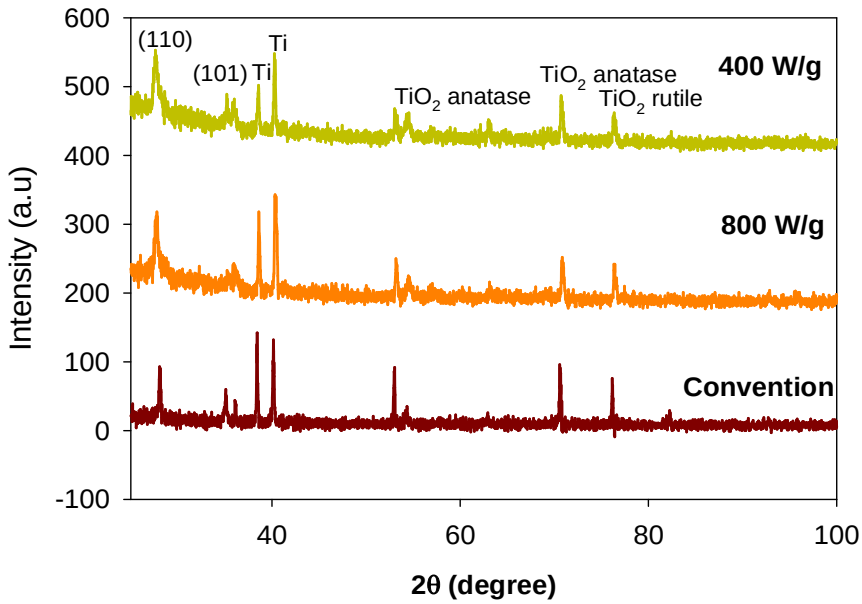

Fig. 4-21. XRD spectra of RuO_2-TiO_2 electrodes made by microwave-assisted and conventional methods.

4.5.4. CV and active surface area

In order to measure the electrochemically active surface area, cyclic voltammetric curves were recorded in the pseudo-capacitive potential range of RuO_2. Figure 4-22 shows the cyclic voltammogram (a) and extrapolated voltammetric charge values (b) from a set of RuO_2-TiO_2 electrodes. As shown in Fig. 4-22 (a), all CV curves are almost symmetrical to zero potential line. Note that the rectangular shape of the cyclic voltammetry of RuO_2-TiO_2 electrodes remains unchanged with scan rate, indicating the good reversibility (redox reaction) of the system resulting from the insignificant iR (ohmic drop) loss. The currents densities from cyclic voltammograms increase in case of the electrodes made by microwave synthesis than the conventional heating method. But the current density decreases when the microwave energy increase from 400 W/g to 800 W/g.

Figure 4-22 (b) shows the extrapolated voltammetric charge q values from a set of RuO_2-TiO_2 electrodes. Since the formations of electrode's morphologies are difference, an effect on the total and outer surface area should be visible. The surface area (voltammetric charge) decrease with the increase of scan rate, which mean that the difficulty of the electrolyte to penetrate to the inner surface of the electrode likes micropore, microcrack, grain boundary. The results show that the q values of the total and outer surface area increase with the order of convention < 800 W/g < 400 W/g, respectively. This is very consistent with the current intensities of these electrodes in cyclic voltammograms. The increasing of the

crack sizes and decreasing of crystal sizes with the electrodes made by microwave synthesis are the explanation of this order.

The total voltammetric charges of microwave-assisted electrodes at 400 W/g, 800 W/g are 35.38 mC/cm^2, 28.92 mC/cm^2 compare to conventional electrode 26.07 mC/cm^2. While the value of outer voltammetric charges are 24.86 mC/cm^2, 22.12 mC/cm^2 and 15.06 mC/cm^2, respectively. Microwave-assisted synthesis method can improve the total and outer surface area of RuO_2-TiO_2 electrodes compare to the conventional procedure. However, when the microwave energy increases, the total and outer surface areas decrease because of the increase of crystal sizes. Note that the outer surface area is more importance that the total surface area in chlorine evolution [14-18]. The electrode made by microwave synthesis shows the higher outer surface area than conventional heating method, so that the chlorine evolution efficiencies are higher.

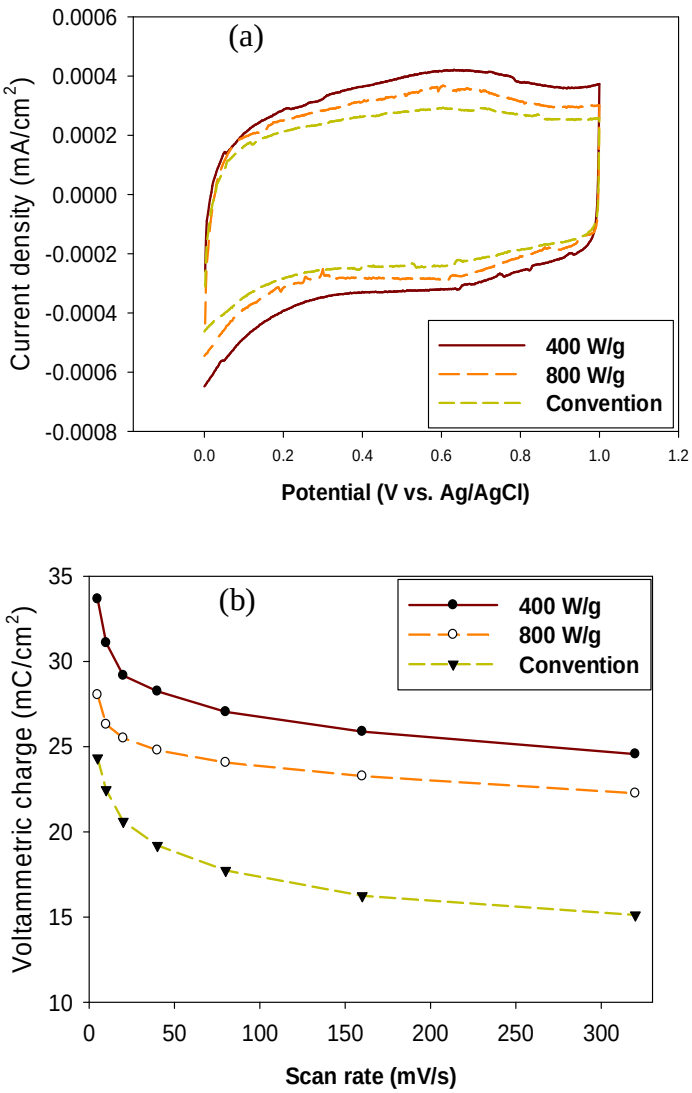

Fig. 4-22. Cyclic voltammetry (a) in 0.5 M H_2SO_4, scan rate 5 mV/s and charge densities (b) at difference scan rates of RuO_2-TiO_2 electrodes made by microwave-assisted and conventional methods.

4.5.5. Accelerated stability test (AST)

In the electrochemical production of chlorine, it is undoubtedly the stability that plays the most important role. The sustainability of the electrode's electro-catalytic capability strongly relies on high electrode stability. Vigorous gas evolution takes place in the solution used in the AST. The applied conditions favor oxygen evolution, which makes the investigated coating less stable than under conditions convenient to chlorine evolution [11]. AST supply the fast information about the electrode's stability. The electrode lifetime in the stability test is defined by the time at which the potential of an anode suddenly escalates under galvanostatic conditions in simultaneous oxygen and chlorine evolution reactions. Figure 4-23 shows the time dependencies of the electrode potential and the appropriate differential curves for the anodes prepared by the microwave-assisted and conventional heating methods. The life time of the RuO_2-TiO_2 electrodes made by microwave synthesis (up to 230 minutes) show the longer service life than the electrode made by conventional heating method (150 minutes). The working life of RuO_2-TiO_2 electrodes made by microwave at 400 W/g is longer than 800 W/g under the same electrolysis condition.

The reason for this observation could either be the larger surface area of the microwave-assisted prepared anodes or the different mechanisms of the catalytic activity loss or both. Two paths for the loss of the electrocatalytic activity have been suggested [94, 96]:

1. The erosion of the coating: simultaneous electrochemical oxidation of Ru species in the coating forming the soluble products move to the electrolyte.

2. The penetration of the electrolyte through pores and cracks toward the substrate, which produces insulating TiO_2 grains on the interface by oxidation of the substrate.

The morphology of the coating may favor any or all of them together. The oxide particles size is smaller and the distributions are more uniform in the case of the microwave synthesis procedure, which produces a larger surface area than in the conventional method. The smaller nanoparticles sizes help the stronger coalescence and connectivity of each nanoparticle, increase the stability. Consequently, the rate of dissolution of the Ru species on the anode obtained by the microwave-assisted procedure is lower. In the same manner, the structures of the catalytic coating of the microwave synthesis prepared anodes are more compact and penetration of the electrolyte toward the titanium substrate is limited. Then it allows less non-conductive intermediate TiO_2 layer formation as compared to the conventional heating anode. Then the erosion of the microwave-assisted electrodes is lower than the conventional heating electrode. It should be noted that the service life mentioned above was obtained in the accelerated life test. Under normal operating conditions (e.g., at current density below 1 A cm^{-2}), the thick electrode would be stable for several years according to many reports [4, 5].

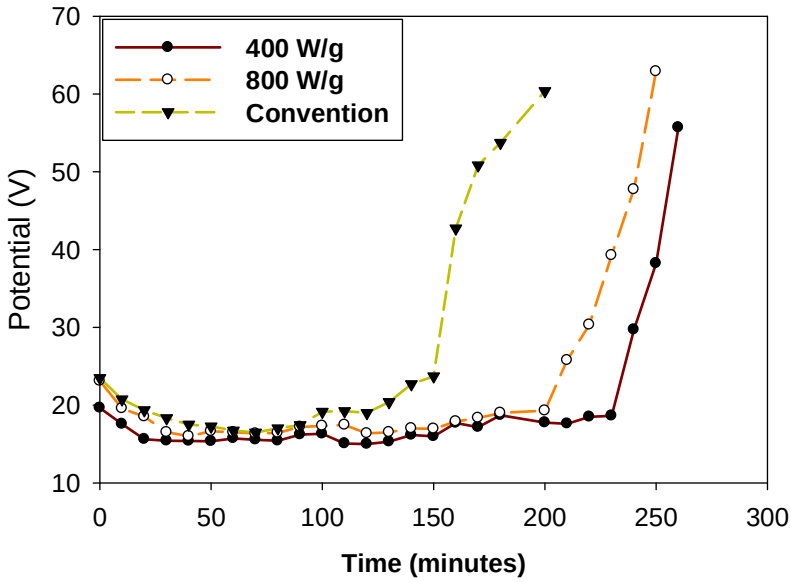

Fig. 4-23. The AST of RuO_2–TiO_2 electrodes prepared by the microwave-assisted and conventional heating methods. Experimental condition: 0.5 M NaCl, pH 2, t = 25^{o}C, current density: 1 A cm^{-2}.

4.5.6. Conclusions

The novel microwave-assisted synthesis RuO_2-TiO_2 electrodes by sol-gel method show considerably higher chlorine evolution efficiency and stability than for those obtained by the conventional heating method. The most importance improvement of microwave-assisted synthesis is the increase of outer active surface area compare to the conventional method. Microwave-assisted synthesis method is rapid, clean, cheap, resulting in uniform, small crystalline size, compact structure and big crack size RuO_2-TiO_2 nanostructures. Increasing of microwave energy intensity reduces efficiency, stability with chorine evolution because of the increasing crystal size. This research proposes a new approach for green synthesis the most popular RuO_2-TiO_2 electrode for chlor-alkaline industry in the future.

5. Summaries and conclusions

This dissertation developed the novel advance RuO_2-based electrocatalysts exhibit an extraordinary surface morphology which provides a high active surface area, improves the catalyst utilization and mass transfer comparing to conventional electrocatalysts, then followed the understanding the mechanism of the electrochemical chlorine evolution at the interface electrode - electrolyte. Lastly, the developments of RuO_2 electrode by using alternative green preparation routes sonoelectrodeposition with control the coating structure, reduce the cost, time, increase the chlorine evolution efficiency and stability can be achieved:

- The effect on chlorine evolution was investigated by focusing on the preparation parameters of the RuO_2 electrodes which included solvents, precursors and calcination times using the thermal decomposition method. It was investigated that using ethanol as solvent played the most critical factor for increasing the chlorine evolution efficiency of the RuO_2 electrode. Using $Ru(AcAc)_3$ as precursor and increase the calcination to 3 h are also the good choices for increasing chlorine electrocatalytic activities. It can be explained that the increasing number and size of the cracks on the electrode surfaces or the outer voltammetric charges were caused by the easily evaporated solvents, decomposed precursors and tensile stress under longer thermal treatments. The chlorine evolution efficiency was not significantly related to the total voltammetric charge but the outer voltammetric charge.

- The RuO_2 nanorod and nanosheet electrodes were synthesized with tailored architecture using organic templates and make the comparison with the conventional nanograin electrode. The organic template precursors as sodium dodecyl sulfate or polyethylene glycol surfactant played a major role in controlling the morphology of RuO_2 electrodes. We have demonstrated that the templated RuO_2 nanorod and nanosheet electrodes can be used as efficient electrocatalyst for chlorine evolution reactions, which show better activity than the nanograin electrode. The chlorine evolution efficiencies increase up to 20% in case of nanorod electrode and 35% in case of nanosheet electrode in comparison with nanograin electrode. These results could be attributed to the better mass transport of RuO_2 nanorod and nanosheet electrodes in comparison with the conventional nanograin electrode, allow more effective surface area to participate in the chlorine evolution reaction. The templated RuO_2 nanorod and nanosheet electrodes are promising materials for high-electrocatalytic performance and reducing the energy consumption in the future chlor-alkali industry.
- Successful fabricated highly electrocatalytically active RuO_2-TiO_2 electrodes for chlorine evolution with a structural ordered macroporous framework using PS microsphere templates (0.1 ~ 1.1 μm). The chlorine evolution efficiency of the macroporous RuO_2-TiO_2 electrodes was up to approximately 1.5 times higher than that of the nontemplated electrode at the same Ru loadings. Interestingly, in the macroporous RuO_2-TiO_2 electrode with the specific templated pore size of PS 0.46 μm, and not that of PS 1.1 μm or PS 0.1 μm, the outer surface area was the most

well-developed, and it led to the highest chlorine evolution efficiency in this study, indicating the existence of an optimal macropore size for an effective chlorine evolution reaction. This result could be attributed to the structural properties of the macroporous electrodes providing easy mass transfer and removal of chlorine gas bubbles with good control over the pore size and pore walls connectivity. The macroporous RuO_2-TiO_2 electrodes can be considered as promising anode materials with high chlorine evolution efficiency and reduced the energy consumption in the future chlor-alkali industry.

- The sonoelectrodeposition synthesis of RuO_2 electrodes was report for the first time for chlorine evolution. The electrodes obtained by the sonoelectrodeposition procedure present a strong improvement about the electrocatalyst efficiency and stability with chlorine evolution in comparison with the one made by conventional stirring electrodeposition. Sonoelectrodeposition can increase the outer surface area of RuO_2 electrodes than the conventional procedure, significance for chlorine evolution enhancement. Increasing of sonoelectrodeposition time of RuO_2 electrode, the chlorine evolution efficiency and electrode's stability also increase. By using sonoelectrodeposition technique, we can successfully synthesize RuO_2 electrodes with broad hemispheres, mushroom-like, and compact structures. Sonoelectrodeposition method also can produce large amount of RuO_2 nanoparticles with more uniform and smaller crystal sizes than the mechanical stirring procedure. Ru metal, which is undesired composition in DSA, is not present by using sonoelectrodedosition route. The critical effect is the increasing of

mass transport, which is high enough to decrease the diffusion layer into a charge controlled system by the capable of degassing produced H_2 free adherent surfaces.

- The novel microwave-assisted synthesis RuO_2-TiO_2 electrodes by sol-gel method show considerably higher chlorine evolution efficiency and stability than for those obtained by the conventional heating method. The most importance improvement of microwave-assisted synthesis is the increase of outer active surface area compare to the conventional method. Microwave-assisted synthesis method is rapid, clean, cheap, resulting in uniform, small crystalline size, compact structure and big crack size RuO_2-TiO_2 nanostructures. Increasing of microwave energy intensity reduces efficiency, stability with chorine evolution because of the increasing crystal size. Microwave-assisted synthesis sol-gel proposes a new approach for green synthesis the most popular RuO_2-TiO_2 electrode for chlor-alkaline industry in the future.

References

[1]. P. Schmittinger, Chlorine: principle and industrial practice, Wiley, New York, 2000, 21-34.

[2]. V. Srinivasan, P. Arora, P. Ramadass, Report on the electrolytic industries for the year 2004, J. Electrochem Soc. 153 (2006) K1.

[3]. M. Kerwick, S. Reddy, A. Chamberlain, D. Holt, Electrochemical disinfection, an environmentally acceptable method of drinking water disinfection? Electrochim. Acta 50 (2005) 5270-5277.

[4]. H. Over, Atomic scale insights into electrochemical versus gas phase oxidation of HCl over RuO_2-based catalysts: A comparative review, Electrochim. Acta 93 (2013) 314–333.

[5]. R. Chen, V. Trieu, B. Schley, H. Natter, J. Kintrup, A. Bulan, R. Weber and R. Hempelmann, Anodic electrocatalytic coatings for electrolytic chlorine production: A review**,** Z. Phys. Chem. 227 (2013) 651-666.

[6]. H. Beer, The invention and industrial development of metal anodes, J. Electrochem. Soc. 127 (1980) 303C-307C.

[7]. S. Trasatti, Electrocatalysis: understanding the success of DSA@, Electrochim. Acta 45 (2000) 2377-2385.

[8]. P. Hayfield, Development of the noble metal/oxide coated Titanium electrode,

Part 1: The beginning of the story, Platinum Met. Rev. 42 (1998) 27-33.
[9]. Y. Matsumoto, E. Sato, Electrocatalytic properties of transition metal oxides for the oxygen evolution reaction, Mater. Chem. Phys. 14 (1986) 397-426.

[10]. J. Jeong, C. Kim, J. Yoon, The effect of electrode material on the generation of oxidants and microbial inactivation in the electrochemical disinfection processes, Water Res. 43 (2009) 895–901.

[11]. B. Zhan, M. White, T. Sham, J. Pincock, R. Doucet, K. Rao, K. Robertson, T. Cameron, Zeolite-confined nano-RuO_2: A green, selective, and efficient catalyst for aerobic alcohol oxidation, J. Am. Chem. Soc. 125 (2003) 2195-2199.

[12]. H. Over, Ruthenium dioxide, a fascinating material for atomic scale surface chemistry, Appl. Phys. A 75 (2002) 37-44.

[13]. S. Trasatti and G. Lodi, Electrodes of conductive metallic oxides, Part A and Part B, Elsevier, Amsterdam, 1980.

[14]. S. Trasatti, Electrocatalysis in the anodic evolution of oxygen and chlorine, Electrochim. Acta 29 (1984) 1503–1512.

[15]. S. Ardizzone, G. Fregonara, S. Trasatti, Inner and outer active surface of RuO_2 electrodes, Electrochim. Acta 35 (1990) 263-267.

[16]. L. Burke and J. O'Neill, Some aspects of the chlorine evolution reaction at Ruthenium dioxides anodes, J. Electroanal. Chem. 101 (1979) 341-349.

[17]. A. R. Zeradjanin, F. L. Mantia, J. Masa, W. Schuhmann, Utilization of the catalyst layer of dimensionally stable anodes - Interplay of morphology and active surface area, Electrochim. Acta 82 (2012) 408-414.

[18]. S. Ardizzone, A. Carugati, G. Lodi, S. Trasatti, Surface structure of Ruthenium dioxide electrodes and kinetics of chlorine evolution, J. Electrochem. Soc. 129 (1982) 1689-1693.

[19]. M. Gopiraman, S. Babu, Z. Khatri, K. Wei, M. Endo, R. Karvembu and I. Kim, Facile and homogeneous decoration of RuO_2 nanorods on graphene nanoplatelets for transfer hydrogenation of carbonyl compounds, Catal. Sci. Technol. 3 (2013) 1485.

[20]. H. Friedrich, P. Jongh, A. Verkleij and K. Jong, Electron tomography for heterogeneous catalysts and related nanostructured materials, Chem. Rev. 109 (2009) 1613-1626.

[21]. R. Liu, J. Duay and S. Lee, Heterogeneous nanostructured electrode materials for electrochemical energy storage, Chem. Commun. 47 (2011) 1384–1404.

[22]. J. Tiwari, R. Tiwari, K. Kim, Zero-dimensional, one-dimensional, two-dimensional and three-dimensional nanostructured materials for advanced electrochemical energy devices, Prog. Mater. Sci. 57 (2012) 724–803.

[23]. J. Chou, Y. Chen, M. Yang, Y. Chen, C. Lai, H. Chiu, C. Lee, Y. Chueh and J.

Gan, RuO_2/MnO_2 core–shell nanorods for supercapacitors, J. Mater. Chem. A 1 (2013) 8753-8759.

[24]. D. Music, J. Breunung, S. Mraz, and J. Schneider, Role of RuO_3 for the formation of RuO_2 nanorods, Appl. Phys. Lett. 100 (2012) 033108.

[25]. G. Zhao, L. Zhang, K. Sun, H. Li, Free-standing $Pt@RuO_2.xH_2O$ nanorod arrays on Si wafers as electrodes for methanol electro-oxidation, J. Power Sources 245 (2014) 892-897.

[26]. S. Neupane, G. Kaganas, R. Valenzuela, L. Kumari, X. Wang, W. Li, Synthesis and characterization of ruthenium dioxide nanostructures, J. Mater. Sci. 46 (2011) 4803–4811.

[27]. Y. Lee, B. Kim, H. Jung, J. Shim, Y. Lee, C. Lee, J. Baik, W. Kim, M. Kim, Hierarchically grown single crystalline RuO_2 nanorods on vertically aligned few walled carbon nanotubes, Mater. Lett. 89 (2012) 115–117.

[28]. J. Han, S. Lee, S. Kim, S. Han, C. Hwang, C. Dussarrat, and J. Gatineau, Growth of RuO_2 thin films by pulsed-chemical vapor deposition using RuO_4 precursor and 5% H_2 reduction gas, Chem. Mater. 22 (2010) 5700–5706.

[29]. M. T. Colomer and J. R. Jurado, Structural, microstructural, and electrical transport properties of TiO_2−RuO_2 ceramic materials obtained by polymeric sol−gel route, Chem. Mater. 12 (2000) 923–930.

[30]. A. Terezo, E. Pereira, Preparation and characterization of Ti/RuO_2 anodes obtained by sol–gel and conventional routes, Mater. Lett. 53 (2002) 339-345.

[31]. J. Ribeiro, M. Moats, A. Andrade, Morphological and electrochemical investigation of RuO_2–Ta_2O_5 oxide films prepared by the Pechini–Adams method, J. Appl. Electrochem. 38 (2008) 767-775.

[32]. J. Jorissen, T. Turek, R. Weber, Energy savings in the electrolysis chlorine production with oxygen depolarized cathode, Chem. Unserer Zeit. 45 (2011) 172-176.

[33]. F. Gestermann, A. Ottaviani, Chlorine production with oxygen-depolarised cathodes on an industrial scale, Modern Alkali Technology. Oxford, UK, 8 (2001) 49-55.

[34]. L. Janssen, Kinetics and mechanism of chlorine evolution on metal oxide electrodes by RuO_2-TiO_2 electrode, Electrochim. Acta 29 (1984) 1607-1612.

[35]. F. Cotton, G. Wilkinson, C. Murillo, M. Bachmann, Advanced Inorganic Chemistry, John Wiley & Sons, Inc: New York, 1999.

[36]. K. Reuter, M. Scheffler, Composition, structure, and stability of RuO_2 (110) as a function of oxygen pressure, Phys. Rev. B 65 (2001) 035406.

[37]. J. Haines, J. Leger, O. Schulte**,** Pa3 modified Fluorite-type structures in metal dioxides at high pressure, Science 271 (1996) 629-631.

[38]. U. Lundin, L. Fast, L. Nordstrom, B. Johansson, M, Wills, O. Eriksson,

Transition metal dioxide with a bulk modulus comparable to diamond, Phys. Rev. B 57 (1998) 4979-4982.

[39]. W. Ryden, A. Lawson, C. Sartain, Electrical transport properties of IrO_2 and RuO_2, Phys. Rev. B 4 (1970) 1494-1500.

[40]. P. Soratin, K. Schwarz, Chemical bonding in rutile-type compounds**,** Inorg. Chem. 31 (1992) 567-576.

[41]. P. Cox, Transition metal oxides: an introduction to their electronic structure and properties, Oxford University Press, Oxford, 1995.

[42]. Y. Takasu, W. Sugimoto, Y. Nishiki, S. Nakamatsu, Structural analyses of RuO_2-TiO_2/Ti and IrO_2–RuO_2–TiO_2/Ti anodes used in industrial chlor-alkali membrane processes, J. Appl. Electrochem. 40 (2010) 1789–1795.

[43]. H. Over, Surface chemistry of Ruthenium dioxide in heterogeneous catalysis and electrocatalysis: from fundamental to applied research, Chem. Rev. 112 (2012) 3356–3426.

[44]. S. Trasatti, Oxide/aqueous solution interfaces, interplay of surface chemistry and electrocatalyst, Mater. Chem. Phys. I6 (1987) 157-114.

[45]. C. Iwahra, K. Hirao and H. Tamura, Preparation of Ruthenium dioxide electrodes and their anodic polarization characteristics in acidic solutions, Electrochim. Acta 22 (1977) 335-340.

[46]. T. Arikado, C. Iwakura, and H. Tamura, Electrochemical behavior of the Ruthenium oxide electrode prepared by thermal decomposition method, Electrochim. Acta 22 (1977) 513-518.

[47]. S. Trasatti, Physical electrochemistry of ceramic oxides, Electrochim. Acta 36 (1991) 225-241.

[48]. S. Ardizzone, A. Daghetti, L. Franceschi and S. Trasatti, The point of zero charge of hydrous RuO_2, Colloids Surf. 35 (1989) 85-96.

[49]. P. Siviglia, A. Daghetti and S. Trasatti, Influence of the preparation temperature of Ruthenium dioxide on its point of zero charge, Colloids Surf. 7 (1983) 16-27.

[50]. P. Castelli, S. Trassati, F. Pollak, W. O'Grady, Single crystals as model electrocatalysts oxygen evolution on RuO_2 (110), J. Electroanal. Chem. 210 (1986) 189-194.

[51]. S. Trasatti, O. Petrii, Real surface area measurements in electrochemistry, Pure Appl. Chem. 63 (1991) 711.

[52]. V. Trieu, B. Schleya, H. Nattera, J. Kintrup, A. Bulan, R. Hempelmann, RuO_2-based anodes with tailored surface morphology for improved chlorine electro-activity, Electrochim. Acta 78 (2012) 188–194.

[53]. J. Fernandez, M. Chialvo, A. Chialvo, Kinetic study of the chlorine electrode reaction on Ti/RuO_2 through the polarization resistance, Part III: proposal of a reaction mechanism, Electrochim. Acta 47 (2002) 1145–1152.

[54]. D. Demon, J. Harrison and R. Knowles, Automation of electrode kinetic IV. The chlorine evolution reaction on a RuO_2-TiO_2 plate electrode, Electrochim. Acta 25 (1978) 1147-1152.

[55]. L. Janssen, Kinetics and mechanism of chlorine evolution on metal oxide electrodes by RuO_2-TiO_2 electrode, Electrochim. Acta 29 (1984) 1607-1612.

[56]. T. Hepel, F. Pollak and W. O'Grady, Chlorine evolution and reduction processes at oriented single crystal RuO_2 electrodes, J. Electrochem. Soc. 133 (1986) 69-75.

[57]. T. Arikado, C. Iwakura, H. Tamura, A consideration of the electrochemical mechanism in the chlorine evolution reaction, Electrochim. Acta 23 (1977) 799-801.

[58]. T. Arikado, C. Iwakura and H. Tamura, Some oxide catalysts for the anodic evolution of chlorine: reaction mechanism and catalytic activity, Electrochim. Acta 23 (1978) 9-15.

[59]. M. Inai, C. Iwakura, H. Tamura, A consideration of the activation energy for the chlorine evolution reaction on RuO_2 and IrO_2 electrodes, Electrochim. Acta 24 (1979) 993–996.

[60]. A. Zeradjanin, N. Menzel, P. Strasser and W. Schuhmann, Role of water in the chlorine evolution reaction at RuO_2-based electrodes - Understanding electrocatalysis as a resonance phenomenon, ChemSusChem 5 (2012) 1897–1904.

[61]. S. Jordanov, B. Conway, Unusual aspects of anodic Cl_2 evolution behaviour at RuO_2 electrodes below room temperature, J. Electroanal. Chem. 326 (1992) 177-195.

[62]. J. Jirkovsky, H. Hoffmannova, M. Klementova and P. Krtil, Particle size dependence of the electrocatalytic activity of nanocrystalline RuO_2 electrodes, J. Electrochem. Soc. 153 (2006) 111-118.

[63]. S. Trasatti, Progress in the understanding of the mechanism of chlorine evolution at oxide electrodes, Electrochim. Acta 32 (1987) 369-382.

[64]. N. Munichandraiah, Electrocatalysis, J. Ind. Inst. Sci. 90 (2010) 261-270.

[65]. L Miller, M. Krenz and R. Landsberg, On the liquid boundary layer near the electrode surface during chlorine evolution, J. EIectroanal. Chem. 180 (1984) 453.

[66]. S. Evdokimov, Kinetics of chlorine evolution on dimensionally stable anodes at high currents: Extending the concept of a self-accelerating electrode process, Russ. J. Electrochem. 36 (2000) 236-239.

[67]. V. Eberil, E. Novikov, A. Mazanko, Reasons for the DSA passivation during chlorate electrolysis and the means for extending the anode service life, Russ. J. Electrochem. 37 (2001) 1054–1058.

[68]. F. Hine, M. Yasuda, T. Noda, T. Yoshida, J. Okuda, Electrochemical behavior of the oxide-coated metal anodes, J. Electrochem. Soc. 126 (1979) 1439.

[69]. C. Comninellis, G. Verceti, Characterization of DSA oxygen evolving electrodes: choice of a coating, J. Appl. Electrochem. 21 (1991) 335-345.

[70]. Y. Takasu, K. Sukalmk, A. Ishimurat, A. Iromine and K. Yahikozawa, An application of the thermal desorption method to the surface characterization of RuO_2-IrO_2 and RuO_2-TiO_2 coated Titanium electrodes, Electrochim. Acta 37 (1992) 1029-1031.

[71]. L. Faria and S. Trasatti, Effect of composition on the point of zero charge of RuO_2 + TiO_2 mixed oxides, J. Electroanal. Chem. 340 (1992) 145-152.

[72]. K. Macounova, M. Makarova, J. Jirkovsky, J. Franc, P. Krtil, Parallel oxygen and chlorine evolution on $Ru_{1-x}Ni_xO_2$ nanostructured electrodes, Electrochim. Acta 53 (2008) 6126–6134.

[73]. L. Burke and M. McCarthy, Oxygen gas evolution at a deterioration of RuO_2/ZrO_2-coated Titanium anodes at elevated temperature in strong base, Electrochim. Acta 29 (1984) 211-216.

[74]. R. Kotz and S. Stuck, Stabilization of RuO_2 by IrO_2 for anodic oxygen evolution in acid media, Electrochim. Acta 31 (1986) 1311-1316.

[75]. A. Battisti, R. Brina, G. Gavelli, A. Benedetti, G. Fagherazzi, Influence of the valve metal oxide on the properties of Ruthenium based mixed oxide electrodes, Part I. Titanium supported RuO_2-Ta_2O_5 layers, J. Electroanal. Chem. 200 (1985) 93-104.

[76]. T. Lassali, S. Castro and J. Boodts, Structural, morphological and surface properties as a function of composition of Ru + Ti + Pt mixed-oxide electrodes, Electrochim. Acta 43 (1998) 2515-2525.

[77]. L. Silva, J. Boodts, L. Faria, ‘In situ’ and ‘ex situ’ characterization of the

surface properties of the $RuO_{2(x)}Co_3O_{4\ (1-x)}$ system, Electrochim. Acta 45 (2000) 2719–2727.

[78]. X. Chen, G. Chen, Stable Ti/RuO_2–Sb_2O_5–SnO_2 electrodes for O_2 evolution, Electrochim. Acta 50 (2005) 4155–4159.

[79]. K. Fernandes, L. Silva, J. Boodts, L. Faria, Surface, kinetics and electrocatalytic properties of the Ti/(Ti+Ru+Ce)O_2-system for the oxygen evolution reaction in alkaline medium, Electrochim. Acta 51 (2006) 2809–2818.

[80]. M. Santana, L. Faria, Oxygen and chlorine evolution on RuO_2 +TiO_2 + CeO_2 + Nb_2O_5 mixed oxide electrodes, Electrochim. Acta 51 (2006) 3578–3585.

[81]. J. Aromaa, O. Forsen, Evaluation of the electrochemical activity of a Ti–RuO_2 –TiO_2 permanent anode, Electrochim. Acta 51 (2006) 6104–6110.

[82]. L. Faria, J. Boodts and S. Trasatti, Electrocatalytic properties of Ru + Ti + Ce mixed oxide electrodes for the Cl_2 evolution reaction**,** Electrochim. Acta 42 (1997) 3525-3530.

[83]. V. Petrykina, K. Macounova, M. Okubea, S. Mukerjeec, P. Krtil, Local structure of Co doped RuO_2 nanocrystalline electrocatalytic materials for chlorine and oxygen evolution, Catal. Today 202 (2013) 63–69.

[84]. L. Gomez, S. Ferro, A. Battisti, Preparation and characterization of RuO_2–IrO_2–SnO_2 ternary mixtures for advanced electrochemical technology, Appl. Catal. B 67 (2006) 34–40.

[85]. X. Zeng, M. Zhang, X. Wanga, X. Chen, X. Su, W. Tang, Effects of Sn content on Ti/RuO_2–SnO_2–TiO_2 anodes used in the generation of electrolyzed

oxidizing water, J. Electroanal. Chem. 677 (2012) 133–138.

[86]. C. Hu, C. Lee, T. Wen, Oxygen evolution and hypochlorite production on Ru-Pt binary oxides**,** J. Appl. Electrochem. 26 (1996) 72-82.

[87]. S. Hoseinieh, F. Ashrafizadeh and M. Maddahi, A comparative investigation of the corrosion behavior of RuO_2–IrO_2–TiO_2 coated Titanium anodes in chloride solutions**,** J. Electrochem. Soc. 1574 (2010) E50-E56.

[88]. G. Chen, X. Chen, and P. Yue, Electrochemical behavior of novel Ti/IrO_x-Sb_2O_5-SnO_2 anodes, J. Phys. Chem. B 106 (2006) 4364-4369.

[89]. L. Naslund, C. Sanchez, A. Ingason, J. Backstrom, E. Herrero, J. Rosen and S. Holmin, The role of TiO_2 doping on RuO_2 coated electrodes for the water oxidation reaction, J. Phys. Chem. C 117 (2013) 6126−6135.

[90]. C. Comninellis and G. Chen (2010) Electrochemistry for the Environment, Springer, 55-69.

[91]. L. D. Burke and N. S. Naser, Metastability and electrocatalytic activity of ruthenium dioxide cathode used in water electrolysis cells, J. Appl. Electrochem. 35 (2005) 931-938.

[92]. Z. Yi, C. Kangning, W. Wei, J. Wang, S. Lee, Effect of IrO_2 loading on RuO_2–IrO_2–TiO_2 anodes: A study of microstructure and working life for the chlorine evolution reaction, Ceram. Int. 33 (2007) 1087–1091.

[93]. R. Burrows, D. Denton, J. Harrison, Chlorine and oxygen evolutions on various compositions of RuO_2/TiO_2 electrodes, Electrochim. Acta 23 (1978) 493-500.

[94]. V. Panic, A. Dekanski, S. Milonjic, R. Atanasoski, B. Nikolic, RuO_2–TiO_2 coated titanium anodes obtained by the sol–gel procedure and their electrochemical behaviour in the chlorine evolution reaction, Colloids Surf. A 157 (1999) 269–274.

[95]. J. Osmana, J. Crayston, A. Pratt, D. Richens, RuO_2–TiO_2 mixed oxides prepared from the hydrolysis of the metal alkoxides, Mater. Chem. Phys. 110 (2008) 256–262.

[96]. V. Panic, A. Dekanski, M. Stankovic, S. Milonjic, B. Nikoli, On the deactivation mechanisms of RuO_2–TiO_2/Ti anodes prepared by the sol–gel procedure, J. Electroanal. Chem. 579 (2005) 67–76.

[97]. R. Chen, V. Trieu, H. Natter, K. Stowe,W. Maier, R. Hempelmann, A. Bulan, J. Kintrup, and R. Webe, In situ supported nanoscale $Ru_xTi_{1-x}O_2$ on anatase TiO_2 with improved electroactivity, Chem. Mater. 22 (2010) 6215–6217.

[98]. R. Chen, V. Trieu, A. Zeradjanin, H. Natter, D. Teschner, A. Bulan, J. Kintrup, W. Schuhmann, R. Hempelmann, Microstructural impact of anodic coatings on the electrochemical chlorine evolution reaction, Phys. Chem. Chem. Phys. 14 (2012) 7392-7399.

[99]. M. Vukovic, Oxygen evolution on an electrodeposited Ruthenium electrode in acid solution - the effect of thermal treatment, Electrochim. Acta 34 (1989) 287-291.

[100]. M. Metikos-Hukovic, R. Babic, F. Jovic, Z. Grubac, Anodically formed oxide films and oxygen reduction on electrodeposited ruthenium in acid solution,

Electrochim. Acta 51 (2006) 1157–1164.

[101]. C. Hu, H. Guo, K. Chang and C. Huang, Anodic composite deposition of $RuO_{2x}H_2O$-TiO_2 for electrochemical supercapacitors, Electrochem. Commun. 11 (2009) 1631-1634.

[102]. J. Jowa, H. Lee, H. Chena, M. Wu, T. Wei, Anodic cathodic and cyclic voltammetric deposition of ruthenium oxides from aqueous $RuCl_3$ solutions, Electrochim. Acta 52 (2007) 2625–2633.

[103]. E. Tsuji, A. Imanishia, K. Fukuia, Y. Nakato, Electrocatalytic activity of amorphous RuO_2 electrode for oxygen evolution in an aqueous solution, Electrochim. Acta 56 (2011) 2009–2016.

[104]. L. Burke and J. Mulcahy, The formation and reduction of anodic films on electrodeposited ruthenium, J. Electroanal. Chem. 73 (1976) 207-218.

[105]. M. Macherzynskia, A. Kasuya, Electrodeposition of uniformly distributed Ru and Ru–Pt nanoparticles onto n-type Si electrodes, Electrochim. Acta 95 (2013) 288–294.

[106]. I. Zhitomirsky, L. Gal-Or, Ruthenium oxide deposits prepared by cathodic electrosynthesis, Mater. Lett. 31 (1997) 155-159.

[107]. Y. Zheng, H. Ding, M. Zhang, Hydrous ruthenium oxide thin film electrodes prepared by cathodic electrodeposition for supercapacitors, Thin Solid Films 516 (2008) 7381–7385.

[108]. B. Park, C. Lokhande, H. Park, K. Jung, O. Joo, Cathodic electrodeposition of RuO_2 thin films from $RuCl_3$ solution, Mater. Chem. Phys. 87 (2004) 59–66.

[109]. J. Garcia, M. Esclapez, P. Bonete, Y. Hernandez, L. Garreton, V. Saez, Current topics on sonoelectrochemistry, Ultrasonics 50 (2010) 318–322.

[110]. J. Garcia, V. Saeza, M. Esclapeza, P. Bonetea, Y. Vargasb, L. Gaeteb, Relevant developments and new insights on sonoelectrochemistry, Phys. Pro. 3 (2010) 117–124.

[111]. M. Hyde, R. Compton, How ultrasound influences the electrodeposition of metals, J. Electroanal. Chem. 531 (2002) 19-24.

[112]. I. Bilecka and M. Niederberger, Microwave chemistry for inorganic nanomaterials synthesis, Nanoscale 2 (2010) 1358–1374.

[113]. G. Chen, Electrochemical technologies in wastewater treatment, Sep. Pur. Technol. 38 (2004) 11–41.

[114]. K. Kim, E. Lee, J. Kim, K. Shin, K. Kim, Study on the electro-activity and non-stochiometry of a Ru-based mixed oxide electrode, Electrochim. Acta 46 (2001) 915-921.

[115]. A. Ananth, S. Dharaneedharan, M. Gandhi, M. Heo, Y. Mok, Novel RuO_2 nanosheets – Facile synthesis, characterization and application, Chem. Eng. J. 223 (2013) 729–736.

[116]. Y. Inoue, M. Uota, M. Uchigasaki, S. Nishi, T. Torikai, T. Watari, and M. Yada, Helical Ruthenium compound templated by 1-Dodecanesulfonate assemblies

and its conversion into helical Ruthenium oxide and helical metallic Ruthenium, Chem. Mater. 20 (2008) 5652–5656.

[117]. C. Malmgren, A. K. Eriksson, A. Cornell, J. Backtrom, S. Eriksson, H. Olin, Nanocrystallinity in RuO_2 coatings - Influence of precursor and preparation temperature, Thin Solid Films 518 (2010) 3615-3618.

[118]. H. P. Klug, L. E. Alexander, X-ray Diffraction Procedures, 2nd edition, Wiley, New York (1974).

[119]. T. L. Luu, J. Kim, J. Yoon, Physicochemical properties of RuO_2 and IrO_2 electrodes affecting chlorine evolutions, J. Ind. Eng. Chem. (2014), in press.

[120]. J. Bennett, Electrodes for generation of hydrogen and oxygen from seawater, Int. J. Hydrogen Energy 5 (1980) 401-408.

[121]. H. K. Abdel-aal, S. M. Sultan, I. A. Hussein, Parametric study for saline water electrolysis: part II – Chlorine evolution, selectivity and determination, Int. J. Hydrogen Energy 18 (1993) 545-551.

[122]. G. Lodi, C. D. Asmundis, S. Ardizzone, E. Siviery and S. Trasatti, Resistivity and temperature coefficient of resistivity of Ruthenium oxide layers influence of morphology, Surf. Tech. 14 (1981) 335-343.

[123]. M. CaO, Y. Wang, C. Guo, Y. Qi, C. Hu, E. Wang, A simple route towards CuO nanowires and nanorods, J. Nanosci. Nanotechnol. 4 (2004) 824–828.

[124]. Z. Li, Y. Xiong, Y. Xie, Selected-control synthesis of ZnO nanowires and nanorods via a PEG-assisted route, Inorg. Chem. 42 (2003) 8105–8109.

[125]. L. Dong and J. Jiao, Dielectrophoretic fabrication and electron microscopy characterization of one dimensional nanomaterial-based devices, Microsc. Microanal. 12 (2006) 482-483.

[126]. Y. Xia, P. Yang, Y. Sun, Y. Wu, B. Mayers, B. Gates, Y. Yin, F. Kim, H. Yan, One dimensional nanostructures: synthesis, characterization, and applications, Adv. Mater. 15 (2003) 353–389.

[127]. X. Wu, Y. Zeng, H. Gao, J. Su, J. Liu and Z. Zhu, Template synthesis of hollow fusiform $RuO_2.xH_2O$ nanostructure and its supercapacitor performance, J. Mater. Chem. 1 (2013) 469–472.

[128]. A. Ponrouch, S. Garbarino, E. Bertin, D. Guay, Ultra high capacitance values of $Pt@RuO_2$ core-shell nanotubular electrodes for microsupercapacitor applications, J. Power Sources 221 (2013) 228-231.

[129]. K. Xiong, Z. Deng, L. Li, S. Chen, M. Xia, L. Zhang, X. Qi, W. Ding, S. Tan, Z. Wei, Sn and Sb co-doped Ru-Ti oxides supported on TiO_2 nanotubes anode for selectivity toward electrocatalytic chlorine evolution, J. Appl. Electrochem. 43 (2013) 847–854.

[130]. H. Cao, D. Lu, J. Lin, Q. Ye, J. Wu, G. Zheng, Novel Sb-doped ruthenium oxide electrode with ordered nanotube structure and its electrocatalytic activity toward chlorine evolution, Electrochim. Acta 91 (2013) 234–239.

[131]. S. Oh and L. Nazar, Direct synthesis of electroactive mesoporous hydrous

crystalline RuO_2 templated by a cationic surfactant, J. Mater. Chem. 20 (2010) 3834–3839.

[132]. C. Sassoye, C. Laberty, H. Khanh, S. Cassaignon, C. Boissiere, M. Antonietti, and C. Sanchez, Block-copolymer-templated synthesis of electroactive RuO_2-based mesoporous thin films, Adv. Funct. Mater. 19 (2009) 1922–1929.

[133]. N. Menzel, E. Ortel, K. Mette, R. Kraehnert, and P. Strasser, Dimensionally stable Ru/Ir/TiO_2 anodes with tailored mesoporosity for efficient electrochemical chlorine evolution, ACS Catal. 3 (2013) 1324−1333.

[134]. E. Ortel, T. Reier, P. Strasser, and R. Kraehnert, Mesoporous IrO_2 films templated by PEO-PB-PEO block-copolymers: self-assembly, crystallization behavior, and electrocatalytic performance, Chem. Mater. 23 (2011) 3201–3209.

[135]. N. Menzel, E. Ortel, R. Kraehnert, and P. Strasser, Electrocatalysis using porous nanostructured materials, Chem. Phys. Chem.13 (2012) 1385–1394.

[136]. F. Jiang, T. Zheng, Y. Yang, Preparation and electrochromic properties of tungsten oxide and iridium oxide porous films, J. Non-cryst. Solids 354 (2008) 1290.

[137]. O. Velev and E. Kaler, Structured porous materials via colloidal crystal templating: from inorganic oxides to metals, Adv. Mater. 7 (2000) 12.

[138]. N. Petkovich and A. Stein, Controlling macro- and mesostructures with hierarchical porosity through combined hard and soft templating, Chem. Soc. Rev. 42 (2013) 3721-3739.

[139]. A. Mallik, B. Ray, An analysis of the temperature-induced supersaturation

effects on structure and properties of sono-electrodeposited copper thin films, Surf. Coat. Tech. 206 (2011) 1947–1954.

[140]. S. Floate, M. Hyde, R. Compton, Electrochemical and AFM studies of the electrodeposition of cobalt on glassy carbon: an analysis of the effect of ultrasound, J. Electroanal. Chem. 523 (2002) 49–63.

[141]. J. Garcia, V. Saez, J. Iniesta, V. Montiel, A. Aldaz, Electrodeposition of PbO_2 on glassy carbon electrodes: influence of ultrasound power, Electrochem. Commun. 4 (2002) 370–373.

[142]. V. Saez, J. Garcia, J. Iniesta, A. Ferrer, A. Aldaz, Electrodeposition of PbO_2 on glassy carbon electrodes: influence of ultrasound frequency, Electrochem. Commun. 6 (2004) 757–761.

[143]. H. Zheng, M. An, Electrodeposition of Zn–Ni–Al_2O_3 nanocomposite coatings under ultrasound conditions, J. Alloys Compd. 459 (2008) 548–552.

[144]. E. Lecina, I. Urrutia, J. Diez, J. Morgiel, P. Indyka, A comparative study of the effect of mechanical and ultrasound agitation on the properties of electrodeposited Ni/Al_2O_3 nanocomposite coatings, Surf. Coat. Tech. 206 (2012) 2998–3005.

[145]. Y. Niu, J. Wei, Y. Yang, J. Hu, Z. Yu, Influence of microstructure on the wear mechanism of multilayered Ni coating deposited by ultrasound-assisted

electrodeposition, Surf. Coat. Tech. 210 (2012) 21–27.

[146]. B. Pollet, J. Hihn, T. Mason, Sonoelectrodeposition (20 and 850 kHz) of copper in aqueous and deep eutectic solvents, Electrochim. Acta 53 (2008) 4248–4256.

[147]. B. Pollet, E. Valzer, Oliver J. Curnick, Platinum sonoelectrodeposition on glassy carbon and gas diffusion layer electrodes, Int. J. Hydrogen Energy 36 (2011) 6248-6258.

[148]. J. Kim, K. Kim, S. Park, K. Kim, Microwave-polyol synthesis of nanocrystalline ruthenium oxide nanoparticles on carbon nanotubes for electrochemical capacitors, Electrochim. Acta 55 (2010) 8056–8061.

[149]. S. Yan, H. Wang, P. Qu, Y. Zhang, Z. Xiao, RuO_2/carbon nanotubes composites synthesized by microwave-assisted method for electrochemical supercapacitor, Synt. Met. 159 (2009) 158–161.

[150]. C. Hu, Y. Yang, T. Lee, Microwave-assisted hydrothermal synthesis of $RuO_2.xH_2O$-TiO_2, nanocomposites for high power supercapacitors, Electrochem. Solid-State Lett. 13 (2010) 173-176.

[151]. A. Devadas, S. Baranton, T. Napporn, C. Coutanceau, Tailoring of RuO_2 nanoparticles by microwave assisted “Instant method” for energy storage applications, J. Power Sources 196 (2011) 4044–4053.

Appendix

Correlation between chlorine evolution and the relevant current densities

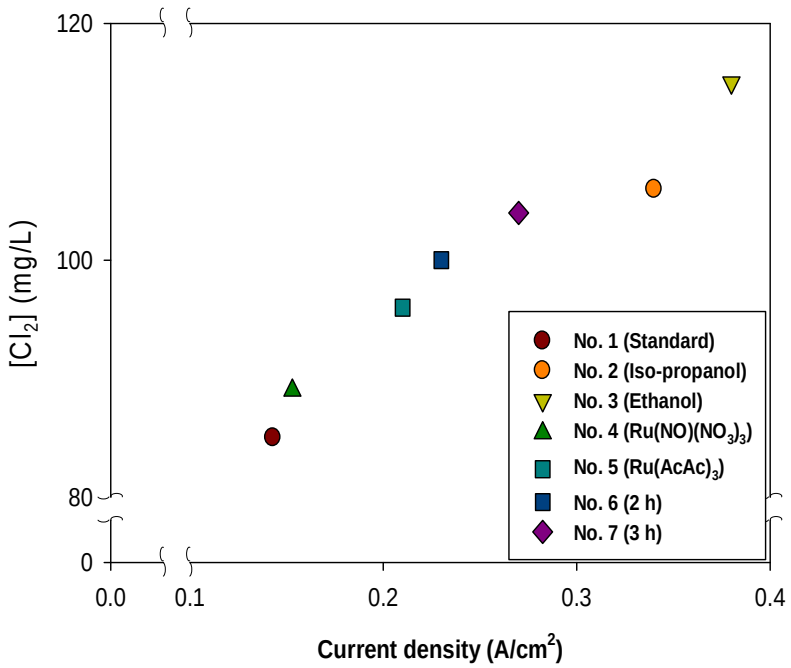

Fig. S1. The correlation between chlorine evolution expressed as the chlorine concentration with the various RuO_2 electrodes fabricated with three different fabrication conditions and their relevant current densities in LSV (at 2.0 V vs. Ag/AgCl): No. 1 (Standard: HCl, $RuCl_3$, 1 h), No. 2 (Iso-propanol), No. 3 (Ethanol), No. 4 ($Ru(NO)(NO_3)_3$), No. 5 ($Ru(AcAc)_3$), No. 6 (2 h), and No. 7 (3 h). Refer to Table 1 for details on the fabrication conditions. The current densities in

Figure S1 were extracted from the LSV in Figure 1 (b) at 2.0 V vs. Ag/AgCl, while the chlorine concentrations are from Figure 1 (a).

CV and voltammetric charge

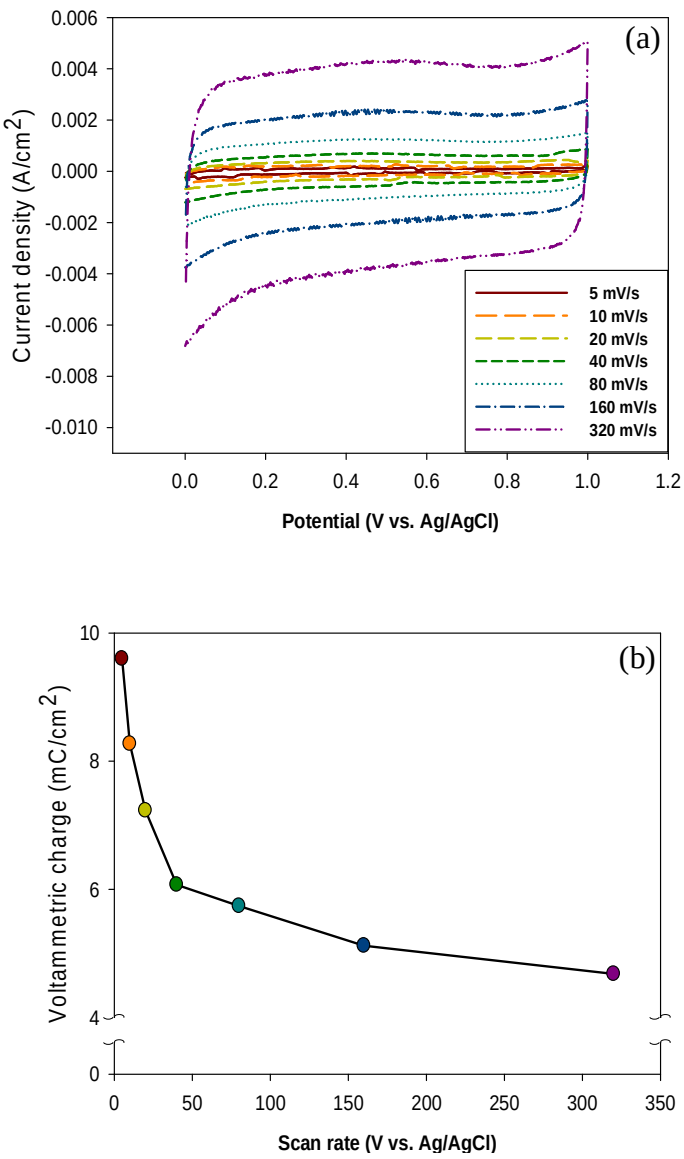

Fig. S2. The representative CV (a) and voltammetric charge (b) with scan rates (5 mV/s - 320 mV/s) for RuO_2 electrode No. 1 (HCl, $RuCl_3$, 1 h).

Figure S2 (a) and (b) shows the representative cyclic voltammogram (No. 1 (HCl, $RuCl_3$, 1 h)) with the scan rates (5 mV/s - 320 mV/s) and their voltammetric charges (q) which were obtained by integrating the cyclic voltammograms. In Figure S2 (a), the current densities from the voltammograms increased as the scan rates increase. Note that the rectangular shape of the cyclic voltammogram was maintained with the increasing the scan rate, showing the good reversibility (redox reaction) of the system resulting from an insignificant iR (ohmic drop) loss. As shown in Figure S2 (b), the voltammetric charge decreased with the increasing scan rates, showing that less accessible surface regions that exist, like micro-cracks and micro-pores, are progressively not participating in the reaction at higher scan rates. In contrast, at lower scan rates, the diffusion process reaches deeper into the oxide structure, resulting in a larger voltammetric charge. The different fabrication conditions including the solvents, precursors, calcination times induced different voltammetric charges in the RuO_2 electrodes.

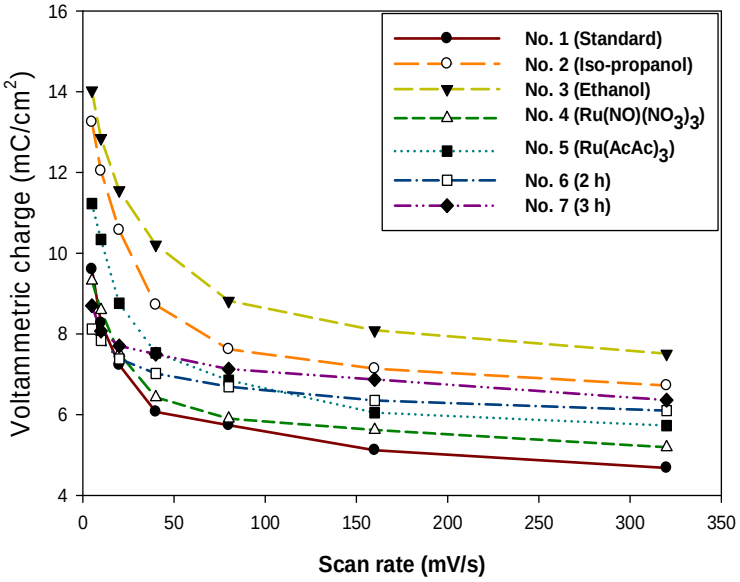

Fig. S3. The voltammetric charges (q) at various scan rates (5 mV/s-320 mV/s) with different fabrication conditions of the RuO_2 electrodes (0.5 M H_2SO_4 solution as electrolyte) with respect to the effect of the solvents: No. 1 (Standard, HCl, $RuCl_3$, 1 h), No. 2 (Iso-propanol), and No. 3 (Ethanol); the effect of the precursors: No. 4 ($Ru(NO)(NO_3)_3$), and No. 5 ($Ru(AcAc)_3$); and the effect of the calcination times: No. 6 (2 h), and No. 7 (3 h). Refer to Table 1 for details on the fabrication conditions.

Correlation between chlorine evolution and total surface area

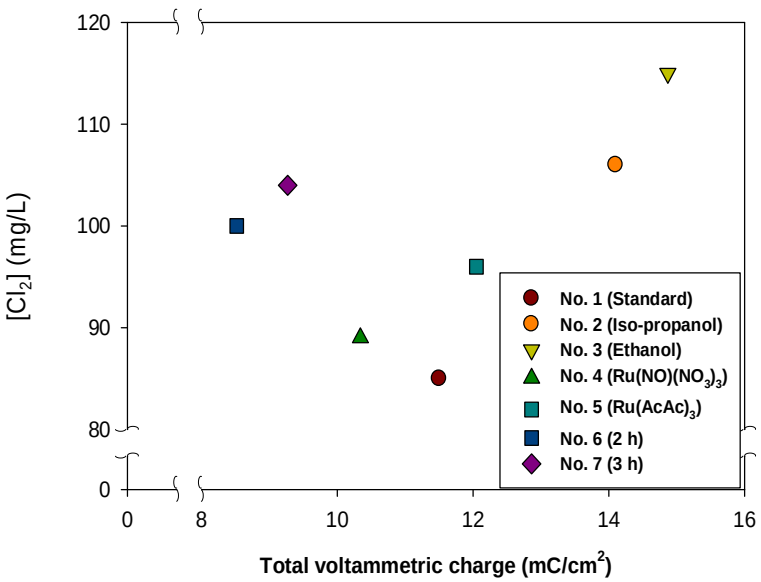

Fig. S4. Relationship between total voltammetric charges (total active surface areas) and the chlorine evolution of the RuO_2 electrodes fabricated with various conditions: No. 1 (Standard: HCl, $RuCl_3$, 1 h), No. 2 (Iso-propanol), No. 3 (Ethanol), No. 4 ($Ru(NO)(NO_3)_3$), No. 5 ($Ru(AcAc)_3$), No. 6 (2 h), and No. 7 (3 h). Refer to Table 1 for details on the fabrication conditions.

XRD spectra with different precursors

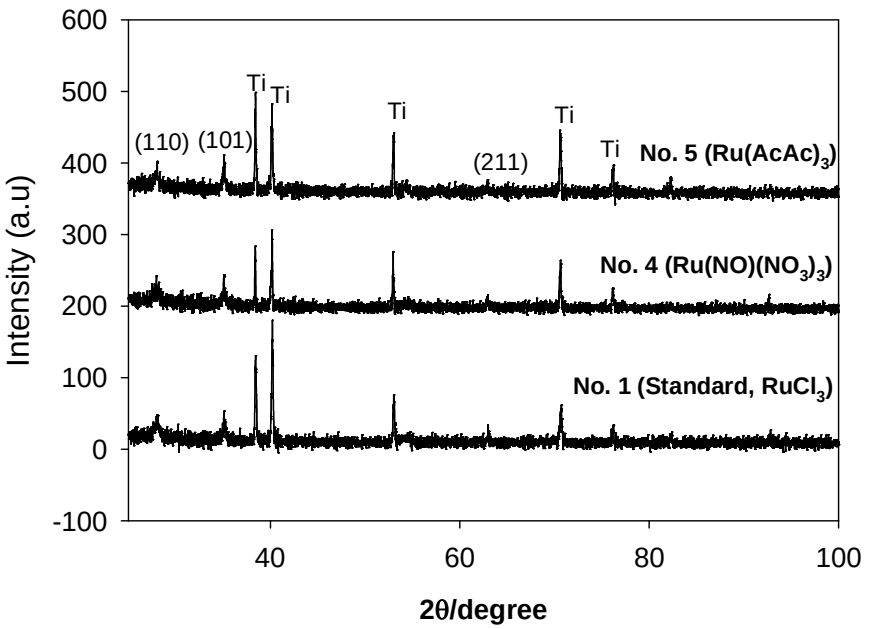

Fig. S5. XRD spectra of the RuO_2 electrodes with different precursors: No. 1 (Standard: HCl, $RuCl_3$, 1 h), No. 4 ($Ru(NO)(NO_3)_3$), and No. 5 ($Ru(AcAc)_3$). Refer to Table 1 for details on the fabrication conditions.

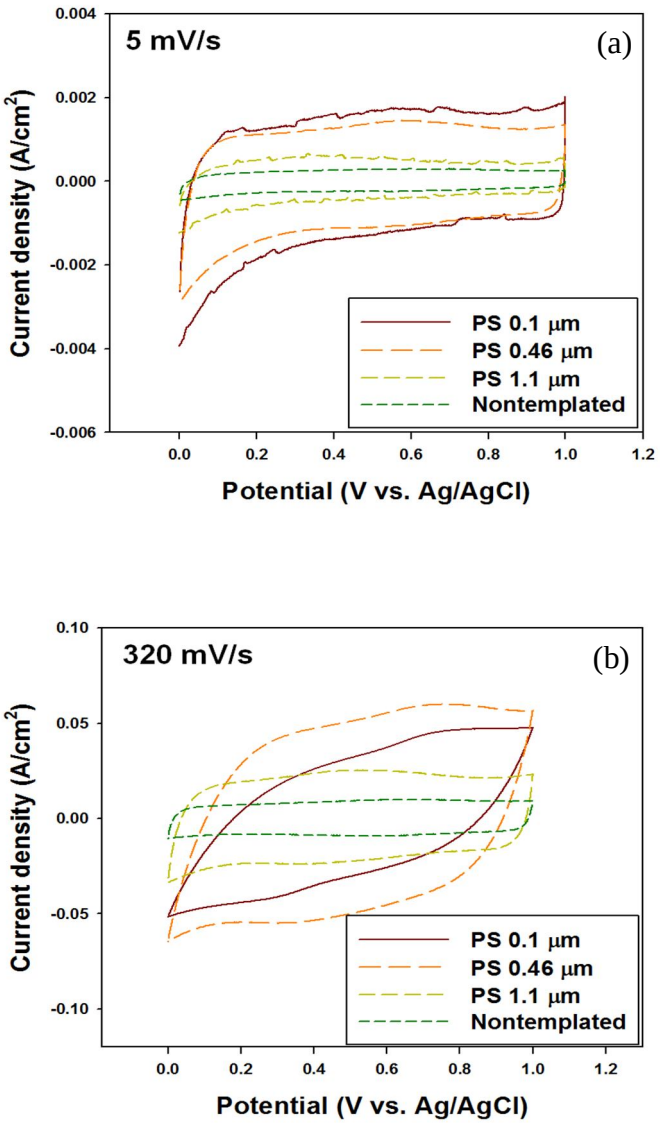

Fig. S6. Cyclic voltammograms of the macroporous RuO_2-TiO_2 electrodes (PS diameter of 0.1 µm, 0.46 µm, PS 1.1 µm) and the nontemplated electrode at two selected scan rates (5 mV/s (a), 320 mV/s (b)).

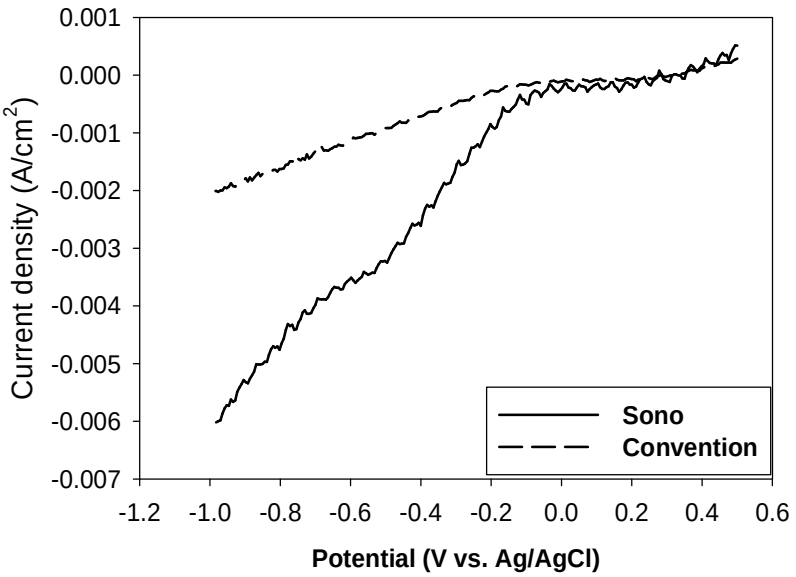

Fig. S7. Cathodic polarization curves of $RuCl_3$ aqueous solution under sonoelectrodeposition and conventional stirring electrodeposition.

Figure S7 shows the cathodic polarization curves of $RuCl_3$ aqueous solution on the Ti substrates under sonoelectrodeposition and conventional stirring electrodeposition. The Ru^{3+} ions in the electrolyte solution are reduced at potential negative than 0.2 V versus Ag/AgCl. A platform of limiting current, and the diffusion current of the reduction of Ru^{3+}, appears at 0 to −0.2 V versus Ag/AgCl. H_2 evolution occurs at potential negative than −0.2 V versus Ag/AgCl. The results showed that the reduced Ru^{3+} ions only possible when H_2 and OH^- are generated on the electrode at potential negative than −0.2 V versus Ag/AgCl. It is very consistent with Zhitomirsky et al.'s results [106], suggested that cathodic deposition is due to the reactions of Ru^{3+} ions with the electrogenerated base on the electrode. Figure S7 clearly shows that sonication affects the RuO_2 deposition process in the potential range studied. Under sonoelectrodeposition process, the cathodic current shifts to the more negative region and the increasing in pseudo limiting current densities is observed compared to conventional stirring electrodeposition. It can be attributed by the highly efficient stirring, decreases the formation overpotential of nucleation sites at the electrode surface caused by the implosion of cavitation H_2 bubbles.